SPECTROSCOPIC INVESTIGATIONS OF NANOEMULSION SURFACES

by

Emma (Ngọc Bích) Tran

A DISSERTATION

Presented to the Department of Chemistry and Biochemistry
and the Divison of Graduate Studies of the University of Oregon
in partial fulfillment of the requirements
for the degree of
Doctor of Philosophy

June 2022

DISSERATION APPROVAL PAGE

Student: Emma (Ngọc Bích) Tran

Title: Spectroscopic Investigations of Nanoemulsion Surfaces

This dissertation has been accepted and approved in partial fulfillment of the requirements for the Doctor of Philosophy degree in the Department of Chemistry and Biochemistry by:

Dr. Larry Scatena	Advisor
Dr. Cathy Wong	Chair
Dr. Jim Prell	Core Member
Dr. Stephanie Majewski	Institutional Representative

and

Krista Chronister	Vice Provost for Graduate Studies

Original approval signatures are on file with the University of Oregon Graduate School.

Degree awarded June 2022.

DISSERTATION ABSTRACT

Emma (Ngọc Bích) Tran

Doctor of Philosophy

Department of Chemistry and Biochemistry

June 2022

Title: Spectroscopic Investigations of Nanoemulsion Surfaces

Interfaces are ubiquitous and diverse in nature, as are surface-active molecules that self-assemble at interfaces. Surfactants and polymers are often found at various interfaces due to their interfacial properties. Such properties can be tuned by the chemical environment and make-up of the interface. For example, the behavior and functionality of surfactants may vary across a solid/liquid, air/liquid, and liquid/liquid interface. The works of this dissertation focuses on the oil/water interface, specifically the surface of oil-in-water nanoemulsions. Nanoemulsions are kinetically stable oil droplets dispersed in water that are 100s of nanometers in diameter. They are stabilized by various types and combinations of surfactants and polymers. From an application standpoint, nanoemulsions are prevalent in cosmetics, food science, drug delivery, and environmental remediation. The droplet surface is a common feature amongst a wide variety of these applications. Thus, emphasis has been placed on understanding how to control and tune droplet stability and interfacial properties.

The studies detailed herein employs a novel surface-specific spectroscopy called vibrational sum frequency scattering spectroscopy to develop molecular-level insights into the self-assembly of surfactants and polymers to nanoemulsion surfaces. Dynamic light scattering, interfacial tensiometry, and ζ-potential measurements are utilized concurrently to complement molecular-level details with results reporting on the macroscopic properties of the system. The adsorption behavior and conformational arrangement of surfactants and polymers to the droplet surface contributes significantly to colloidal stability and interfacial properties. Specifically, the chemical environment, constituents of the adsorbed species, polymer layering behavior, and surface charge are important details that influence nanoemulsion properties. This kind of knowledge on interfacial phenomena and colloidal chemistry aids in the advancement of technological, commercial, and industrial applications involving emulsions.

This dissertation contains published and unpublished co-authored material.

CURRICULUM VITAE

NAME OF AUTHOR: Emma (Ngọc Bích) Tran

GRADUATE AND UNDERGRADUATE SCHOOLS ATTENDED:

University of Oregon, Eugene
University of Nevada, Las Vegas

DEGREES AWARDED:

Doctor of Philosophy, Chemistry, 2022, University of Oregon
Masters of Science, Chemistry, 2018, University of Oregon
Bachelor of Science, Chemistry, 2017, University of Nevada, Las Vegas

AREAS OF SPECIAL INTEREST:

Surface and colloid chemistry
Interfacial phenomena of surfactants and polymers
Nonlinear spectroscopy

PROFESSIONAL EXPERIENCE:

Graduate Research Assistant in the Richmond Laboratory, Department of Chemistry and Biochemistry, University of Oregon, Eugene (2018–Present)

General chemistry lecture sequence Head Teaching Assistant, Department of Chemistry and Biochemistry, University of Oregon, Eugene (2020–2021)

Presidential Undergraduate Research Scholars (PURS) Co-instructor, Department of Chemistry and Biochemistry, University of Oregon, Eugene (2020–2021)

General chemistry laboratory sequence Head Teaching Assistant, Department of Chemistry and Biochemistry, University of Oregon, Eugene (2019–2020)

General chemistry laboratory sequence Teaching Assistant, Department of Chemistry and Biochemistry, University of Oregon, Eugene (2017–2018)

GRANTS, AWARDS, AND HONORS:

Keana Fellowship, University of Oregon, 2021–2022

Graduate Student Award for Excellence in the Teaching of Chemistry, University of Oregon, 2019–2020

PUBLICATIONS:

Tran, E., Richmond, G. L. "Interfacial steric and molecular bonding effects contributing to the stability of neutrally charged nanoemulsions" *Langmuir*, 2021

Tran, E., Mapile, A. N., Richmond, G. L. "Peeling back the layers: Investigating the effects of polyelectrolyte layering on surface structure and stability of oil-in-water nanoemulsions" *Journal of Colloid and Interface Science*, 2021 599, 706-716.

Tran, E., Carpenter, A. P., Richmond, G. L. "Probing the Molecular Structure of Coadsorbed Polyethylenimine and Charged Surfactants at the Nanoemulsion Droplet Surface" *Langmuir*, 2020 36, 31, 9081-9089.

Carpenter, A. P., Tran, E., Altman, R. M., Richmond, G. L. "The Formation and Surface Stabilizing Contributions to Bare Nanoemulsions Created with Negligible Surface Charge" Proceedings of the National Academy of Sciences, 2019 116 (19) 9214-9219.

ACKNOWLEDGEMENTS

The most valuable thing PhD school taught me is that nothing great is ever truly accomplished alone. My deepest appreciation goes to each and every one of you:

To the Richmond Lab: Dr. Geri Richmond–Thank you for pushing me to be a more confident scientist. You have shown me that strong and accomplished women in science need not fit a single mold. Dr. Larry Scatena–I am amazed with the amount of work you accomplish while prioritizing your work/life balance. I am happy and proud to have you as an interim advisor. Thank you for stepping up and giving us your all. Dr. Fred Moore–Despite everything, you have always brought so much positivity and joy to the lab. We could all use a kind heart like yours. Priscilla Lewis–You are the backbone of the lab. Without you, everything would be in shambles. Thank you for taking incredible care of us. To all Richmond lab members past and present–Thank you for all the support, mentorship, and friendly SFG banter. I also thank the Department of Energy for the funding that made this work possible.

To my committee: Dr. Cathy Wong, Dr. Jim Prell, and Dr. Stephanie Majewski–Thank you for believing in me and in my work, especially when I struggled to believe in anything at all.

To the chemistry department: Dr. Deb Exton–I don't think many people truly understand and appreciate how challenging teaching general chemistry is. I will always admire your dedication to your students. Thank you for supporting me in all my teaching efforts. Dr. Jeff Cina–I have enjoyed each and every one of our conversations and how unapologetically honest you are with your thoughts and advice. Christi Mabinuori–You have done so much for our department, have always been in our corner, and have never expected anything in return. I (and likely so many others) cannot thank you enough. Dr. Mark Lonergan–Despite having so much on your plate as department head, you have always made time to talk to me and worked hard to support all our DEI efforts. Your thoughtfulness and commitment to the chemistry department is inspiring.

To my dearest friends: Jack Maurer–I'm not sure if you remember, but you were the first person I met in our cohort. We were checking in at the rec center for CPR training. You are one of the few people I know who can talk about science so passionately without making me feel insecure about my own knowledge and abilities.

Not many people have that skill. Thank you for being such a great friend and making us bomb food in astronomical portions (i.e., the meatball the size of my head). Becca Schaefer–I admire your creativity, talent, honesty, and the fun activities (with prizes!) you prepare for us when we're all together. Ashley Mapile–Between working with you in the lab, serving on the DEI committee, conversations about the good, bad, and ugly, and all of our outdoor excursions, you have become one of my closest friends. Your unshakeable kindness motivates me to believe that (just maybe) humans aren't the absolute worst. Lola Schaefer Maurer–I've said it before and I'll say it again: I like dogs more than I like humans. Your zoomies make my day. Lydia Dysart–I value your commitment to our friendship and keeping in touch, especially when we're 2,500 miles apart. Morgan Mann–Thank you for being a source of never-ending love and support. To Cassidi Howard, Phil Lotshaw, Marc Foster, Deepika Sundarraman, Claire Albrecht, Dylan Heussman, and Bia Assunção–the past five years wasn't always a smooth ride, but having you all around made the bumps much more manageable.

To Tiemo Landes: Danke for providing me with your relentless patience, understanding, and so much more, even during my worst days. You are my best friend and I appreciate all our adventures together. Also, I'm looking forward to getting my honorary PhD in physics after the countless times I've listened to you talk about "entangled two-photon absorption."

To the friends I call family: Lynne Truong–No words will ever truly capture how I appreciate you. You've been my rock since we were kids. For always showing up and never being too busy for me, *cảm ơn*. Sarah Molina–No matter how busy our lives are, you've always kept me in your thoughts and never stopped telling me how proud you are of me. You are one of the strongest, most resilient people I know. For all your encouragement and love since we were teenagers, *maraming salamat*.

To my family: Although the generational, cultural, and language barriers will always keep us from seeing eye-to-eye, everything I've done up to this point is for you.

To Dr. Kathleen Robins: Everything I've done up to this point is because of you. Thank you for the unwavering support and guidance I never knew I needed. If it weren't for you, I would not be here writing this today, because I would not have even gotten a Bachelor's degree, let alone a doctorate. Truly.

A final acknowledgement goes to my Vietnamese-American community. This is long overdue, but it wasn't until a couple years ago that I felt proud of my Vietnamese culture and where I came from. My Vietnamese name is Ngọc Bích and I was always ashamed of it (it's still a constant struggle for me), and I trust that people can imagine why. The Model Minority Myth paints all Asian-Americans in the same light and sets the expectation that we can all be successful if we just work hard enough. But the truth is that success does not revolve around work alone. Success relies on resources, guidance, support, and luck–all things many Vietnamese immigrants do not have.

I used to be consumed with anger. I was angry that my parents didn't speak English, didn't help me with homework, didn't teach me how to ride a bike, or swim, or ski, didn't expose me to the recreational activities that I now love, didn't understand nor appreciate what a PhD is, let alone the science. But I've learned that those aren't truly the reasons that made me upset. I shouldn't have been upset at my parents for the things they didn't do, and I should have been more grateful for the things they did do. To leave behind your home, comfort, and all of your family to settle in foreign land with unfamiliar faces takes an enormous amount of courage–an amount of courage I wish I had.

Instead, I was upset because people didn't see and understand the hardships of a Vietnamese immigrant, yet casually assumed that "Asians are good at math and intelligent and successful" and expected the most from us. I encourage you all to think about the number of times you've seen a Vietnamese name on a publication, as the face of a recreational sport, the lead of a research group or project. The reason why there is so few of us is because we are from a country that was devastated by colonization and war, leaving most of my family living well below the poverty line. When those are your circumstances, you can work as hard as you want, and will never be where most are. So this acknowledgement goes to Vietnamese-Americans who have defied all odds and paved the way for my journey and my story.

Whatever I do next, I will pay it forward.

TABLE OF CONTENTS

Chapter **Page**

LIST OF FIGURES

Figure **Page**

LIST OF TABLES

CHAPTER I

BACKGROUND AND THEORY

Colloid and Interfacial Chemistry

A colloid is a type of mixture in which particles with nanometer to micron diameters are evenly distributed throughout an aqueous solution. In order to maintain colloidal stability, surface-active agents (i.e., surfactants) and polymers are often used to modify the surfaces of colloids. Thus, the intersection of colloids and interfacial chemistry is an area of research that provides necessary insights into controlling the properties, functionality, and stability of colloidal systems.

Nanoemulsions are an example of a colloid. Oil-in-water nanoemulsions, specifically, are oil droplets measuring between 20-500 nm in diameter. The oil (dispersed phase) is dispersed through an aqueous solution of emulsifiers (continuous phase) via low- and high-energy processes.[1–3] Unlike two immiscible liquids—such as oil and water—spontaneously forming a planar oil/water interface that is thermodynamically stable, nanoemulsions are kinetically stable and will eventually phase separate over time. However, based on the stabilizing agents, nanoemulsions can be stable for weeks, months, and in some cases, years, making them advantageous for applications.[4–6]

Applications utilizing nanoemulsions include food science,[5, 7] cosmetics,[8] drug delivery systems,[9–11] and material synthesis.[1] In each of these applications, nanoemulsions play a variety of roles from improving the appearance of food to encapsulating and increasing the bioavailability of active pharmaceutical ingredients. Their functionality and properties depend on environmental considerations such as pH, salinity, and temperature, as well as the surfactants and polymers coating the droplet surface. Thus, by developing a strong understanding of the interfacial chemistry occurring at the droplet surface, nanoemulsions can be designed for diverse applications with specific properties and tunable behavior.

Liquid/liquid interfaces are notoriously challenging to study experimentally, especially in a way that provides molecular-level details on conformational structure. Surface techniques such as X-ray photoelelectron spectroscopy require a vacuum and is therefore incompatible for probing liquid/liquid interfaces. Other scattering techniques such as neutron scattering and ellipsometery are able to provide information regarding the thickness and composition of thin layers at an interface (including liquid/liquid interfaces), but do not provide molecular-level information. Moreover,

none of these techniques are able to probe the surfaces of liquid droplets suspended in another liquid medium. This dissertation sheds light on nanoemulsion surfaces by providing molecular-level information using vibrational sum frequency scattering spectroscopy, complemented by pendant drop tensiometry, dynamic light scattering, and ζ-potential measurements.

In this dissertation, the contents of Chapters III, IV, and V have been published with co-authors. Chapter VI contains work that is not yet published, but is currently under review at the time of submission. Chapter VI also contains co-authors.

Vibrational Sum Frequency Spectroscopy at Planar Interfaces

Prior to discussing the details of probing a droplet liquid/liquid interface, it is necessary to first review sum frequency generation at planar liquid/liquid interfaces. Vibrational sum frequency spectroscopy (VSFS) is a powerful experimental tool for probing interfaces because it is inherently surface-specific with chemical selectivity.[12, 13]

As light moves through a material, the electric field of that light exerts a force on the valence electrons of the molecules making up the material. With low intensity, non-coherent light (e.g., ambient light), the force exerted is small. In an isotropic (uniform in all orientations and direction) medium, the induced electric dipole $\vec{\mu}$ is given as:

$$\vec{\mu} = \vec{\mu}_o + \alpha\vec{E}, \tag{1}$$

where $\vec{\mu}_o$ is the permanent dipole of the material and α is the polarizability of the electrons.

In condensed phase, the sum of all the molecular electric dipoles yields a dipole moment per unit volume known as the bulk polarization $\vec{P}$. Very few materials have a permanent dipole, thus if $\vec{\mu}_o$ is omitted, the bulk polarization can be described as

$$\vec{P} = \varepsilon_o \chi^{(1)} \vec{E}, \tag{2}$$

where $\chi^{(1)}$ is the macroscopic average of α, known as the first-order, linear susceptibility. ε_o is vacuum permittivity. The induced dipole emits light that oscillates at the same frequency as the incident electric field and describes linear processes such as reflection and refraction.

For high intensity, coherent light (e.g., laser), the non-linearity of the material response must be considered. This non-linearity is accounted for by additional terms

in the induced electric dipole given by

$$\vec{\mu} = \vec{\mu}_o + \alpha\vec{E} + \beta\vec{E}^2 + \gamma\vec{E}^3 + \cdots, \tag{3}$$

where β and γ are the first- and second-order hyperpolarizabilities, respectively. Again, if it is assumed that most materials do not have a permanent dipole moment and omit $\vec{\mu}_o$, then the bulk polarization becomes

$$\begin{aligned} \vec{P} &= \vec{P}^{(1)} + \vec{P}^{(2)} + \vec{P}^{(3)} + \cdots & (4) \\ &= \varepsilon_o(\chi^{(1)}\vec{E} + \chi^{(2)}\vec{E}^2 + \chi^{(3)}\vec{E}^3 + \cdots), & (5) \end{aligned}$$

where $\chi^{(2)}$ and $\chi^{(3)}$ are the second- and third-order non-linear susceptibilities, respectivity. Like $\chi^{(1)}$ and α, $\chi^{(2)}$ and $\chi^{(3)}$ are the macroscopic average of β and γ, respectively.

The sum frequency component of the second-order non-linear polarization can be expressed as

$$\vec{P}_i(\omega_{\mathrm{SF}}) = \chi^{(2)}_{\mathrm{ijk}}\vec{E}_j(\omega_{\mathrm{IR}})\vec{E}_k(\omega_{\mathrm{vis}}), \tag{6}$$

where $\vec{E}_j$ and $\vec{E}_k$ are the electric fields of the IR and visible pulse, respectively, and $\chi^{(2)}_{\mathrm{ijk}}$ is a third-rank tensor describing the material surface response. For sum frequency generation, the induced second-order polarization will oscillate at the sum of the incident IR and visible frequencies. Note that additional second-order non-linear processes such as second harmonic generation and difference frequency generation exist, but the focus here is placed on sum frequency generation.

The surface-specificity of the VSFS technique lies in the second-order non-linear susceptibility, $\chi^{(2)}_{\mathrm{ijk}}$, which is a third-rank tensor containing 27 possible non-zero elements. In centrosymmetric media, inversion symmetry requires the following relationship to be true:

$$\chi^{(2)}_{\mathrm{ijk}} = \chi^{(2)}_{\mathrm{-i-j-k}} = -\chi^{(2)}_{\mathrm{ijk}} \tag{7}$$

This necessarily results in $\chi^{(2)}_{\mathrm{ijk}} = 0$. The outcome here is that sum frequency generation is strictly allowed only where inversion symmetry is broken. The interface of two immiscible liquids is a primary example of where inversion symmetry is broken, enabling VSFS to specifically probe the interface and ignore all bulk contributions.

Interfaces can be described with $C_{\infty\mathrm{v}}$ symmetry in the plane of the interface. By applying the symmetry operators in the $C_{\infty\mathrm{v}}$ (or $C_{4\mathrm{v}}$ for simplicity) point group to each element of $\chi^{(2)}_{\mathrm{ijk}}$, the result is that out of the 27 tensor elements, only 7 is non-zero. Further, of the 7 non-zero tensor elements, only 4 are unique because the interface is

isotropic within the plane of the interface (i.e., $x = y$). Ultimately, VSFS probes the following tensor elements: $\chi^{(2)}_{xxz} = \chi^{(2)}_{yyz}$, $\chi^{(2)}_{xzx} = \chi^{(2)}_{yzy}$, $\chi^{(2)}_{zxx} = \chi^{(2)}_{zyy}$, and $\chi^{(2)}_{zzz}$.

Experimentally, the polarization of the IR, visible, and generated SF light can be selected to probe specific elements of $\chi^{(2)}_{ijk}$. The polarization denoted as S or P are with respect to the plane of incidence (i.e., the plane in which the beams are traveling) with S being perpendicular and P being parallel. The polarization schemes and tensor elements probed with VSFS are summarized below:

Polarization scheme	$\chi^{(2)}_{ijk}$ element probed
SSP	$\chi^{(2)}_{xxz}$
SPS	$\chi^{(2)}_{xzx}$
PSS	$\chi^{(2)}_{zxx}$
PPP	$\chi^{(2)}_{zzz}$, $\chi^{(2)}_{yyz}$, $\chi^{(2)}_{yzy}$, $\chi^{(2)}_{zyy}$

$\chi^{(2)}_{ijk}$ is a macroscopic quantity related to the molecular hyperpolarizability, $\beta^{(2)}_{abc}$, by

$$\chi^{(2)}_{ijk} = N \langle T_{ia} T_{jb} T_{kc} \rangle \beta^{(2)}_{abc} \tag{8}$$

where N is the density of molecules, T_{mn} represents the coordinate transformation from the molecular frame (a, b, c) to the laboratory frame (i, j, k), and the $\langle\rangle$ denotes averaging over all molecular orientations. The molecular hyperpolarizability is expressed as

$$\beta^{(2)}_{abc} = \frac{1}{2\hbar} \frac{M_{ab} A_c}{(\omega_\nu - \omega_{IR} - i\Gamma)} \tag{9}$$

where M_{ab} and A_c are the Raman and IR transition moments, respectively, which necessitates that all sum frequency-active vibrational resonances must be both Raman-*and* IR-active. ω_ν is the frequency of the vibrational resonance, ω_{IR} is the frequency of the IR beam, and Γ^{-1} is the relaxation time of the excited vibrational resonance. It can be seen that as ω_{IR} is tuned to be resonant with ω_ν, the term $(\omega_\nu - \omega_{IR}) \rightarrow 0$ and the magnitude of $\chi^{(2)}_{ijk}$ increases. Thus, the sum frequency response is enhanced at the resonant frequency. Measuring the sum frequency response as a function of IR frequencies ultimately yields a vibrational spectrum of only surface-adsorbed molecules, and all interference from bulk contributions are ignored.

While traditional planar sum frequency generation has been employed to study interfaces since 1987, sum frequency scattering was developed by Roke et. al. relatively recently in 2003.[13, 14] Similar to the description above, centrosymmetry is broken at the surfaces of nanoemulsions and thus, a scattered sum frequency response can be generated to provide molecular-level information on suspended droplets. At the far field, sum frequency photons interfere to generate a scattering pattern. The scattered sum frequency response is given by

$$E_{0,\mathrm{i}} \propto \Gamma^{(2)}_{\mathrm{i,j,k}}(\chi^{(2)}, R, \theta) : E_{1,\mathrm{j}} E_{2,\mathrm{k}} \tag{10}$$

where $\Gamma^{(2)}$ is the effective particle susceptibility, which depends on the non-linear second order susceptibility $\chi^{(2)}$, particle radius R, and scattering angle θ. The complete derivation for the expressions describing $\Gamma^{(2)}$ can be found elsewhere.[14–18] Our focus here is to briefly describe the relation between $\Gamma^{(2)}$ and $\chi^{(2)}$ which is given by

$$\begin{pmatrix} \Gamma_1 \\ \Gamma_2 \\ \Gamma_3 \\ \Gamma_4 \end{pmatrix} = \begin{pmatrix} 2F_1 - 5F_2 & 0 & 0 & 0 \\ F_2 & 2F_1 & 0 & 0 \\ F_2 & 0 & 2F_1 & 0 \\ F_2 & 0 & 0 & 2F_1 \end{pmatrix} \begin{pmatrix} \chi_1 \\ \chi_2 \\ \chi_3 \\ \chi_4 \end{pmatrix}. \tag{11}$$

Under the Rayleigh-Gans-Debye approximation for second-order scattering, F_1 and F_2 are form factor functions that are expressed as

$$F_1(qR) = 2\pi i \left(\frac{\sin(qR)}{(qR)^2} - \frac{\cos(qR)}{qR} \right) \tag{12}$$

$$F_2(qR) = 4\pi i \left(3\frac{\sin(qR)}{(qR)^4} - 3\frac{\cos(qR)}{(qR)^3} - \frac{\sin(qR)}{(qR)^2} \right). \tag{13}$$

Note that $q = ||\vec{q}|| = 2|\vec{k_o}| \sin(\frac{\theta}{2})$ and R is the particle radius.

The resulting scattered electric field amplitudes are given by

$$\begin{aligned} E_{\mathrm{ppp}} &\propto \cos\left(\frac{\theta}{2}\right)\cos\left(\frac{\theta}{2}-\alpha\right)\cos\left(\frac{\theta}{2}-\alpha+\beta\right)\Gamma_1^{(2)} \\ &+ \cos(\theta-\alpha+\beta)E_{\mathrm{ssp}} \\ &+ \cos(\theta-\alpha)E_{\mathrm{sps}} \\ &+ \cos(\beta)E_{\mathrm{pss}} \qquad (14) \\ E_{\mathrm{ssp}} &\propto \cos\left(\frac{\theta}{2}-\alpha\right)\Gamma_2^{(2)} \qquad (15) \\ E_{\mathrm{sps}} &\propto \cos\left(\frac{\theta}{2}-\alpha+\beta\right)\Gamma_3^{(2)} \qquad (16) \\ E_{\mathrm{pss}} &\propto \cos\left(\frac{\theta}{2}\right)\Gamma_4^{(2)}. \qquad (17) \end{aligned}$$

The angle between the incident IR and visible beams is β and the angle between the IR wavevector and the phase-matched wavevector is α. Ultimately, by careful design of the experimental and detection geometry, the polarization combinations PPP, SSP, SPS, and PSS for scattering experiments are analogous to planar experiments in that they probe equivalent tensor elements.[14, 15, 17]

CHAPTER II

EXPERIMENTAL DETAILS

Nanoemulsion Preparation

All nanoemulsions prepared for this work were done via ultra-sonication with a Branson Sonifier 250 sonicator. The materials and recipe for each nanoemulsion system vary depending on each project, which are outlined below. In general, all nanoemulsion samples were sonicated with an output control of ~3 for 3 minutes. For each formulation, the final nanoemulsion concentration is 1% v/v. That is, 1% v/v hexadecane is sonicated into the aqueous phase. All glassware used was soaked for a minimum of 12 hours in a solution of concentrated sulfuric acid and AlNOCHROMIX oxidizer. After soaking, each piece of glassware was thoroughly rinsed with ultra-pure water (18.2 MΩ-cm resistivity) and dried in a 140°C oven. This cleaning routine is important for removing surface-active impurities and contaminants that may interfere with the spectroscopic measurements.[19] It is implied that each recipe below may use either hydrogenated or deuterated versions of a chemical, whichever is necessary for the experimental conditions. The specific chemical used is specified in each chapter.

Chapter III. *Chemicals used:* Hexadecane, sodium dodecyl sulfate (SDS), dodecyltrimethylammonium bromide (DTAB), polyethylenimine (PEI), HCl, and NaOH. This chapter contains nanoemulsions stabilized by PEI/surfactants and surfactants alone. For PEI/SDS-stabilized nanoemulsions, a stock solution of nanoemulsions was made by ultra-sonicating 2% v/v hexadecane into an aqueous solution containing twice the desired concentration of SDS. Separately, a PEI stock solution was also prepared at twice its desired concentration. When equal volumes of the stock 2% v/v SDS-stabilized nanoemulsions and stock PEI solution were mixed, a final nanoemulsion sample with 1% v/v hexadecane stabilized by the target concentration of SDS and PEI is obtained. The same method was used for preparing DTAB/PEI-stabilized nanoemulsions.

For SDS-stabilized nanoemulsions, a similar approach was taken. A stock solution of nanoemulsions was made by ultra-sonicating 2% v/v hexadecane into an aqueous solution containing twice the desired concentration of SDS. By mixing equal volumes of the 2% v/v SDS-stabiized nanoemulsions and water, a final 1% v/v nanoemulsion sample is made with the desired SDS concentration. The same procedure was used

to prepare DTAB-stabilized nanoemulsions.

For pH dependent studies, small amounts of NaOH or HCl were added to the PEI stock solutions made in H_2O to adjust the pH accordingly. MilliporeSigma MColorpHast pH strips were used to measure the pH of nanoemulsion samples. Analogously, for stock solutions made in D_2O, small amounts of NaOD or DCl were added to adjust the pD of the deuterated solution. We note that although we do not measure pD, but rather pH in a D_2O solution, it has been reported that a constant value of 0.45 is the difference between measured pH in D_2O versus pD.[20] Thus, it is assumed that this fixed value will not affect the trends in which conclusions were drawn from.

Chapter IV. *Chemicals used:* Hexadecane, dodecyltrimethylammonium bromide (DTAB), polyethylenimine (PEI), poly(styrene sulfonate) (PSS), HCl, and NaOH. This chapter contains nanoemulsions that are stabilized by DTAB alone, and DTAB in conjunction with *either* one or two polymer layers: PEI (under different pH conditions) and PSS. For nanoemulsions stabilized by only DTAB, a stock nanoemulsion sample is prepared by ultra-sonicating 2% v/v hexadecane with an aqueous solution containing twice the desired concentration of DTAB. By mixing equal volumes of the 2% v/v DTAB-stabilized nanoemulsions with water, a final 1% v/v DTAB-stabilized nanoemulsion sample is obtained with the desired DTAB concentration.

For DTAB/PSS-stabilized nanoemulsions, a 2% v/v stock nanoemulsion sample is prepared with twice the desired concentration of DTAB (as described above). Separately, a stock PSS solution is prepared at twice its desired concentration. Upon mixing equal volumes of the nanoemulsion sample and the PSS solution, a final 1% v/v nanoemulsion sample is obtained with the desired DTAB and PSS concentrations.

For DTAB/PSS/PEI-stabilized nanoemulsions, a similar approach is used with slight modifications. Here, a stock nanoemulsion sample is prepared by ultra-sonicating 2% v/v hexadecane with an aqueous solution containing twice the desired concentrations of DTAB *and* PSS. Separately, acidic (pH 3) and basic (pH 10) PEI solutions at twice their desired concentrations are prepared and set aside. By mixing equal volumes of the 2% v/v stock nanoemulsions stabilized by DTAB/PSS with *either* the acidic or basic aqueous PEI solutions, a final 1% v/v nanoemulsion solution is obtained and stabilized by the appropriate polymer/surfactant combination at the desired pH and concentrations. Again, MilliporeSigma MColorpHast pH strips were used to measure the pH of the PEI solutions, as well as the final nanoemulsion samples.

Chapter V. *Chemicals used:* Hexadecane, sodium dodecyl sulfate (SDS), and poly(N-

vinylacetamide) (PNVA).
This chapter contains nanoemulsions stabilized by a combination of SDS and PNVA, as well as SDS alone. To prepare the SDS/PNVA-coated nanoemulsions, 2% v/v hexadecane was sonicated with an aqueous solution containing SDS at twice the desired concentration. Separately, a PNVA solution was also prepared at twice the desired concentration. Upon mixing equal volumes of the nanoemulsion sample and the PNVA solution, a final 1% v/v nanoemulsion sample was obtained with the desired surfactant and polymer concentrations.

For SDS-stabilized nanoemulsions, a stock solution of nanoemulsions was made by ultra-sonicating 2% v/v hexadecane into an aqueous solution containing twice the desired concentration of SDS. By mixing equal volumes of the 2% v/v SDS-stabilized nanoemulsions and water, a final 1% v/v nanoemulsion sample is made with the desired SDS concentration.

Chapter VI. *Chemicals used:* Hexadecane, sodium dodecyl sulfate (SDS), dodecyltrimethylammonium bromide (DTAB), dodecyl-N,N-dimethyl-3-ammonio-1-propanesulfonate (DDAPS), NaCl, and $MgCl_2$.
This chapter contains nanoemulsions prepared with DDAPS in conjunction with one of the following: SDS, DTAB, NaCl, or $MgCl_2$. Unlike previous projects, these emulsions were created by ultra-sonicating 1% v/v hexadecane into an aqueous solution containing the chemical components of interest at the desired concentrations (as opposed to *twice* the desired concentration). Because DDAPS alone cannot form stable nanoemulsions, it must be mixed with the other co-additives prior to sonication.

Dynamic Light Scattering

Sample size distribution, average (Z-average) diameter, and the polydispersity index (PDI) were measured with a Malvern Zetasizer Nano via dynamic light scattering (DLS) measurements.[21–23] Using DLS, the Brownian motion of the nanoemulsions were measured by illuminating the sample with a 633 nm laser and detecting the scattered light at a back-scatter detection angle of 173°. This detection set-up is advantageous for a few reasons:

1. By measuring the back-scattered light, the incident beam does not need to travel through the entire sample volume, thus shortening the path length of the sample. With a shorter path length, samples that are more concentrated may still be measured before reaching the saturation threshold.

2. Reduces the probability for multiple scattering events to occur, which also allows for higher concentrations to be measured.

3. Minimizes contributions from larger contaminants and particulates. Larger particles will scatter light primarily in the forward direction. Thus, by measuring the back-scatter, the probability of detecting light scattering off contaminants is reduced.

The fluctuations in intensity of the light scattered by the sample is analyzed with a correlation function, $G(\tau)$, given by

$$G(\tau) = \langle I(t)T(t+\tau)\rangle\,, \tag{18}$$

where $I(t)$ is the intensity at time zero and $I(t+\tau)$ is the intensity at some time later. A cumulant analysis fits the log of the intensity correlation function to a third-order polynomial to obtain the decay rate, Γ (i.e. the first cumulant):

$$\Gamma = q^2 D, \tag{19}$$

where q is the scattering vector and D is the diffusion coefficient. The Stokes-Einstein formula is used to relate the diffusion coefficient to the hydrodynamic radius, R:

$$D = \frac{k_B T}{6\pi\eta R}, \tag{20}$$

where k_B is the Boltzmann constant, T is temperature, and η is the solvent viscosity.

This cumulant analysis provides a cumulant mean or a "Z-average" particle size. This mean is considered to be the most stable size value obtained by DLS, and is the size to report if a number is required for quality control. This Z-average size is only comparable to other size measurement techniques if the sample is spherical, monodisersed, and monomodal.

ζ-potential Measurements

ζ-potential (ZP) measurements were determined with a Malvern Zetasizer Nano to characterize the potential at the slip plane boundary of nanoemulsions, which is used as an indicator of surface charge and emulsion stability.[23, 24] In a colloidal system, there exists a layer of tightly bound ions referred to as the Stern layer. Ions of opposite charge are attracted to the Stern layer and form a layer of loosely bound ions, called

the diffuse layer. As a voltage is applied, causing charged particles to move, solvent molecules and ions within the diffuse layer will move with the particles, while ions in the Stern layer remain stagnant. The boundary separating the Stern layer and the diffuse layer is called the slip plane.

Using Laser Doppler Velocimetry, the change in frequency of back-scattered light, Δf, can be measured upon illuminating the sample with a 633 nm laser. The change in frequency of the back-scattered light is related to the particle speed, ν, by:

$$\Delta f = \frac{2\nu \sin\left(\frac{\theta}{2}\right)}{\lambda}, \tag{21}$$

where θ is the scattering angle and λ is the laser wavelength.

For particles moving at a constant speed under a uniform electric field, E, the particle electrophoretic mobility, μ, is given by:

$$\mu = \frac{\nu}{E} \tag{22}$$

By measuring Δf, one can determine the particle speed and then the electrophoretic mobility. Finally, applying the Smoluchowski approximation, the electrophoretic mobility and the electrokinetic potential at the slip plane (i.e., the ζ-potential), ϕ_ζ, can be determined:

$$\mu = \frac{\phi_\zeta \varepsilon \varepsilon_o}{\eta}, \tag{23}$$

with ε as the dielectric constant of the continuous phase, ε_o as the vacuum permittivity, and η as the solvent viscosity.

Pendant Drop Tensiometry

Interfacial tension (IFT) measurements were conducted using a KSV Instruments Attension Theta pendant drop tensiometer. The experimental set-up is dependent on the oil phase, which is either carbon tetrachloride (CCl_4) or hexadecane, for the studies detailed in this dissertation. For IFT measurements using CCl_4 as the oil phase (which is more dense than water), a droplet of aqueous solution containing the chemical system of interest (e.g., surfactants, polymers, salts, etc.) at the desired concentrations was suspended in a quartz cuvette of CCl_4. For IFT measurements using hexadecane as the oil phase (which is less dense than water), a droplet of hexadecane is suspended in a cuvette containing the aqueous chemical system. In both cases, a Hamilton Gastight syringe with a hooked needle (~0.771 mm in diameter)

was used to create the droplet.

The pendant drop tensiometer illuminates the cuvette such that a camera is able to capture images of the droplet silhouette. For all IFT experiments, the first image was taken immediately upon creating the droplet and then subsequently after at a specified fixed rate for a specified number of frames. By fitting the droplet silhouette of each frame to mathematical models derived from the Laplace-Young equation, the IFT was calculated using the tensiometry software. The error bars included in all IFT traces shown herein represent the standard deviation of at least three different scans measured on different days.

Tensiometry data can be reported and visualized in different ways. In the work discussed herein, there are reports of surface pressure (SP) values as well as IFT over time, both in units of mN/m. In Chapter 3, SP is reported which is the IFT value of a clean CCl_4/water interface minus the equilibrated IFT value of the chemical system of interest. Thus, the more surface active a system is, the greater the SP value. For these experiments, the measurement continues until the IFT value reaches a plateau (i.e., the equilibrium IFT). Alternatively, for highly surface active systems where a plateau is not observed within a reasonable time frame, the IFT value at ~8 hours is used. In Chapter 5, IFT values over time is reported, which shows the evolution of IFT. Here, after the first image of the droplet is taken, each subsequent image is taken at a rate of 1 frame per minute for a total of 60 minutes. With this approach, although some chemical systems will not reach their equilibrated IFT value by the end of 60 minutes, one can compare the shape of the traces over time.

VSFSS Laser Set-Up

For the vibrational sum frequency scattering spectroscopy (VSFSS) experiments conducted in the Richmond lab, a Ti:Sapphire Libra regenerative amplifier laser from Coherent generates a fundamental 800 nm beam that becomes the IR and visible beams used for sum frequency generation (SFG). Within the amplifier is a Vitesse (Coherent) oscillator and an Evolution pump laser (Coherent). The Vitesse oscillator outputs the 800 nm seed beam at an 80 Mhz repetition rate. The seed beam is stretched temporally via a diffraction grating and then enters the amplification cavity. The Evolution pump laser outputs a ~15 W 532 nm beam, which was used to amplify the seed beam. The amplified beam exits the amplification cavity, travels through a compressor, and then exits the Libra amplifier with femtosecond pulse widths at a 1 kHz repetition rate and a power of ~3 W.

The now amplified seed beam travels into an OPERA-SOLO 2 (Light Conversion) optical parametric amplifier (OPA), where a portion of the beam immediately exits the OPA to the experimental line of the VSFSS set-up, while the remaining portion is used to generate the IR beam at the appropriate wavelengths needed to probe specific vibrational resonances. The 800 nm seed beam that is allowed to travel through the OPA is split once more, where ~5% of the beam is sent to a saphhire crystal to generate white light. This is the pre-amplification step, where the white light is spatially chirped and overlapped with the 800 nm seed beam inside a Beta barium borate (BBO) non-linear crystal. This step generates a signal and idler beam via optical parametric generation. The generated signal beam is overlapped with the remaining 800 nm seed beam that was not used in the pre-amplification step in another BBO crystal. During this step, an amplified signal and idler pair is generated with ~100x the power of the original signal and idler from the pre-amplification step. The amplified signal and idler beams recombine in a GaSe crystal to generate the IR beam via difference frequency generation. This IR beam exits the OPA and continues to the experimental line of the VSFSS set-up. By adjusting the white light timing in the pre-amplification step and optimizing the crystal angles, IR beams with wavelengths of 3–10 μm can be generated.

The experimental line of our VSFSS set-up follows the design of others in literature.[14, 15, 25, 26] The portion of the 800 nm beam that immediately exits the OPA (described above) is used as the visible beam for SFG. The visible beam travels through an etalon, half-wave plate, polarizer cube, half-wave plate configuration to allow for the control of the visible power and polarization. The visible beam then travels off a retroflector, which is used to control the beam's path length and hence, the temporal overlap of the visible and IR beams. The broadband IR beam that exits the OPA travels through two BaF_2 wire grid polarizers and is then focused to a spot size of ~80 μm with a gold parabolic mirror (focal length = 50 mm). The IR beam is focused insight the sample cuvette, while the visible beam is focused behind the sample cuvette with a spot size of ~500 μm. The sample cuvette consists of a CaF_2 front window (CeNing Optics) and a quartz back cuvette (Helma QS, path length = 200 μm) to allow for proper transmission of the incident beams and sum frequency response, respectively. The visible and IR beams are incident on the sample cuvette with an opening angle of ~20° and the scattered sum frequency response is collected at ~60° from the phase-matched direction.

The scattered sum frequency response is collimated by a plano-convex lens (focal length = 20 mm) and travels through a half-wave plate, polarizer cube configura-

tion, which allows for filtering and controlling the polarization of the sum frequency response. Finally, the collimated sum frequency response travels through another lens (focal length = 100 mm), which focuses the light into a spectrometer (IsoPlane Princeton Instruments) that spectrally disperses the signal onto a CCD (PIMAX 4 Princeton Instruments).

VSFS Laser Set-Up

The majority of this dissertation contains spectroscopic measurements using VSFSS, which is specific to nanoemulsion interfaces. Chapter VI, however, contains work that is a collaboration and includes traditional vibrational sum frequency spectroscopy (VSFS) measurements made off of a planar carbon tetrachloride (CCl_4)/water interface. For the VSFS experiments discussed in Chapter VI, a brief overview of the laser set-up is provided here, but more detailed descriptions can be found in publications[27–29] and dissertations[30–32] from the Richmond lab.

The VSFS employed a commercially available Nd:YAG laser system manufactured by Ekspla. A flash-lamp pumped Nd:YAG rod generates a 1064 nm seed beam, with ~30 ps pulse widths, at a repetition rate of 50 Hz. The seed beam is split into three different beams, two of which are frequency doubled to 532 nm. One of the two 532 nm beams is sent directly to the CCl_4/water interface. The other 532 nm beam and the remaining seed 1064 nm beam are sent to an Ekspla optical parametric oscillation/optical parametric generation/difference frequency generation (i.e., OPO/OPG/DFG) process to generate the tunable IR beam for experiments. The IR wavelength can be tuned between the range of 2-10 μm. The IR beam is directed—via a bottom-up geometry—to the sample cell containing the CCl_4 as the oil phase, and the aqueous phase containing the chemical system of interest. The sample cell for VSFS experiments was custom machined from Kel-F with a CaF_2 window for the incident beams and a BK7 glass window for the outgoing beams.

As the IR beam travels through the sample cell, it impinges with the visible beam at 68° and 76°, such that total internal reflection is achieved. A half-wave plate and a Glan-Taylor polarizer were used to control the polarization of the visible beam; while a periscope was used to control the polarization of the IR beam. Upon spatial and temporal overlap of the visible and IR beams at the sample, the generated sum frequency signal is sent through a series of filters and another half-wave plate/Glan-Taylor polarizer combination for polarization selection. Finally, the sum frequency signal is detected by a monochromator (model MS2001) and photomultiplier tube (Hamamatsu R7899), with a 3 cm^{-1} resolution.

The sum frequency response from a planar or droplet surface is generated by the spatial and temporal overlap of a visible and IR beam, where the visible beam is at a fixed wavelength and the IR beam is chosen to be resonant with the vibrational mode of interest. The intensity of the sum frequency response is proportional to the square modulus of the second-order susceptibility, $\chi^{(2)}$. The $\chi^{(2)}$ tensor contains both non-resonant and resonant contributions where

$$\chi^{(2)}_{\text{resonant}} \propto \frac{N}{\varepsilon_o} \langle \beta_\nu \rangle , \tag{24}$$

where N is the number density of molecules at the droplet surface, ε_o is the vacuum permittivity, and $\langle \beta_\nu \rangle$ is the macroscopic average of the molecular hyperpolarizability. Thus, the SF response is dependent on both the population and net conformational ordering of surface adsorbed species.

A standard fitting routine described by Bain et. al.[33, 34] was used to deconvolve the non-resonant signal and each individual resonant vibrational modes. This fitting procedure fits all experimental spectra to the following equation:

$$\chi^{(2)} = \left| \chi^{(2)}_{NR} e^{i\phi_{NR}} + \sum_\nu \int_{-\infty}^{+\infty} \frac{A_\nu e^{i\phi_\nu} \exp\left[-\frac{(\omega_L - \omega_\nu)^2}{\Gamma_\nu^2} \right]}{\omega_L - \omega_{IR} + i\Gamma_L} d\omega_L \right|^2 . \tag{25}$$

The first term describes the non-resonant susceptibility with an amplitude $\chi^{(2)}_{NR}$ and phase ϕ_{NR}. The second term describes the resonant susceptibility as a sum of all SF-active vibrational transitions, where A_ν is the peak amplitude, ϕ_ν is the phase, Γ_L is the Lorentzian linewidth describing the homogenous broadening, and Γ_ν is the Gaussian linewidth describing the inhomogenous broadening. The frequencies of the Lorentzian, IR, and resonant vibrational modes are described by ω_L, ω_{IR}, and ω_ν, respectively. The Lorentzian linewidths were chosen to reflect the vibrational lifetime of the transition of interest. All spectra shown herein were fit and analyzed with Igor Pro 6, using code developed by Moore et. al.[35]

CHAPTER III

INTERFACIAL BEHAVIOR OF pH-TUNABLE POLYETHYLENIMINE

This work was published in Volume 36 of the journal *Langmuir* in July 2020. Emma Tran designed the study, performed the experiments, analyzed the data, and wrote the manuscript. Andrew Carpenter provided initial training on the laser system and general feedback on the manuscript. Geraldine Richmond was the principal investigator for this work and provided editorial assistance and general feedback.

Introduction

In pharmaceutical applications, many active ingredients are water-insoluble, making it difficult to stabilize, protect, and increase the bioavailability of the active ingredient. Research in this area has been directed towards developing nanocarrier drug delivery systems, which utilize emulsions to encapsulate a hydrophobic drug to then be delivered to a target site within the body.[36] A layering of surfactants and polymers around the oil core is often implemented in the design of nanocarrier templates to enhance the stability and efficacy of the nanocarrier. The performance and versatility of the nanocarrier depends heavily on the tunability of the interfacial polymer–surfactant (PS) behavior that emerges from altering physiological conditions such as pH, ionic strength, and temperature.[37, 38]

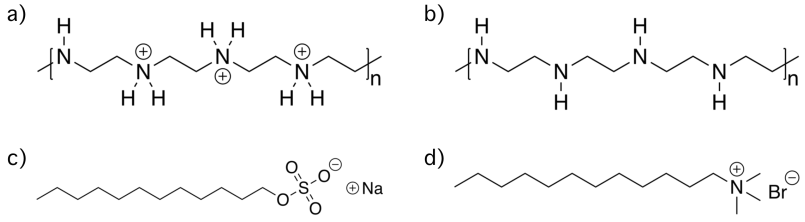

Figure 3.1. Molecular structures of (a) protonated PEI, (b) deprotonated PEI, (c) sodium dodecyl sulfate (SDS), and (d) dodecyltrimethylammonium bromide (DTAB).

In this work, polyethylenimine (PEI) is studied in conjunction with either sodium dodecyl sulfate (SDS) or dodecyltrimethylammonium bromide (DTAB) to investigate the molecular factors contributing to the stabilization of nanoemulsions that occur during PS coadsorption. Molecular structures of PEI, SDS, and DTAB are shown in

Figure 3.1. Central to this study is measuring changes to the molecular conformational arrangement of the polymer and co-surfactants upon variation of the polymer electrostatics by altering the solution pH. PEI is a biocompatible, partially cationic polymer whose charge density can be tuned by adjusting the solution pH, making it an attractive option as the polymer shell in nanocarrier templates.[10] Approximately 70%, 30%, and 5% of the amine groups in PEI are protonated at pH 2.5, 5-6, and 10, respectively.[39] While many previous studies of PEI employed interfacial techniques such as surface tensiometry,[40–44] neutron reflectivity,[40–46] and ellipsometry,[47, 48] molecular-level details regarding PEI bonding and conformational ordering are largely lacking, especially at the droplet interface. Due to the tunable cationic character of PEI, understanding its adsorption behavior and molecular conformational ordering at a surfactant-stabilized nanoemulsion surface is essential for controlling its performance as a nanocarrier layer under different environmental conditions.

To achieve this level of understanding, vibrational sum frequency scattering spectroscopy (VSFSS) has been employed herein to probe the vibrational dipoles of PS complexes at the nanoemulsion interface, yielding insight into PEI/SDS and PEI/DTAB molecular structure and behavior at the droplet surface. These spectroscopic studies are complemented with ζ-potential (ZP) and surface pressure measurements. The findings reported in this chapter provide insights into the molecular factors that contribute to the enhancement of PEI when coadsorbed with a similarly or oppositely charged surfactant, and how the interfacial molecular properties vary as the charge density on the polymer is altered by solution pH. Most notable is the strong variation with pH in the conformational ordering of the polymer at the nanoemulsion surface when coadsorbed with either surfactant. These results have significant implications for both nanoemulsion stability and functionality in the application of drug delivery as different organs and membranes within the human body exist under a wide range of pH values.

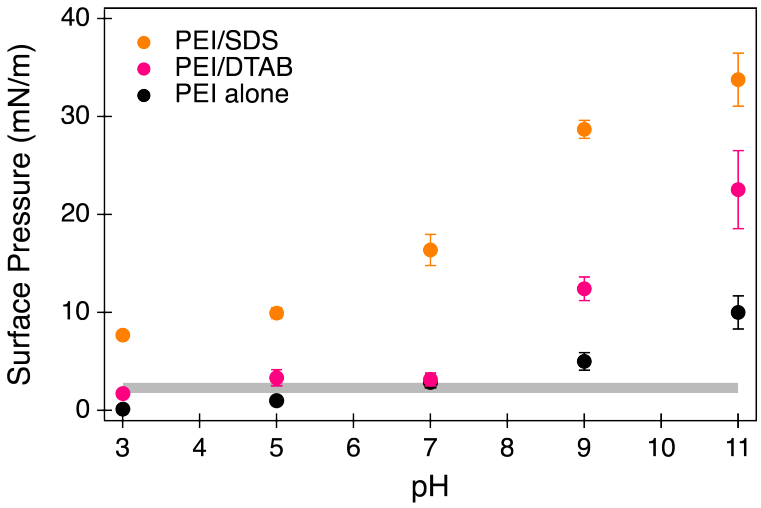

Figure 3.2. Surface pressure measurements as a function of pH of PEI alone (black ●), PEI/SDS (orange ●), and PEI/DTAB (pink ●). PEI concentration was kept constant at 0.52 mM, while surfactant concentration was fixed at 0.01 mM. For comparison, the gray horizontal bar represents the surface pressures exerted by 0.01 mM SDS and 0.01 mM DTAB individually.

The adsorptive behavior of PEI to a planar oil/water interface was determined through pendant drop tensiometry, represented by the black ● in Figure 3.2. Although surface tensiometry provides information about surface activity at a planar (rather than a droplet) oil/water interface, such studies can still be informative regarding PS adsorption to the nanoemulsion oil/water surface. At low pH, PEI alone at a concentration of 0.52 mM is not surface active. In acidic conditions, PEI is highly soluble due to the high charge density. Thus, bulk solvation of the polymer is more energetically favorable than adsorption. As the solution becomes more basic, its surface pressure increases slightly, indicative of higher surface activity. This result is consistent with previous studies from this laboratory showing pH-tunable polymers desorb from a planar oil/water interface when the polymer is ~20% charged.[28, 49, 50] PEI becomes more hydrophobic as pH increases into the basic regime, allowing for polymer adsorption in part due to hydrophobic interactions between the polymer backbone and oil phase, and because bulk solvation is less energetically favorable as PEI becomes less charged. Additionally, weakly charged PEI has been shown to form multilayers due to strong hydrophobic interactions coupled with ion-dipole interactions between the SDS sulfate ion and NH dipole.[40] The enhanced surface pressure

observed may also be indicative of more PEI adsorption, potentially forming thicker layers. It is noted later, regardless of the slight enhancement in PEI surface activity as pH increases at the planar oil/water interface, we find that PEI alone does not form and stabilize nanoemulsions at any pH. Emulsion samples created with 15 mM PEI alone were on the order of microns and destabilized within ~10 min by visual observation.

Effect of Charged Surfactants on PEI Adsorption

PEI adsorption in the presence of SDS. Although PEI alone showed minimal adsorption to the planar oil/water interface, its surface activity can be enhanced with the addition of surfactants. The orange ● in Figure 3.2 depict the surface activity of PEI/SDS in solutions of different pH, with PEI and SDS concentrations fixed at 0.52 mM and 0.01 mM, respectively. For comparison, the horizontal gray bar in Figure 3.2 represents the pH-independent surface activity of 0.01 mM SDS at a planar oil/water interface under various pH conditions. PEI/SDS is surface active across the entire pH range studied. The enhanced adsorption for this system increases with pH, indicating that PEI/SDS surface activity is strongest when PEI becomes increasingly neutral as pH becomes more basic.

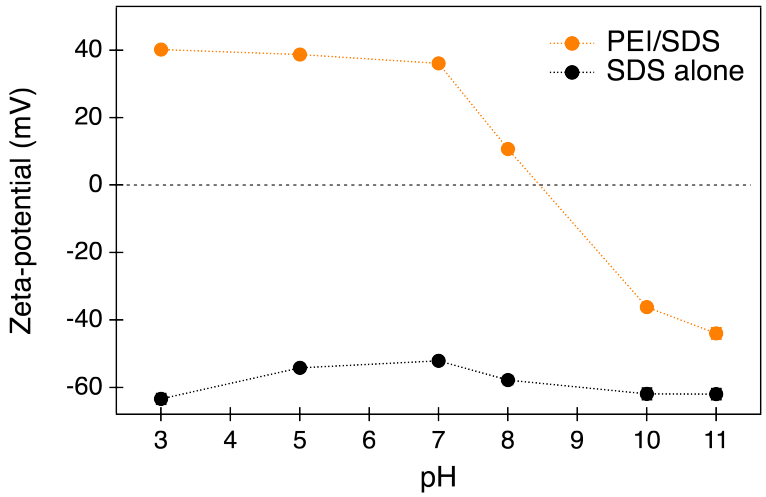

Figure 3.3. ζ-potential measurements as a function of pH for nanoemulsions stabilized by SDS (black ●) and PEI/d-SDS (orange ●). The polymer and surfactant concentrations are 5.2 mM and 0.1 mM, respectively. Uncertainty bars are present, but comparable to the size of the markers.

The addition of SDS to PEI also enhances nanoemulsion formation throughout the pH regime of 311. As noted above, PEI alone does not form stable nanoemulsions

at any pH. ZP measurements of these SDS/PEI-stabilized nanoemulsions are shown in Figure 3.3 (orange ●) along with ZP measurements of nanoemulsions stabilized with SDS alone (black ●). For nanoemulsions stabilized by SDS only, the ZP remains highly negative and largely invariant to changes in pH.

The ZP values of PEI/SDS-stabilized nanoemulsions start highly positive at pH 3 and become progressively less positive as pH increases. At low pH, PEI behaves as a cationic polymer, making the surface of PEI/SDS-stabilized nanoemulsions highly positive. Between pH 3 and 7 (Figure 3.3), ZP measurements for these samples are constant, despite PEI going from ~70% charged (pH 3) to ~30% charged (pH 7). Previous sum frequency studies at the planar solid/aqueous interface by Windsor et al. and neutron reflectivity studies at the emulsion surface by Penfold et al. suggest PEI encourages SDS adsorption.[44, 51] Enhanced SDS adsorption due to the presence of PEI would result in increasingly negative ZP values between pH 3 and 7, which we do not observe. There are two possibilities that may explain the constant ZP from acidic to neutral pH. With the concentrations used, the number of SDS molecules (and hence, negative charge) in solution is ~2 orders of magnitude less than the number of positively charged monomer units of PEI at pH 3 and ~1 order of magnitude less at pH 7. Thus, it is feasible that if additional SDS molecules adsorb to the droplet surface, PEI counters the influence SDS has on the ZP because the amount of positively charged monomer units is so much greater than the amount of negatively charged SDS. It is also likely that cooperative interactions between PEI and SDS enhance the adsorption of both species such that the net change in magnitude of ZP is nominal. While it is unclear from ZP results alone whether PEI assists the adsorption of SDS, our VSFSS results discussed below revisit this hypothesis in more detail.

Beyond pH 7, ZP values of PEI/SDS become increasingly negative, indicative of deprotonated PEI contributing less positive charge to the interface. At pH $\geqslant$ 10, PEI is considered to behave essentially as a neutral polymer.[39, 52] The highly negative ZP originates from the negatively charged headgroup of coadsorbed SDS. However, even in highly basic conditions, nanoemulsions stabilized by PEI and SDS exhibit ZP values less negative than those of nanoemulsions stabilized by SDS alone. In addition to the strong surface activity of PEI/SDS complexes in the basic regime, these results confirm PEI is still interfacially present, even when it is only marginally positive.

As change in pH alters PEI charge density, knowledge of how the surfactant and polymer surface structure are affected will aid in the informed design of nanocarrier architecture. While both SDS and PEI are present at the interface stabilizing the

nanoemulsions, the molecular structure of these two species at the droplet interface is still unknown. Past studies have reported PEI/SDS layer formation and thickness at various interfaces,[40–46] but these studies do not provide molecular-level details about PS conformational ordering around a nanoemulsion surface. Thus, in later sections, we turn to VSFSS to determine the orientation of net dipoles of the SDS alkyl tail and polymer backbone relative to the oil/water droplet surface, and how that orientation changes under different pH conditions. We now investigate how changing the surfactant headgroup from a negative to a postiive charge influences PEI adsorptive behavior.

PEI adsorption in the presence of DTAB. Studies of PEI in conjunction with DTAB provide an opportunity for further investigation of surface complexation between a positively charged surfactant and a charge-tunable polymer. PEI/DTAB solutions at a planar oil/water interface (Figure 3.2) are surface active at pH $\geqslant$ 9, albeit less surface active than the PEI/SDS system.

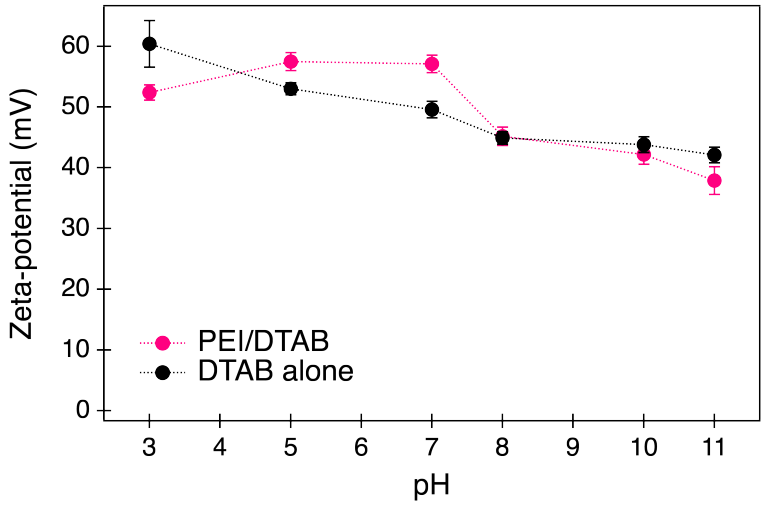

Figure 3.4. ζ-potential measurements as a function of pH for nanoemulsions stabilized by DTAB (black ●) and PEI/d-DTAB (pink ●). The polymer and surfactant concentrations were fixed at 5.2 mM and 0.1 mM, respectively.

To confirm the presence of PEI at the droplet surface, mixtures of 5.2 mM PEI and 0.1 mM DTAB were used to form stable nanoemulsions. ZP measurements made on these PEI/DTAB-stabilized nanoemulsions at varying pH are shown in Figure 3.4. Though both species are cationic, changes in the magnitude of the ZP values aid in the deduction of whether PEI is present at the surface. As can be seen in Figure 3.4,

there is minimal deviation between the ZP values of DTAB-stabilized nanoemulsions (black ●) and PEI/DTAB-stabilized nanoemulsions (pink ●) at all pH values.

In acidic conditions, the nominal deviation in ZP values between the DTAB and PEI/DTAB system, along with the significantly low surface activity discussed above (Figure 3.2), suggests that a PS complex is not present at the nanoemulsion surface. In basic conditions, while the surface activity of the PEI/DTAB system increases at the planar oil/water interface (Figure 3.2), the changes in ZP values of nanoemulsions stabilized by DTAB alone versus PEI/DTAB are not substantial enough to be conclusive. Therefore, to investigate this system in more detail, we turn to VSFSS to corroborate our ZP results as well as determine the structural ordering of the PEI/DTAB complexes.

Effect of Charged Surfactants on PEI Surface Structure

PEI surface structure in the presence of SDS. Surface spectroscopic measurements of nanoemulsions confirm not only the presence of interfacial species but also their molecular structure relative to the interface and thus, provide insight into their interfacial bonding behavior. Recall that all nanoemulsions were prepared with deuterated hexadecane as the dispersed phase and D_2O as the continuous phase. Thus, in all spectra hereafter, there are no CH contributions from hexadecane, and IR absorption by the continuous phase has been minimized.

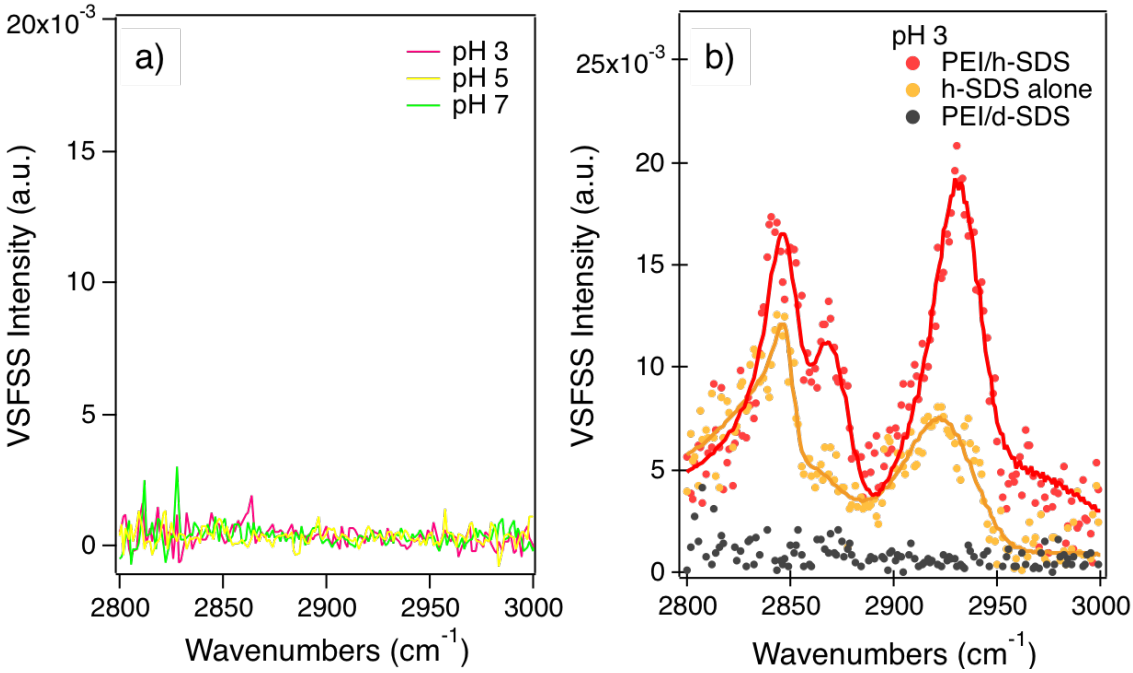

Figure 3.5. (a) VSFSS measurements of the CH stretching region of PEI/d-SDS nanoemulsions at pH 3 (pink), 5 (yellow), and 7 (green). PEI and d-SDS concentrations were fixed at 5.2 mM and 0.1 mM, respectively. (b) VSFSS spectra of the CH stretching region of nanoemulsions stabilized by PEI/d-SDS (gray), h-SDS alone (orange), and PEI/h-SDS (red). Here, PEI concentration remained the same at 5.2 mM, while the surfactant concentration was increased to 1 mM. All spectra were collected in SSP and where appropriate, lines are fits to data following the Richmond fitting routine.

As shown in Figure 3.5, VSFSS measurements in the CH stretching region of nanoemulsions stabilized by 5.2 mM PEI and 0.1 mM deuterated SDS (d-SDS) at pH 3, 5, and 7 all result in a lack of signal from the CH stretching vibrational modes of PEI. Since ZP results show PEI is adsorbed to the nanoemulsion surface under these pH conditions and surface pressure measurements confirm PEI adsorption at the planar interface, the lack of SF signal under acidic conditions is attributed to a lack of net dipole orientation of the polymer CH modes relative to the interface. Such scenario is indicative of a disordered polymer molecular structure around the droplet surface (e.g., tangled polymer strands). Highly charged PEI is reported to adopt an extended conformation due to a high degree of intrachain chargecharge repulsion.[53] While this would allow PEI to adsorb flatly to a planar surface, especially one with a tightly packed surfactant monolayer, PEI adsorption to the nanoemulsion surface geometry likely adopts more gauche defects, especially when the surfactants are isotropically distributed in a diffuse monolayer, making the polymer chains more disordered.

To monitor the structural ordering of the surface adsorbed surfactant in the presence of interfacial PEI, SDS concentration was increased from 0.1 mM to 1 mM to surpass the limit of detection of SDS with our laser system. VSFSS spectra in the CH stretching region collected for nanoemulsions stabilized by PEI/d-SDS, PEI/h-SDS, and h-SDS alone are shown in Figure 3.5b. Because the CH modes of PEI are SF inactive at pH 3 and contribute no signal, as can be seen by the featureless gray trace in Figure 3.5b, any spectroscopic signal from the CH stretching region is attributed to the SDS alkyl tails. VSFSS measurements probing the SDS tails in the absence (orange trace) and presence (red trace) of PEI show that with the addition of PEI, the SF signal from the SDS CH vibrational modes increases. These vibrational modes have been attributed to the CH_2 symmetric stretch (d^+) at ~2850 cm^{-1}, CH_3 symmetric stretch (r^+) at ~2873 cm^{-1}, and a broad peak corresponding to a mixture of modes that include the CH_3 asymmetric stretch and a Fermi resonance arising from a CH_3 bend overtone with a CH_3 stretch at ~2935 cm^{-1}.[54, 55] Fits to all SF spectra herein follow the Richmond laboratory fitting routine, which was discussed above in

Chapter 2.[34] The fitting parameters along with the uncertainties corresponding to the fits in Figure 3.5 can be found in Table A.2 in the Appendix.

The enhanced intensities from each vibrational mode observed in samples stabilized by PEI/h-SDS compared to samples stabilized by only h-SDS indicate that more SDS has adsorbed to the droplet surface with PEI present. Furthermore, analysis of the intensity ratios between the CH2 symmetric stretch and CH_3 symmetric stretch (i.e., the d^+/r^+ ratio) yields a lower d^+/r^+ ratio for samples stabilized by both PEI/h-SDS relative to h-SDS alone, which corresponds to a higher degree of conformational ordering in the SDS alkyl tails and less gauche defects.[54, 56] We note that despite the change in surfactant concentration, and thus the polymer/surfactant concentration ratio, the PEI/SDS system with 1 mM d-SDS behaves the same as with 0.1 mM d-SDS (i.e., both polymer/surfactant concentration ratios result in a completely disordered PEI surface structure). While it has been shown that PS complexation and interfacial aggregation behavior depend greatly on polymer/surfactant concentration ratios,[57] it is evident that in this work, whether the polymer/surfactant concentration ratio is ~50:1 or ~5:1, the disorder in PEI interfacial structure is comparable between the two. Together, these results illustrate that at the droplet oil/water interface, PEI is present and encourages more SDS to adsorb, leading to more conformational ordering of the surfactant tails. Our conclusions at the nanoemulsion surface are consistent with the previous studies mentioned above, confirming that PEI promotes the adsorption of SDS.[44, 51] Moreover, these results show that coadsorption also promotes SDS chain ordering.

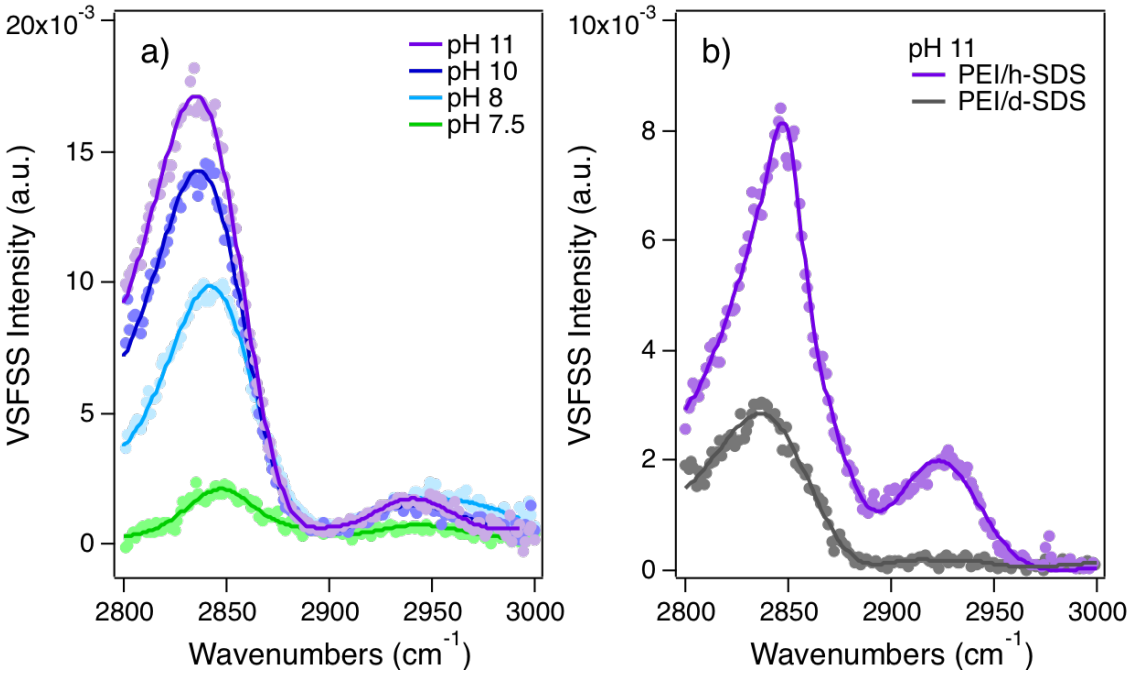

Figure 3.6. (a) VSFSS measurements of the CH stretching region of PEI/d-SDS stabilized nanoemulsions at pH 7.5 (green), 8 (cyan), 10 (blue), and 11 (purple). PEI and d-SDS concentrations were fixed at 5.2 mM and 0.1 mM, respectively. (b) VSFSS spectra of the CH stretching region of nanoemulsions stabilized by PEI/h-SDS (purple) and PEI/d-SDS (gray) at pH 11. Here, PEI concentration remained the same at 5.2 mM, while the surfactant concentration was increased to 1 mM. Spectra were taken under the SSP polarization scheme and lines are fits to data.

As pH increases, the charge density on PEI decreases, making it increasingly neutral. To investigate the effects that deprotonation has on PEI surface behavior, VSFSS spectra of the CH stretching region of nanoemulsions stabilized by 5.2 mM PEI and 0.1 mM d-SDS at pH 7.5, 8, 10, and 11 were measured (Figure 3.6a). The observed broad peak at 2851 cm^{-1} corresponds to the CH_2 symmetric stretch of PEI for all traces. This SF intensity grows with increasing pH, consistent with its surface activity at the planar oil/water interface (Figure 3.2). Note from Figure 3.5a, that this mode was not observed for PEI/SDS nanoemulsions prepared in acidic pH. Minor contributions near 2870 cm^{-1} from the CH_3 symmetric stretch and 2935 cm^{-1} from the CH_3 asymmetric stretch of the polymer end-caps are also acknowledged (see Table A.3 and A.4 for fitting parameters). The spectral presence of the terminal CH_3 indicate that they too have a preferential surface orientation with their CH modes having a perpendicular component relative to the nanoemulsion surface. These spectroscopic studies provide strong evidence not only that PEI is interfacially present but that the

polymer backbone and terminal methyl groups adopt an ordered and net orientation to the droplet surface.[14, 15, 19, 58] The VSFSS results herein reveal the unique conformational reorientation PEI undergoes between pH 7 to 7.5 from being largely disordered in the acidic regime to progressively more ordered in the basic regime.

To determine the influence that nonionic PEI has on SDS structural ordering, VSFSS measurements of the SDS alkyl tails were obtained for 1 mM SDS in the presence of 5.2 mM PEI at pH 11 (Figure 3.6b). Recall that the surfactant concentration was increased in order for it to be spectroscopically detectable with our laser system. The gray and purple traces in Figure 3.6b are the VSFSS spectra of nanoemulsions stabilized by PEI/d-SDS and PEI/h-SDS, respectively. Similar to the discussion above surrounding polymer/surfactant concentration ratios, PEI orders itself similarly with 0.1 mM d-SDS as it does with 1 mM d-SDS. With a comparison of the spectrum of PEI with those of 0.1 mM d-SDS at pH 11 (Figure 3.6a, purple trace) and 1 mM d-SDS at pH 11 (Figure 3.6b, gray trace), it is clear that the similar traces are both indicative of ordered interfacial PEI, regardless of d-SDS concentration. While the spectrum of PEI/d-SDS contains polymer contributions, specifically from the CH_2 symmetric stretch mode near 2851 cm^{-1} (gray trace), the spectrum of PEI/h-SDS contains contributions from both the polymer and surfactant CH_2 and CH_3 modes (purple trace). Because it is not possible to decouple CH modes between PEI and h-SDS, a quantitative d^+/r^+ analysis is not applicable here. Nevertheless, the overall enhanced signal intensity and additional CH3 spectral features near ~2935 cm^{-1} observed for nanoemulsions stabilized by PEI/h-SDS are indicative of conformationally ordered interfacial SDS molecules. Therefore, in basic conditions at the nanoemulsion surface, PEI and SDS form ordered complexes.

PEI surface structure in the presence of DTAB. We now investigate the effects of surfactant charge on PEI interfacial ordering by switching anionic SDS to cationic DTAB. Spectroscopic measurements taken in the SSP polarization scheme of nanoemulsions stabilized by PEI/d-DTAB, PEI/h-DTAB, and h-DTAB only are shown in Figure 3.7. These experiments were performed at pH 3 with 5.2 mM PEI and 1 mM DTAB. Though the polymer/surfactant concentration ratio has changed here, we are confident that PEI interfacial conformational structure is similar even with higher DTAB concentrations, as it resulted in a lack of signal, very much like it did with 0.1 mM d-DTAB (not shown).

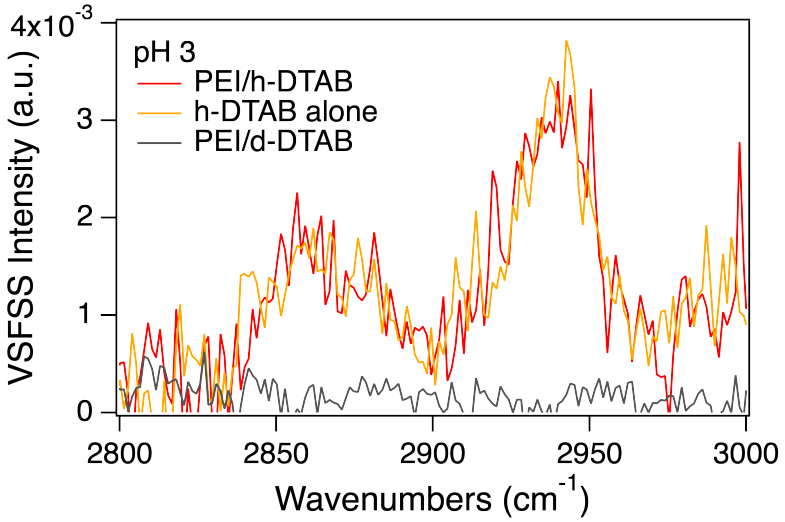

Figure 3.7. VSFSS spectra of the CH stretching region of nanoemulsions stabilized with 5.2 mM PEI and 1 mM h-DTAB (red) and 1 mM h-DTAB alone (orange). All spectra were collected in SSP and all samples were prepared at pH 3.

We note that although there are differences in signal-to-noise between PEI/SDS and PEI/DTAB, the VSFSS results obtained for the PEI/DTAB system are similar to the results obtained for the PEI/SDS studies above, in that, no CH stretching vibrational modes of PEI were detected (gray trace). However, unlike the PEI/SDS system, VSFSS measurements of DTAB in the absence (orange trace) and presence (red trace) of PEI resulted in nearly identical spectra. The orange and red spectra in Figure 3.7 are characteristic of the DTAB alkyl tails stretching modes, consisting of the CH_2 symmetric stretch, CH_3 symmetric stretch, and a combination of the CH_3 asymmetric stretch with a Fermi resonance.[59, 60] This result combined with the ZP measurements indicates that at pH 3, PEI and DTAB do not appear to form a surface complex at the nanoemulsion surface. PEI likely remains solvated in the bulk aqueous phase under these conditions, leaving the nanoemulsion surface polymer-free.

In basic conditions, PEI is no longer in its highly charged form. With less cationic character on the polymer, there is less chargecharge repulsion between DTAB and PEI, allowing for PEI to adsorb more readily to DTAB-stabilized nanoemulsions. The surface pressure measurements (Figure 3.2) show PEI/DTAB mixtures exhibit higher surface activity in basic conditions than acidic conditions. This enhanced surface activity is also evident in the spectroscopic measurements of the nanoemulsions.

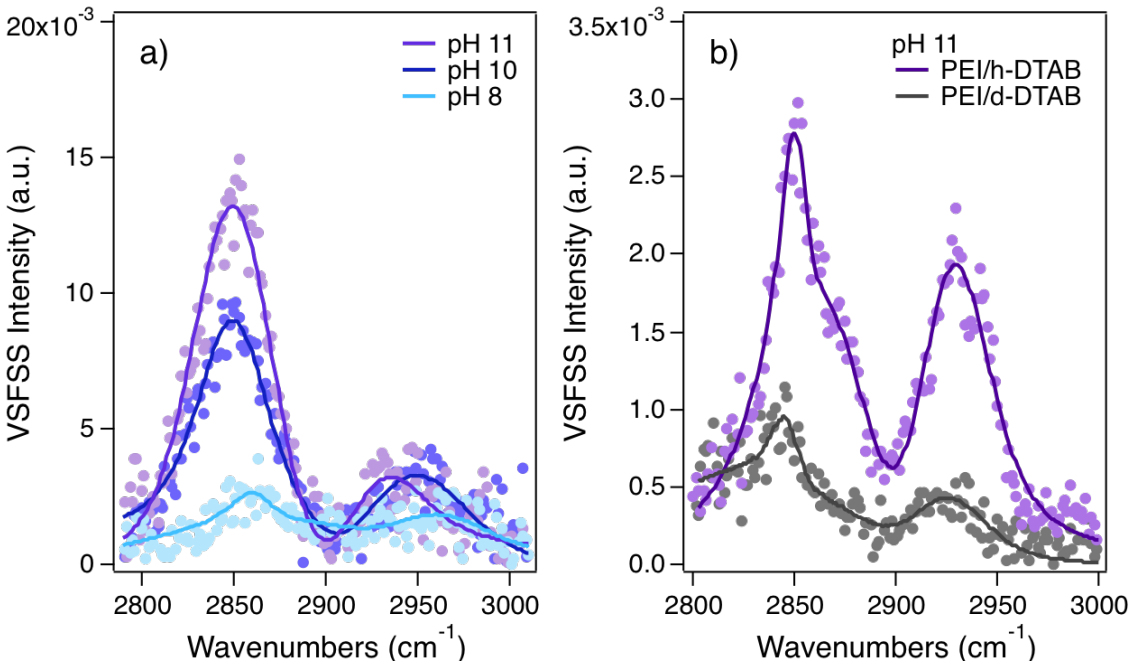

Figure 3.8. (a) VSFSS spectra of the CH stretching region of nanoemulsions stabilized by 5.2 mM PEI and 0.1 mM d-DTAB at pH 8 (cyan), 10 (blue), and 11 (purple). (b) VSFSS measurements of the CH stretching region of nanoemulsions stabilized by PEI/h-DTAB (purple) and PEI/d-DTAB (gray) at pH 11. PEI concentration was fixed at 5.2 mM, while surfactant concentration was increased to 1 mM. Spectra were collected in SSP and solid lines are fits to data.

VSFSS spectra of the CH stretching region of nanoemulsions stabilized by PEI and d-DTAB at pH 8, 10, and 11 are shown in Figure 3.8. Similar to the results obtained from the PEI/d-SDS nanoemulsions above (Figure 3.6), SF intensity increases with increasing pH (Figure 3.8a), showing conclusively that PEI, in the presence of DTAB, is adsorbed to the nanoemulsion surface under basic conditions. Moreover, the strong CH response from the CH_2 backbone modes indicates a net dipole orientation along the polymer chains, which increases with pH. The most pronounced peak corresponds to the CH_2 symmetric stretch at 2851 cm^{-1} with additional contributions arising from the CH_3 modes from the polymer end-caps. It is noted that for nanoemulsions stabilized with PEI/d-SDS in basic conditions (Figure 3.6a), there is elevated SF intensity at lower frequencies of the CH stretching region and an apparent frequency shift in the PEI CH_2 symmetric stretch. This is not observed for samples stabilized with PEI/d-DTAB (Figure 3.8a). This observation of seemingly higher background SF signal around 2800 cm^{-1} for SDS versus DTAB has also been acknowledged by other groups and corresponds to OD modes of D_2O that are enhanced by the presence

of SDS and constructively interfere with the CH_2 modes.[61–65] These OD modes are also present in chemical systems involving DTAB, but the cationic charge likely results in a destructive interference with the CH_2 modes and hence, lower intensity.[61]

With a comparison of the spectra of nanoemulsions stabilized by PEI/d-DTAB (gray) to PEI/h-DTAB (purple) at pH 11 (Figure 3.8b), information regarding DTAB tail ordering can be inferred, despite contributions from the polymer CH modes. In these experiments, the polymer and surfactant concentrations were fixed at 5.2 mM and 1 mM, respectively. Again, we note that despite the change to the polymer/surfactant concentration ratio, the spectrum of PEI with 0.1 mM d-DTAB (Figure 3.8a, purple trace) versus 1 mM d-DTAB (Figure 3.8b, gray trace) are very comparable, indicating that coadsorbed PEI/DTAB complexes structure themselves similarly whether the surfactant concentration is 0.1 mM or 1 mM. In the presence of h-DTAB, the SF intensity is increased due to the additional CH_2, CH_3, and Fermi resonances from the surfactant alkyl tails that are no longer deuterated. For fitting paramters corresponding to Figure 3.8, see Table A.5 and A.6 in the Appendix. Together, these results demonstrate that in basic conditions, in conjunction with ordered PEI, DTAB also possesses a net ordering at the nanoemulsion surface.

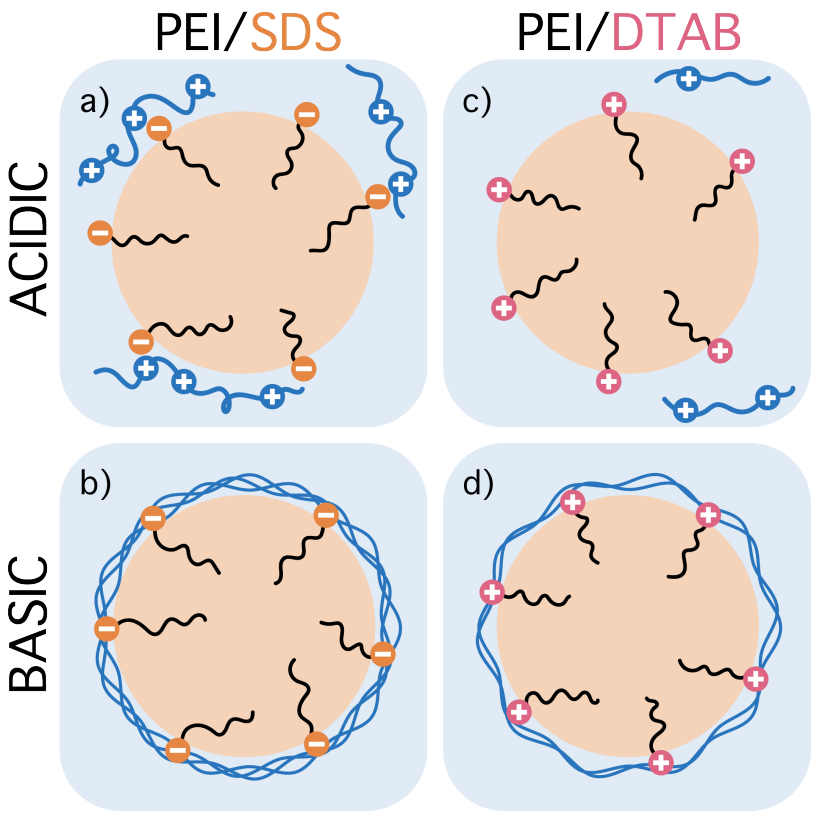

Figure 3.9. A pictorial representation of PEI/SDS in (a) acidic and (b) basic conditions and PEI/DTAB in (c) acidic and (d) basic conditions. Molecules and nanoemulsions are not illustrated to scale.

This study examines how PEI adsorption and structural ordering at a nanoemulsion surface can be tuned with surfactant charge and solution pH. Illustrated by Figure 3.9a, in the presence of anionic SDS at low pH, PEI is disordered and polymer adsorption to the droplet surface is predominantly influenced by attractive electrostatic interactions between the positively charged amine groups on PEI and the negatively charged sulfate group on SDS. When PEI is highly charged, adsorption is limited due to competitive bulk solvation of the polymer. At high pH when PEI is less charged, bulk solvation is no longer energetically favorable and thus, the degree of PEI adsorption in basic conditions is stronger than in acidic conditions. Hydrophobic interactions between PEI, SDS, and the oil phase encourage PEI adsorption to the droplet surface. In conjunction with hydrophobic interactions, attractive chargecharge and ion-dipole interactions between the sulfate anion and the polymer NH dipole assist in PEI adopting a net ordering at the interface, depicted by Figure 3.9b, similar to

what previous studies have concluded with tensiometry[40–44, 66, 67] and neutron reflectivity[40–46, 66, 67] experiments at the air/water and oil/water interfaces.

For the PEI/DTAB system in acidic conditions, the lack of attractive electrostatic interactions between the polymer and surfactant leaves PEI fully solvated in the bulk and DTAB as the only interfacially active component stabilizing the nanoemulsion, as seen in Figure 3.9c. In basic conditions, PEI/DTAB exhibit similar adsorption behavior and polymer structuring as PEI/SDS. For the PEI/DTAB system at pH>8, hydrophobic interactions between PEI, DTAB alkyl tails, and the oil phase accompanied by attractive ion-dipole interactions between the DTAB cation and NH dipole govern polymer adsorption and ordering. These combined intermolecular interactions drive PEI adsorption and impart a net ordering to the polymer chains. However, illustrated by Figure 3.9d, the lack of attractive chargecharge interactions between PEI and DTAB limits the overall surface activity of PEI/DTAB when compared to PEI/SDS, where repulsive forces do not exist.

Being partially cationic, the surface behavior of PEI is dependent on its charge density. Due to the pH-dependent behavior PEI exhibits, the amount of adsorption and degree of ordering can be tuned to create nanoemulsions with contrasting interfacial structures, demonstrating the versatility of PEI for industrial and commercial applications. The direct comparison between PEI/SDS versus PEI/DTAB confirms that chargecharge interactions, ion-dipole interactions, and hydrophobic interactions are all contributing to the strong adsorption and ordering of PEI in basic conditions, which corroborates assumptions in literature regarding the strong interactions between PEI and SDS at high pH.[40–42, 44, 46, 51, 68] Moreover, the results in this work demonstrate PEI structural ordering at a droplet surface and its sensitivity to pH perturbations. Using VSFSS, molecular-level detail about the polymer at a buried oil/water interface has been revealed, which is information that has not accessible until now.

These findings provide valuable insight into the tunable nature of PEI and how it behaves at the nanoemulsion surface, which has direct implications for the informed design of nanocarrier templates containing PEI as the polymer layer. Within half a pH unit, PEI reorients itself from being completely disordered to adopting a net ordering that persists with increasing pH. This suggests that the net structural ordering of PEI is insensitive to pH values within the acidic regime but responds to changes in pH values within the basic regime. Future work investigating the mechanism that drives this reorientation would be necessary to take full advantage of PEI surface behavior for both fundamental knowledge and layer-by-layer applications. These results provide

molecular-level details about a PS system at a nanoemulsion surface, which aids in the optimization of nanocarrier technology and sets the foundation for future work investigating polymerpolymer ordering at a curved interface.

CHAPTER IV

POLYELECTROLYTE LAYERING ON DROPLET SURFACES

This work was published in Volume 599 of the *Journal of Colloid and Interface Science* in April 2021. Emma Tran designed the study, performed some of the experiments, analyzed the data, and wrote the manuscript. Ashley Mapile performed some of the experiments and provided general feedback on the manuscript. Geraldine Richmond was the principal investigator for this work and provided editorial assistance and general feedback.

Introduction

In the previous chapter, we studied nanoemulsions coated by a single polymer layer at a molecular-level. In this chapter, we add a secondary polymer layer and investigate the complexities of such a system from both a macroscopic and molecular perspective.

Since the early 1990s, layer-by-layer (LbL) deposition has become a popular technique employed to prepare multiple layer thin films of oppositely charged polyelectrolytes through electrostatic-driven adsorption.[69, 70] Today, this technique is still widely prevalent in applications involving the design of devices,[71] coatings,[70, 72, 73] sensors,[74, 75] quantum dots,[76] and drug delivery systems.[9, 11, 77, 78] While most research conducted on LbL assembly has been primarily done to understand thin film formation on a flat solid substrate, knowledge regarding LbL assembly at curved surfaces or liquid/liquid interfaces is much more limited. As more drug delivery applications are incorporating LbL deposition and emulsions into their design, having knowledge about multi-polymer layering behavior at the curved surface is essential for intuiting structure-function relationships. Structural characterization of thin films prepared via LbL deposition has been done using various reflectivity[79–82] and microscopy techniques,[74, 82, 83] which provides information such as layer thickness and composition. Additionally, surface-specific techniques such as reflection-absorption infrared spectroscopy[84] and sum frequency generation[84, 85] has been utilized to determine the conformational ordering of polyelectrolyte layers on planar surfaces. Yet, the molecular-level structural ordering of polymer layers coating a curved surface has yet to be investigated.

In this work, we show on a molecular level the role that charged surfactant dodecyltrimethylammonium bromide (DTAB) (Figure 4.1a) plays in the stabilization

of nanoemulsions with either a single- or two-polymer system. The polymers used in this study are poly(styrene sulfonate) (PSS) (Figure 4.1b) and polyethylenimine (PEI) (Figure 4.1c). While PSS is an anionic polymer, PEI is a cationic polymer in acidic environments and a nonionic polymer in basic environments (Figure 4.1c).[39, 52] Thus, this polymer combination provides a unique opportunity to control the interfacial electrostatics of the system through the addition of a secondary polymer and solution pH. Ultimately, the effects of PEI as a secondary polymer on both PSS conformational ordering and overall nanoemulsion stability have been carefully described in this work.

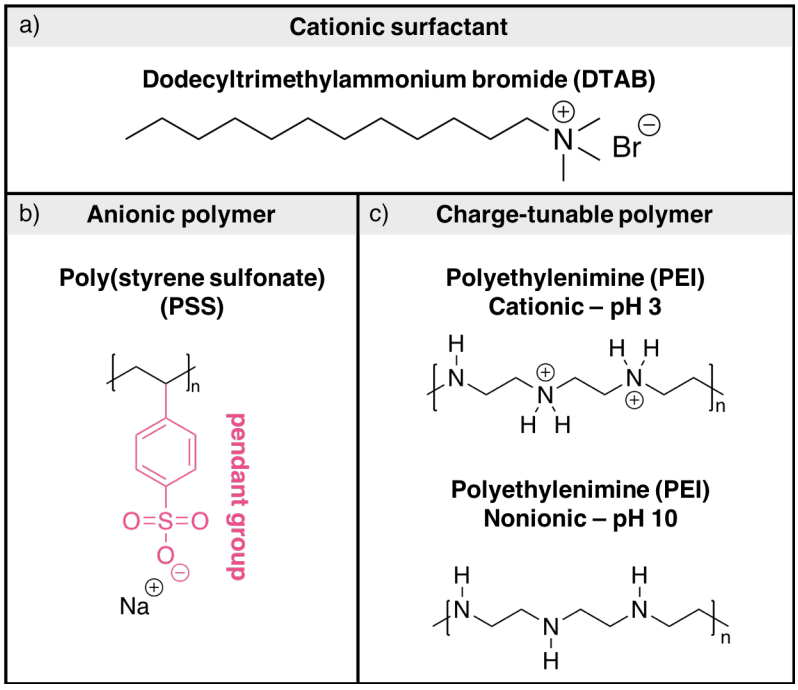

Figure 4.1. Molecular structures of (a) surfactant DTAB, (b) anionic polymer PSS, and (c) partially cationic polymer PEI.

We characterize nanoemulsion quality and stability by monitoring the sample size distribution, Z-average diameter, polydispersity index (PDI), and ζ-potential (ZP) over 30 days with dynamic light scattering (DLS), as these metrics are important for industrial and commercial applications. To complement our macroscopic characterization, we also employ vibrational sum frequency scattering spectroscopy (VSFSS) to unveil molecular-level structural details at the nanoemulsion surface. Specifically, we are able to determine the interfacial assembly and conformational ordering of the anionic PSS layer, with and without the secondary polymer PEI, allowing us to understand the contributions from added electrostatics and steric effects. Together, our

DLS and VSFSS results provide a fundamental understanding of how LbL processes at curved oil/water interfaces affect both macroscopic and molecular-level surface properties of nanoemulsions. Moreover, the molecular-level insights gained in this work are important for the rational design of applications involving foods,[86, 87] cosmetics,[88, 89] and drug delivery systems,[9, 11, 77, 78] as these applications often employ emulsions coated by alternating layers of oppositely charged polyelectrolytes.

DTAB/PSS complexes on nanoemulsion stabiity

Since the formation of nanoemulsions is a nonspontaneous event, understanding and controlling nanoemulsion stability (i.e. sample size distributions, polydispersity, ζ-potential) is important for many applications involving a shelf life such as creams and cosmetics, or time-sensitive functions such as targeted drug delivery. The time-dependent stability of nanoemulsions stabilized by d-DTAB/PSS at the natural solution pH of 7 is summarized in Figure 4.2. The top panel (Figure 4.2a–c) shows size distributions of nanoemulsion samples stabilized by a fixed PSS concentration of 5 mM with 0, 0.1, and 1 mM d-DTAB, respectively. The bottom panel (Figure 4.2d–f) shows the diameters, PDIs, and ZP, respectively, for 5 mM PSS in conjunction with 0, 0.1, and 1 mM d-DTAB.

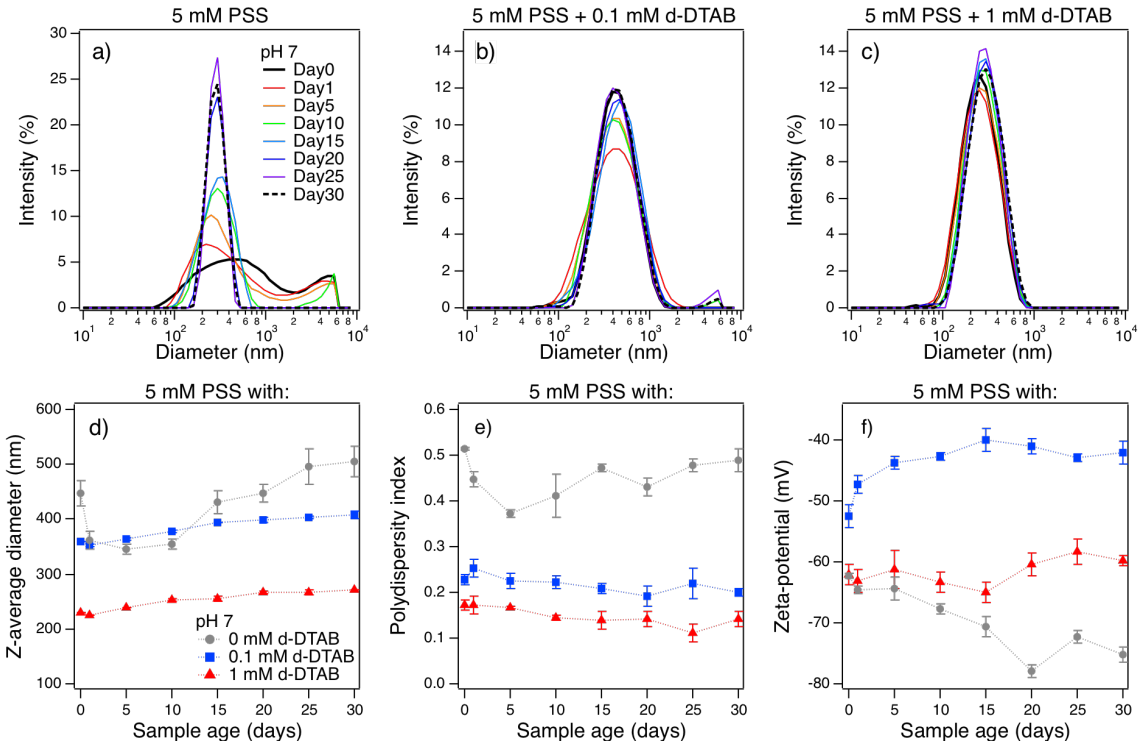

Figure 4.2. Top panel: Size distribution measurements of nanoemulsions stabilized by (a) 0 mM DTAB, (b) 0.1 mM DTAB, and (c) 1 mM DTAB, all in conjunction with 5 mM PSS. Bottom panel: (d) Nanoemulsion Z-average diameter, (e) PDI, and (f) ZP for samples stabilized by 5 mM PSS with 0 mM DTAB (gray ●), 0.1 mM DTAB (blue ■), and 1 mM DTAB (red ▲).

Fresh samples (Day 0) of nanoemulsions created with 5 mM PSS alone (i.e., no added surfactants) had a broad size distribution with two distinct populations (Figure 4.2a, solid black). A broad size distribution has been reported to be due to a variety of structures in solution.[90, 91] The broadness we observe is indicative of a combination of nanoemulsions, micron-sized emulsions, and bulk PSS aggregates in solution. Over time, depletion of larger sized emulsions is observed accompanied by an increase in smaller sizes until eventually, the distribution becomes uni-modal (Figure 4.2a). We attribute the depletion of larger size populations to the destabilization of micron-sized emulsions. Over time, the sample becomes less opaque, a visual indicator of phase separation and emulsion destabilization (Figure 4.3, left panel).[87, 92–94]

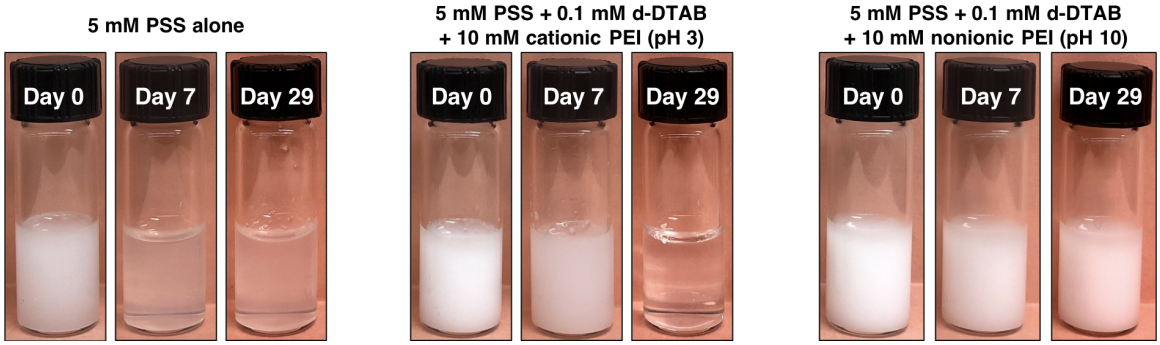

Figure 4.3. Photograph images of nanoemulsion samples stabilized by 5 mM PSS alone (left), 0.1 mM d-DTAB, 5 mM PSS, and 10 mM cationic PEI (pH 3) (center), 0.1 mM d-DTAB, 5 mM PSS, and 10 mM nonionic PEI (pH 10) (right) taken on Days 0, 7, and 29 of the 30-day period.

With no surfactant present, diameters of nanoemulsions stabilized with only PSS fluctuate between ~350–500 nm (Figure 4.2d, gray ●) with PDI values (Figure 4.2e, gray ●) indicating non-uniformity in the sample. A nanoemulsion sample is considered to be monodispersed and suitable for application when the PDI < 0.3,[2, 77, 95] which is not the case for these samples. The measured ZP starts highly negative and becomes progressively more negative as the sample ages (Figure 4.2f, gray ●). From the size distribution plots, the reduction in larger size population frees PSS from stabilizing larger emulsions. Thus, with free PSS in solution, the formation of bulk PSS

complexes can contribute to both the more negative ZP values and the increase in size populations with time, as observed from the distribution plots.

Nanoemulsions created with PSS in conjunction with 0.1 mM d-DTAB and 1 mM d-DTAB resulted in uni-modal size distributions that remained as such for 30 days, which can be seen in Figure 4.2b and 4.2c, respectively. Additionally, nanoemulsion diameters decrease with fewer fluctuations. Smaller nanoemulsions are obtained with 1 mM d-DTAB (Figure 4.2d, red ▲) as compared to 0.1 mM DTAB (Figure 4.2d, blue ■); and while both samples show steady growth over time, they remain monodispersed based on their steady PDI values < 0.3 (Figure 4.2e, blue ■ and red ▲). ZP measurements are summarized in Figure 4.2f, showing that with the addition of 0.1 mM (Figure 4.2f, blue ■) and 1 mM d-DTAB (Figure 4.2f, red ▲) to 5 mM PSS, ZP becomes less negative compared to samples containing only PSS (Figure 4.2f, gray ●). This confirms d-DTAB is adsorbed to the droplet surface, resulting in a less net negative surface charge. Samples containing 1 mM d-DTAB have more negative ZP than 0.1 mM d-DTAB, despite having a greater bulk concentration of cationic surfactant. We conclude that a higher bulk d-DTAB concentration increases the amount of d-DTAB adsorbed to the nanoemulsions, which recruits more PSS to the surface, making the net interfacial charge more negative. We note that it is possible for the negatively charged sulfonate groups of PSS to re-orient in such a way that can result in more negative ZP measurements without necessarily an increase in PSS adsorption. However, previous surface tensiometry experiments have shown that the interfacial population of PSS increases with increasing amounts of d-DTAB, which is consistent and further supports our interpretation here.[60, 96, 97]

Altogether, we conclude that nanoemulsions stabilized by d-DTAB/PSS are stable over a month's time based on the robustness of the size distribution plots and minimal variation in diameters, PDIs, and ZPs. We note that for d-DTAB concentrations 2–14 mM, visible aggregation was observed, prior to the creation of nanoemulsions. This is commonly attributed to low-charged (near the isoelectric point) PS complexes resulting in precipitation.[98, 99] Upon sonication, aggregation and precipitation prevented the formation of stable nanoemulsions for this work, as nanoemulsions near the isoelectric point are highly prone to flocculation.[100, 101]

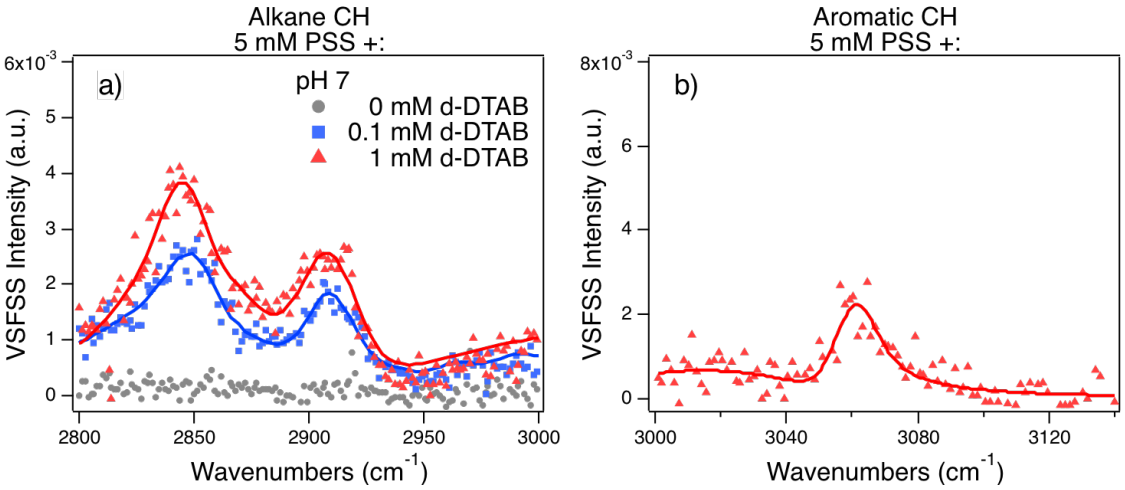

Figure 4.4. VSFSS spectra of the (a) alkane CH stretching region and the (b) aromatic CH stretching region of nanoemulsions stabilized by 0 mM d-DTAB (gray ●), 0.1 mM d-DTAB (blue ■), and 1 mM d-DTAB (red ▲), all in conjunction with 5 mM PSS. All samples are at the solution natural pH of 7 and all spectra were collected in the SSP polarization scheme. Spectra in the aromatic CH stretching region of samples made with 0 mM d-DTAB/5 mM PSS and 1 mM d-DTAB/5 mM PSS resulted in no signal and thus, are not shown.

From above, it is clear that d-DTAB concentration influences the long-term emulsion stability and sample quality based on the sample size distributions, diameters, PDIs, and ZPs (Figure 4.2). To better understand the surface properties of nanoemulsions coated with d-DTAB and PSS at the molecular-level, we have employed VSFSS to investigate the conformational ordering of PSS induced by adsorbed d-DTAB. VSFSS spectra of 5 mM PSS sonicated with 0, 0.1, and 1 mM d-DTAB is shown in Figure 4.4. The use of deuterated DTAB removes its spectral contributions in the CH stretching region, allowing us to investigate the conformational structure of strictly PSS. Figure 4.4a and 4.4b are VSFSS spectra of the aromatic CH and alkane CH stretching modes of PSS, respectively. As these spectra were taken with the SSP polarization combination, any resultant signal is indicative of vibrational modes with a component of their dipoles perpendicular relative to the droplet surface. Without the addition of d-DTAB, PSS yields no spectral response (Figure 4.4b, gray ●) even though the highly negative ZP of these samples (Figure 4.2f, gray ●) indicates that PSS is adsorbed to the droplet surface.

As noted above from ZP measurements, the addition of d-DTAB to PSS results in increased co-adsorption to the nanoemulsion surface (Figure 4.2f). The impact of co-adsorbed d-DTAB on the conformational arrangement and orientation of the

PSS pendant group and backbone is shown in Figure 4.4. All spectra shown herein have been fit according to previous Richmond publications. While the details of the fitting routine can be found elsewhere,[33, 34] the fit parameters for this work can be found in Table A.7 in the Appendix. Spectral contributions from the aromatic sp^2 CH stretching mode of PSS near 3060 cm^{-1} are observed with 1 mM d-DTAB (red ▲) and shown in Figure 4.4a.[60, 85] The alkane CH signatures corresponding to the CH_2 symmetric stretch (ss) near 2850 cm^{-1}, CH_3 ss near 2880 cm^{-1}, CH_2 asymmetric stretch (as) near 2910 cm^{-1}, and CH_3 as near 2975 cm^{-1} are observed with 0.1 mM (blue ■) and 1 mM d-DTAB (red ▲) and depicted in Figure 4.4b.[60, 85] As cationic d-DTAB populates the droplet surface, it creates an interfacial electric field that interacts with the anionic groups on PSS. We attribute the net ordering of the PSS backbone to interfacial electrostatics, in contrast to the surface behavior of adsorbed PSS alone, which does not show any net orientation. While a net orientation of the aromatic CH modes of PSS appears only at a bulk d-DTAB concentration of 1 mM (Figure 4.4a), the backbone CH modes are aligned starting at a much lower bulk d-DTAB concentration of 0.1 mM. We note that we do not achieve the same spectral sensitivity to the aromatic CH modes as we do with the alkane CH modes until the d-DTAB concentration is at 1 mM; however, the spectral appearance of both types of CH modes are indicative of significant conformational ordering of PSS perpendicular to the surface normal, in the presence of co-adsorbed d-DTAB. It is interesting to note that the appearance of the aromatic CH modes (Figure 4.4a) occurs at d-DTAB concentrations that increase PSS adsorption, as shown in the ZP measurements (Figure 4.2f, red ▲). As mentioned previously, bulk concentrations of d-DTAB between 2 and 14 mM resulted in complex aggregation, making it difficult to create monodispersed nanoemulsions for this study and therefore, we refrained from using higher bulk d-DTAB concentrations.

Ultimately, we attribute these orientation effects to electrostatic interactions between the cationic d-DTAB head group and the anionic sulfonate pendant group of PSS, which then influences the net orientation of the polymer backbone. This is in contrast to the surface behavior of adsorbed PSS alone, which is facilitated predominantly by hydrophobic interactions. In the absence of co-adsorbed d-DTAB, the system lacks electrostatically driven interactions and thus, PSS does not show any net orientation.

The effects of cationic PEI: Added electrosterics

With the adsorption of a secondary polymer, the effects of additional steric repulsion and intermolecular interactions on emulsion stability were investigated. In this section, we focus on the addition of cationic PEI at pH 3 as the second polymer whereas later, we focus on this system at pH 10 for which PEI is then nonionic.[39, 52] For these studies, d-DTAB and PSS were sonicated together as described above in Chapter 2 in *Nanoemulsion Preparation*, followed by PEI being added to the nanoemulsion sample and allowed to adsorb to the droplet surface via electrostatic interactions, mimicking common LbL adsorption techniques.[36, 102] The size distribution of nanoemulsions stabilized by 0.1 mM d-DTAB, 5 mM PSS, and either 0, 1, or 10 mM PEI is shown in Figure 4.5a–c, respectively. Figure 4.5d–f summarizes the nanoemulsion diameters, PDIs, and ZPs, respectively, for samples containing 0.1 mM d-DTAB, 5 mM PSS, and varying cationic PEI concentrations.

Samples stabilized with 0 mM (Figure 4.5a) and 1 mM PEI (Figure 4.5b) show a constant, narrow, and largely uni-modal size distribution throughout the duration of the study, demonstrating that the stability of the sample is preserved with the addition of 1 mM PEI. For 0 and 1 mM PEI, the nanoemulsions display similar diameters (Figure 4.5d, orange ● and green ■), and exhibit little change over the 30-day span. PDI values for these samples (Figure 4.5e, orange ● and green ■) remain largely invariant over time and are all < 0.3, indicating a monodispersed sample. Comparison of the ZP measurements of samples with 0 mM PEI (Figure 4.5f, orange ●) and 1 mM PEI (Figure 4.5f, green ■) shows that the addition of 1 mM cationic PEI results in a more negative ZP reading than the DTAB/PSS system. We attribute these observations to an increase in PSS adsorption through enhanced electrostatic interactions with the presence of surface adsorbed cationic PEI, similar to the enhanced PSS adsorption observed with a greater concentration of cationic d-DTAB described above. Consequently, the overall net surface charge is more negative with more adsorbed PSS. This enhanced adsorption of PSS will be confirmed below with our spectroscopic results. Overall, the unchanging size distributions, diameters, PDIs, and ZP values with the addition of 1 mM cationic PEI confirm that the nanoemulsions are stable with a second polymer layer.

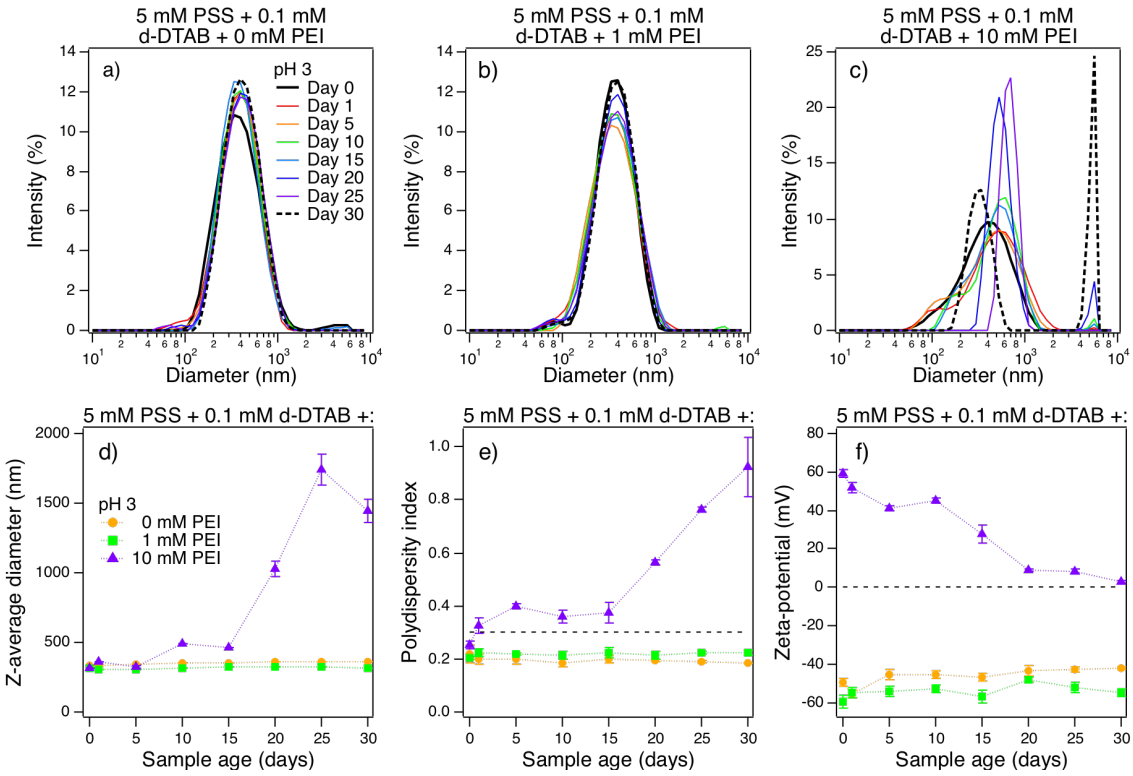

Figure 4.5. Top panel: Size distribution measurements of nanoemulsions stabilized by 0.1 mM DTAB, 5 mM PSS, and (a) 0 mM PEI, (b) 1 mM PEI, and (c) 10 mM PEI. Bottom panel: (d) Nanoemulsion Z-average diameter, (e) PDI, and (f) ZP for samples stabilized by 0.1 mM DTAB, 5 mM PSS, and 0 mM PEI (orange ●), 1 mM PEI (green ■), and 10 mM PEI (purple ▲). All samples were prepared at constant pH 3 with the DTAB/PSS + PEI preparation scheme, in which DTAB and PSS were first sonicated together to create nanoemulsions, then PEI was added and allowed to adsorb to the droplet surface.

Contrary to the observed robustness and stability of the system with 1 mM PEI, the addition of 10 mM PEI at pH 3 shows more dynamic behavior over the course of 30 days. The initial size distribution is comparable to that of samples containing 0 and 1 mM PEI (Figure 4.5c, solid black). Over time, the distribution shifts to slightly larger sizes, accompanied by an increase in size populations exceeding 1000 nm. The shift in size distribution to larger diameter is representative of the coalescence process, as the nanoemulsions are collectively becoming larger. After Day 15, the broad uni-modal distribution becomes bi-modal with changes to the relative intensities between the smaller and larger size populations. Specifically by Day 30, the relative amount of emulsions > 5000 nm in diameter surpasses that of emulsions < 500 nm, which is evident of Ostwald ripening.[78, 91] Destabilization via Ostwald ripening occurs when smaller droplets join with larger droplets, adding to the volume of larger droplets while

decreasing the population of smaller droplets.[78, 90, 91] Complementing the dynamic behavior of the size distribution over time for the 10 mM PEI sample are diameters, PDIs, and ZPs results (Figure 4.5d–f, purple ▲). Both the emulsion diameter and PDI begins to significantly increase after Day 15, when the size distribution becomes bi-modal. The ZP for samples containing 10 mM cationic PEI begins highly positive around +60 mV, but continually decreases to a near-zero surface charge by Day 30.

Long-term droplet stability relies not only on the adsorption of chemical species, but also the energetics that keep them there. While instantaneous PEI adsorption to the droplet surface provides initial stability, as represented by the size distribution and PDI results of fresh samples (Day 0), the sample quality degrades over time as size increases and the sample becomes more polydispersed. ZP values also support sample destabilization. As the surface charge goes to zero, there is decreased inter-droplet electrostatic repulsion, which increases the probability of flocculation and coalescence. Under the current solution conditions, PEI is highly charged and soluble which presents an issue of competitive bulk solvation versus adsorption.[103] Altogether, the increased variability in size distribution over time, the increase in diameter and PDI, and the decrease in ZP magnitude indicate that PEI is desorbing from the droplet surface and catalyzing the destabilization process. While we do not quantify the amount of polymer desorption, the near-zero surface charge by Day 30 illustrates the depletion of charged PSS/PEI complexes at the droplet surface. Thus, without any surface-active species at the droplet surface, there is no stabilizing mechanism for the nanoemulsions. We note that while the size distribution of samples containing 10 mM PEI (Figure 4.5c, dotted black) show a population of sizes measuring ~500 nm, we are confident that these are bulk polymer structures in solution, rather than nanoemulsions. By Day 30, the sample is visually no longer opaque and instead, largely transparent (see Figure 4.3, middle panel), confirming that an emulsion is no longer present.[87, 92–94]

To understand how the amount of adsorbed charged PEI influences the backbone and pendant group ordering of PSS, VSFSS measurements are used to probe the droplet surface coated by d-DTAB, PSS, and PEI at constant pH 3. We only perform spectroscopic studies on fresh samples, prepared the day of our spectroscopic experiments, to ensure the most uniform size distributions and PDIs < 0.3, making them most suitable for VSFSS. In this preparation scheme, d-DTAB and PSS were sonicated together. Upon dilution with a PEI solution, the final concentrations of d-DTAB and PSS were fixed at 0.1 mM and 5 mM, respectively, while the final concentration of PEI varied between 0, 1, and 10 mM. Though many applications use

much higher bulk surfactant concentrations to stabilize emulsions, we have carefully chosen to work with 0.1 mM d-DTAB for our spectrosopic studies to stay below maximum surfactant surface coverage.[25, 104, 105] This allows us to focus primarily on how steric hindrance contributes to droplet stability. Additionally, this ensures that any changes observed in the aromatic CH modes of PSS can then be attributed to the added cationic PEI, since 0.1 mM d-DTAB has been shown to not impart any detectable net alignment in the PSS pendant groups (Figure 4.4a).

Recall from above that samples containing d-DTAB/PSS leads to the polymer displaying measurable conformational ordering of the PSS backbone and pendant groups (Figure 4.4). Figure 4.6a shows the VSFSS spectra of the alkane CH stretching region of nanoemulsions stabilized with 0.1 mM d-DTAB, 5 mM PSS, and either 0 mM PEI (orange ●), 1 mM (green ■), or 10 mM PEI (purple ▲). These spectra contain peaks characteristic of CH modes from an alkane chain, such as the backbone of PEI and PSS.[51, 60, 85] The polymers both contain alkane CH stretching modes, making it impossible to decouple the alkane CH stretches of PEI from those of PSS. The SF response observed in this region is evidence that the alkane CH modes of either PSS, PEI, or a combination of the two possess a net ordering perpendicular to the droplet surface.

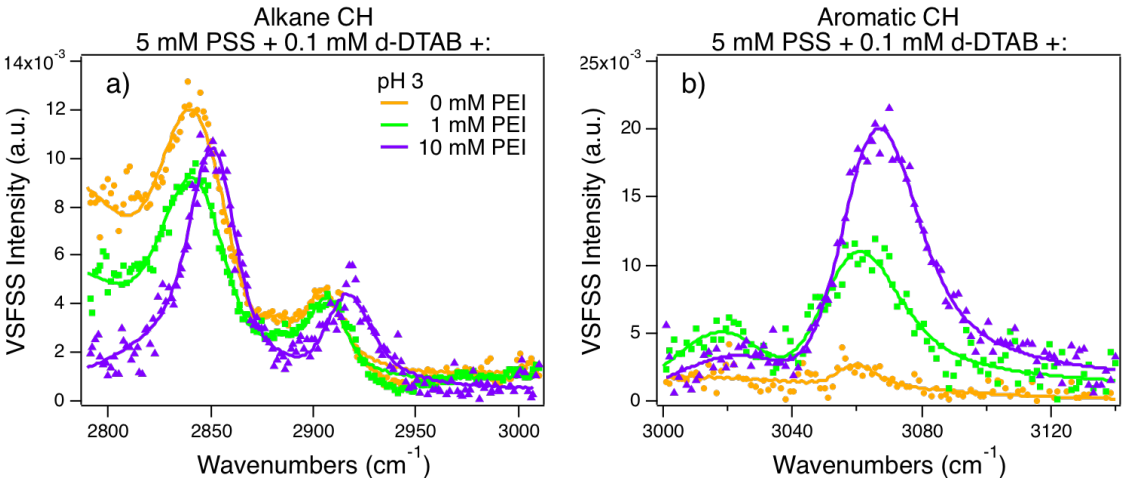

Figure 4.6. VSFSS spectra of the (a) alkane CH stretching region and the (b) aromatic CH stretching region of nanoemulsions stabilized by 0.1 mM d-DTAB, 5 mM PSS, and 0 mM PEI (orange ●), 1 mM PEI (green ■), and 10 mM (purple ▲), all at constant pH 3. Spectra were collected in the SSP polarization scheme and lines are fits to normalized data.

Additional information can be gained from the rise in intensity at and below 2800 cm^{-1}, which corresponds to the tail of the OD stretching modes of highly coordinated

interfacial (heavy) water molecules. As shown in recent studies from this laboratory, surface D_2O has a broad stretch and libration combination mode in this region that is highly sensitive to surface charge.[106] This mode interferes with the CH modes, with its phase flipping by 180° as a surface goes from positive to negative. The increase in this water signal with decreasing PEI concentration (shown in Figure 4.6a) mirrors the change from a positively charged surface to one that is negatively charged, which is consistent with ZP results in Figure 4.5f. By accounting for this mode in our fits (see Appendix, Table A.8) the overall intensities of the CH modes are found to increase with the addition of PEI. This is consistent with our ZP results above showing that in the presence of cationic PEI as a secondary polymer layer, more PSS is recruited to the surface (Figure 4.5f, orange ● and green ■). In the presence of 10 mM cationic PEI, the ZP becomes highly positive and alkane CH intensities are the highest (Table A.8). Since 1 mM PEI enhances PSS adsorption, we intuit 10 mM PEI would further enhance PSS adsorption, leading to the increased intensities in the fits for the alkane CH stretches. While PEI itself can contribute to the increased signal observed between 2800 cm^{-1} and 3000 cm^{-1}, we believe the signal increase is mostly due to a higher interfacial PSS population as PEI has been reported to possess no net orientation at the droplet surface in acidic conditions.[103]

Although the backbone CH modes of PEI and PSS are indistinguishable, only PSS contains the aromatic CH modes.[60, 85] Figure 4.6b shows the VSFSS response from the aromatic CH modes of the PSS pendant groups in the presence of 0.1 mM d-DTAB and varying concentrations of PEI at pH 3. As shown, this mode near 3060 cm^{-1} increases with increasing PEI concentration. We attribute this signal increase to enhanced surface PSS adsorption (and consequently, orientation) when more PEI is adsorbed to the droplet surface. Recall ZP results demonstrate that a greater amount of PSS is interfacially present with the addition of cationic PEI (Figure 4.5f). This is further confirmation that PEI is interfacially present, as without it (Figure 4.6b, orange ●), the aromatic CH modes are not detectable.

The effects of nonionic PEI: Added hydrophobicity and sterics

As pH increases from 3 to 10, PEI loses its cationic character and behaves as a nearly neutral polymer.[39, 52] In this section, we address how nanoemulsion stability and interfacial PSS ordering is altered upon the addition of a secondary nonionic polymer. The size distributions of d-DTAB/PSS and either 0, 1, or 10 mM PEI nanoemulsions at pH 10 were measured over 30 days and are shown in Figure 4.7a–c,

respectively (top panel). In Figure 4.7d–f (bottom panel), we summarize the results from diameter, PDI, and ZP measurements, respectively, of nanoemulsions stabilized by d-DTAB/PSS and 0, 1, or 10 mM nonionic PEI.

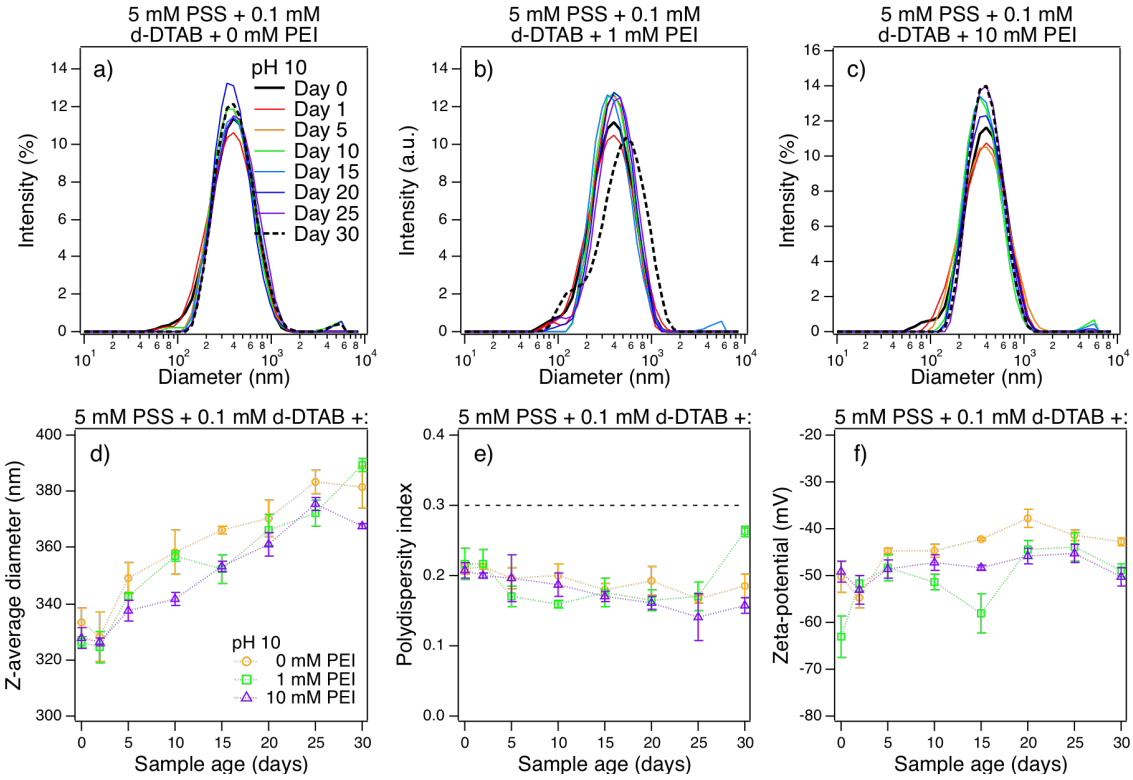

Figure 4.7. Top panel: Size distribution measurements of nanoemulsions stabilized by 0.1 mM DTAB, 5 mM PSS, and (a) 0 mM PEI, (b) 1 mM PEI, and (c) 10 mM PEI. Bottom panel: (d) Nanoemulsion Z- average diameter, (e) PDI, and (f) ZP for samples stabilized by 0.1 mM DTAB, 5 mM PSS, and 0 mM PEI (orange), 1 mM PEI (green), and 10 mM PEI (purple). All samples were prepared at constant pH 10 with the DTAB/PSS + PEI preparation scheme, in which DTAB and PSS were first sonicated together to create nanoemulsions, then PEI was added and allowed to adsorb to the droplet surface.

As can be seen by the consistent, robust, and invariant size distributions over 30 days for all samples containing 0 mM PEI (Figure 4.7a), 1 mM PEI (Figure 4.7b), and 10 mM PEI (Figure 4.7c), hydrophobic PEI preserves the nanoemulsion stability with time at both low and high concentrations. Unlike what was observed for samples containing 10 mM cationic PEI above at pH 3 (Figure 4.5c), with nonionic PEI, competing factors such as bulk solvation no longer poses an issue to nanoemulsion stability. For each PEI concentration, steady growth in diameter (Figure 4.7d) is observed, while the PDI (Figure 4.7e) and ZP (Figure 4.7f) remains comparable and

largely constant. This demonstrates that under these preparation conditions, PEI desorption is not occurring as it did with higher concentrations of cationic PEI. These results present another avenue for droplet surface tunability because now, a higher concentration of PEI can be used to coat the droplet surface without jeopardizing the sample quality.

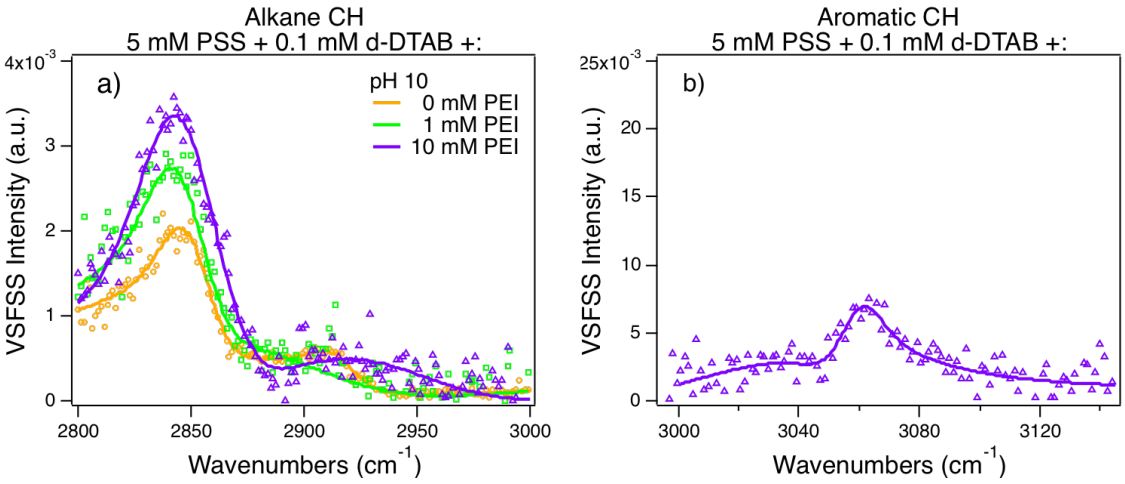

Figure 4.8. VSFSS spectra of the (a) alkane CH stretching reigon and the (b) aromatic CH stretching region of nanoemulsions stabilized by 0.1 mM d-DTAB, 5 mM PSS, and 0 mM PEI (orange ○), 1 mM PEI (green □), and 10 mM (purple △), all at constant pH 10. Spectra were collected in the SSP polarization scheme and lines are fits to normalized data. Spectra collected in the aromatic CH stretching regions of samples containing 0 and 1 mM PEI resulted in no signal and thus, has been omitted for clarity.

Figure 4.8 shows the VSFSS measurements, collected in the SSP polarization scheme, of the two polymers alkane CH modes (a) and the PSS aromatic CH modes (b) for nanoemulsions stabilized with 0.1 mM d-DTAB, 5 mM PSS, and varying concentrations of PEI at pH 10. In Figure 4.8a, the alkane CH stretching modes increase (see Table A.9 in the Appendix for fit parameters) with increasing PEI concentration from 0 mM (orange ○) to 10 mM (purple △). Although it is difficult to interpret the alkane CH region for this two-polymer system where both polymers contain alkane CH signatures,[51, 60, 85] we conclude that both PSS and PEI are interfacially present and arranged with their net dipoles perpendicular to the droplet surface. We note the striking absence of the CH_2 asymmetric stretch near ~2910 cm^{-1} in Figure 4.8a. The ways in which the two polymers can complex with each other at the droplet surface may cause interferences between the CH_2 asymmetric stretches from the two different

polymers, ultimately resulting in a diminished net signal near ~2910 cm^{-1}. It is difficult to determine the exact orientation of the polymers to describe the interference between a CH_2 asymmetric stretch of PSS and a CH_2 asymmetric stretch of PEI. However, it is possible that the two together interacts in such a way that suppresses this vibrational mode.

ZP measurements for these nanoemulsions (Figure 4.7f) are negative for all concentrations of PEI, evidence that PSS is coating the droplet surface, as PEI possesses minimal charge at pH 10. Note that with increasing amounts of nonionic PEI, the ZP values do not show significant changes that would suggest more PSS is recruited to the droplet surface. With PEI being neutral in basic environments, PSS adsorption is not enhanced as it was with increasing d-DTAB (Figure 4.2f) and cationic PEI (Figure 4.5f) concentrations, due to the absence of additional electrostatics. Thus, changes to the VSFSS spectra depicted in Figure 4.8a confirm that PEI is also present at the droplet surface and contributing to the increase in spectral intensity.

The reduction in positive charges along PEI greatly reduces the net ordering of PSS pendant groups, as shown in Figure 4.8b. At pH 3 (Figure 4.6b, green ■), 1 mM cationic PEI imparts an appreciable SF response in the aromatic stretching region. Conversely, at pH 10, 1 mM nonionic PEI results in no discernible signal (not shown for clarity). When the amount of charge on PEI is significantly reduced in basic conditions, 10 mM PEI is needed to impart a very low-lying, yet measurable level of net ordering amongst the PSS pendant groups (Figure 4.8b, purple △).[60, 85] We conclude that with nonionic PEI, the electric field it induces at the droplet surface is not strong enough to achieve the level of net ordering in PSS as observed with its highly cationic form.

Previously with highly cationic PEI, electrostatic interactions are the dominant intermolecular forces influencing PSS adsorption and net orientation. This resulted in nanoemulsion samples that are coated with highly ordered PSS pendant groups, but are not stable for the 30-day period. Conversely, at pH 10, although the lowered solubility of PEI caused the reduction in net alignment of the PSS pendant groups, the nanoemulsions *did* remain stable during the study, even with higher PEI concentrations. At pH 10, electrostatic interactions between d-DTAB and PSS still exist, but without competitive bulk solvation of PEI causing its desorption (as occurred above at pH 3), nanoemulsions containing hydrophobic PEI remain stable for much longer. Thus, it is the balance of electrostatics between d-DTAB and PSS, as well as the hydrophobic interactions between d-DTAB/PSS complexes and nonionic PEI that contributes to the long-term stability of the sample.

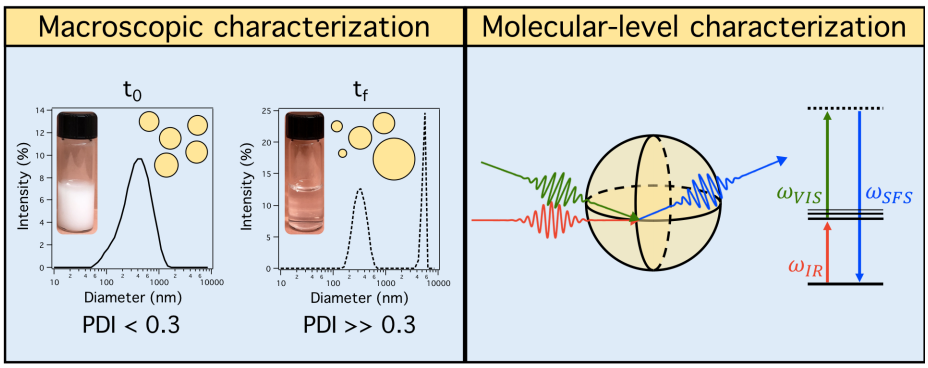

Figure 4.9. Summary illustration of macroscopic and molecular-level studies of polymer multilayering on nanoemulsion surfaces.

LbL deposition on planar surfaces has been employed for a broad range of applications, as it is a convenient method for tuning surface properties.[71, 73–76] Specifically with the multi-layering of polymers around cargo-loaded emulsions for biopharmaceutical advancements, both the macroscopic sample properties as well as molecular-level interfacial properties of the system are of interest.[9, 11, 77, 78] In this study, we have demonstrated that nanoemulsions < 500 nm with PDI < 0.3 can be created with a stabilizing surfactant layer and coated with two different polymers: anionic PSS and charge-tunable PEI, but the long-term stability of this system is highly dependent on factors such as surfactant concentration, PEI concentration, and solution pH. Moreover, these multipolymer coated nanoemulsions are highly versatile, in which many routes can be taken to modify their macroscopic and molecular surface properties. While many applications rely on high bulk concentrations of small molecule surfactants to stabilize emulsions, with the combined effects of two polymers, nanoemulsions can be prepared with much lower bulk surfactant concentrations.

By adjusting the balance of electrostatic, hydrophobic, and steric interactions, nanoemulsions with long- and short-term stability can be made with varying degrees of conformationally ordered polymer layers. DTAB/PSS-stabilized nanoemulsions remained stable throughout the 30-day span, and while varying DTAB concentration influences PSS adsorption and backbone alignment, the effect it has on the ordering of the PSS pendant groups is minimal. Alternatively, the charge density of PEI plays an important role in altering both the amount of PSS adsorption and its net interfacial ordering, as well as the duration in which the nanoemulsion sample remains stable. In the DTAB/PSS/PEI combination, cationic PEI encourages more PSS to adsorb to

the droplet surface with highly oriented pendant groups, in comparison to its nonionic counterpart. This is caused by the increased electrostatic interactions at the interface when PEI is charged. However, over time, highly charged PEI is shown to desorb from the droplet surface, catalyzing sample destabilization. Conversely, within the 30-day period, destabilization does not occur for nanoemulsion samples containing nonionic PEI due to its enhanced hydrophobicity, making desorption from the interface to the bulk less energetically favorable. The added steric effects from PEI as a secondary polymer layer also preserves the stability of the sample.

Together, our time-dependent nanoemulsion sample characterization and spectroscopic investigations of PSS/PEI polymer layering behavior at the curved oil/water interface demonstrate how nanoemulsions can be made to have both tunable stability and interfacial properties. The versatility of this surfactant/two-polymer system is highly advantageous for applications such as drug delivery systems, which depend on timely destabilization of the nanoemulsion to release the encapsulated cargo, or applications that require a long shelf life such as cosmetics and emulsified foods.

CHAPTER V

NANOEMULSION STABILIZATION VIA STERIC EFFECTS

This work was published in Volume 37 of the journal *Langmuir* in October 2021. Emma Tran designed the study, performed the experiments, analyzed the data, and wrote the manuscript. Geraldine Richmond was the principal investigator for this work and provided editorial assistance and general feedback.

Introduction

In the work discussed thus far, the focus has been placed on how polyelectrolytes influence not only the surface functionality, but also the overall quality (i.e., droplet size distribution, PDI, growth rate) of the nanoemulsion samples. From a more fundamental perspective, colloidal stability depends on a balance of different intermolecular forces. As mentioned previously, nanoemulsions are kinectically stable and thus, over time, will destabilize and phase separate into immiscible oil and water layers (i.e., the thermodynamically stable system). To enhance the stability of nanoemulsions for applications, ionic surfactants and polyelectrolytes are frequently used as emulsifying agents, effectively adding a layer of electrostatic charge around the droplet surface. Common polyelectrolytes used in applications include PEI and PSS, as discussed in Chapter 3 and Chapter 4 above. As a result, the charge–charge repulsion between droplets acts as a stabilizing factor. However, the incorporation of nonionic surfactants and polymers in application design has gained interest due to their advantageous properties such as low cost, lowered toxicity, and increased biodegradability.[107] A deeper understanding of the stabilizing mechanisms that nonionic emulsifiers provide is important for guiding the informed design of these products.

This chapter is aimed towards better understanding the stabilizing effects due to steric hindrance from nonionic polymer layers. For these studies, we have created polymer/surfactant-stabilized nanoemulsions that have roughly no surface charge, yet are stable for upwards of a month. The stabilizing agents used are a combination of surfactant sodium dodecyl sulfate (SDS) and nonionic polymer poly(N-vinylacetamide) (PNVA). Although SDS is anionic, under specific PNVA concentrations, the stable nanoemulsions possess nearly zero ζ-potentials. Using a combination of experimental techniques such as dynamic light scattering, ζ-potential, and surface spectroscopic measurements, we characterize the properties of these "uncharged" nanoemulsions to learn about the intermolecular factors contributing to their stability.

Additionally, we calculated interaction pair potentials using the framework of extended DLVO (named after Derjaguin, Landau, Verwey, and Overbeek) theory to better understand how the thickness of the polymer layer contributes to the stability of these droplets.

Our calculations show that extended DLVO theory can be applied to these "uncharged" nanoemulsions to explain the significant forces that contribute to droplet stability. But beyond simply steric effects, we learn from our spectroscopic results that the interfacial-bonding network surrounding the droplet surface is critical for maintaining the stability of nanoemulsions with a negligible ζ-potential (ZP). The strongly bonded, rigid polymer networks that are formed act as shells, protecting the oil droplets from colliding and ultimately being destabilized. The insights from this investigation provide a better understanding of the factors governing the interfacial behavior of nonionic polymers. This opens up avenues for applications to integrate more nonionic emulsifiers into their designs for a variety of purposes.

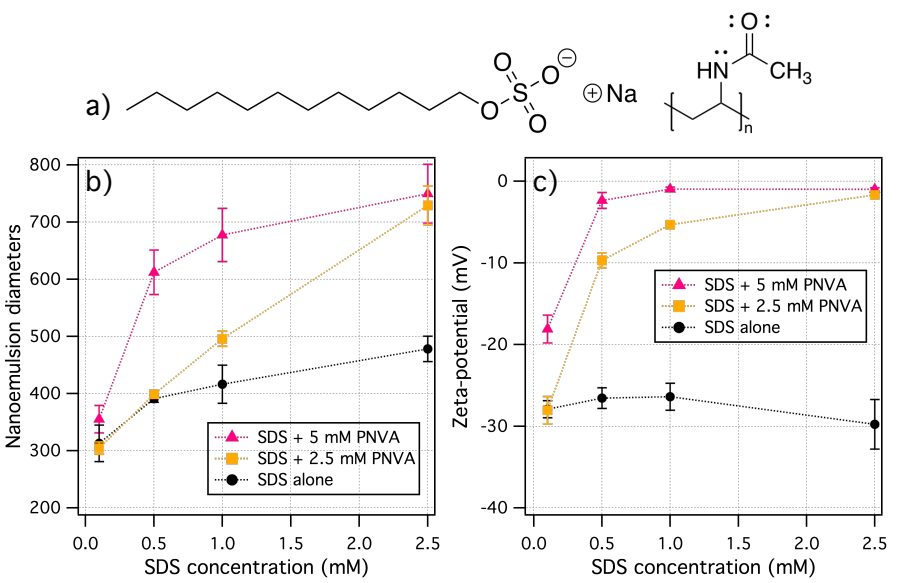

Figure 5.1. (a) Molecular structures of surfactant SDS and polymer PNVA. (b) Droplet diameters and (c) ZP measurements as a function of SDS concentration for nanoemulsions stabilized by SDS alone (black ●), SDS with 2.5 mM PNVA (orange ■), and SDS with 5 mM PNVA (pink ▲). Error bars represent error-propagated standard deviations from triplicate measurements of 5-7 different samples prepared on different days.

The diameter and ζ-potential (ZP) of nanoemulsions are informative of initial

droplet stability. Nanoemulsions are in the size range of 100s of nanometers in diameter. A highly charged surface typically reflects a stable colloid system.[2, 108] Figure 5.1a shows the molecular structures of surfactant SDS and polymer PNVA. Figure 5.1b,c depicts the measured diameters and ZP, respectively, for nanoemulsions stabilized by SDS and PNVA, as a function of SDS concentration. The black, orange, and pink traces represent samples containing SDS in conjunction with 0, 2.5, and 5 mM PNVA, respectively. It can be seen that nanoemulsions stabilized by only SDS (black ●) measure between 300 and 500 nm and possess a highly negative ZP, which is characteristic of SDS-stabilized nanoemulsions.[59, 103] As PNVA is added to the sample and adsorbs to the droplet surface, two notable phenomena are observed: the nanoemulsion size increases significantly (Figure 5.1b) and the magnitude of the ZP decreases to ~0 mV (Figure 5.1c). It is noteworthy that these droplets have roughly zero ZP values when coated with the polymer. In previous literature reports, nanoemulsions stabilized by nonionic surfactants with minimal ZP were stable for only 5-10 days.[108, 109] In other reports, nanoemulsions prepared with nonionic surfactants have been shown to still possess an appreciable ZP (−20 to −50 mV).[110, 111] It has been noted that the observed charge is attributed to trace impurities within the surfactants and/or surface-active contaminants.[19, 112] Thus, we are careful to ensure that the nanoemulsions we have prepared are as clean as possible.[19]

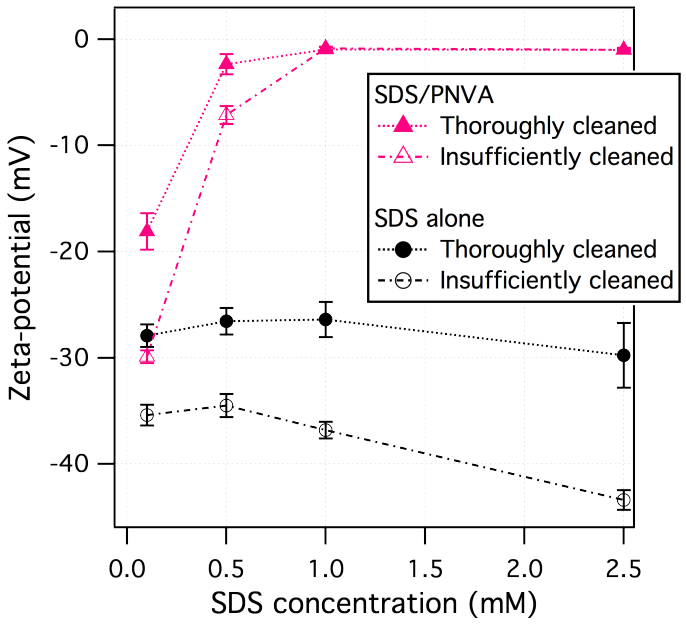

Figure 5.2. ZP measurements of nanoemulsions stabilized by SDS alone (black ● or ○) and SDS/PNVA (pink ▲ or △). The SDS concentration was varied from 0.1, 0.5, 1, and 2.5 mM, while the PNVA concentration was fixed at 5 mM. The solid traces depict samples prepared with thoroughly cleaned glassware (see Chapter 2, *Nanoemulsion Preparation*), and the dashed traces depict samples prepared with loosely cleaned glassware (which we refer to as "insufficiently cleaned").

In Figure 5.2, we demonstrate that insufficiently cleaned glassware can influence the overall magnitude of the ZP of the prepared nanoemulsions. While we cannot control any impurities that may be present in the purchased SDS or PNVA, we can control the cleanliness of our system. Figure 5.2 shows the ZP measurements for nanoemulsions stabilized by SDS alone and SDS/PNVA prepared in "cleaned" (▲ or ●) and "insufficiently cleaned" (△ or ○) glassware. The PNVA concentration was fixed at 5 mM, while the SDS concentration ranged from 0.1, 0.5, 1, and 2.5 mM. It can be seen that between "cleaned" and "insufficiently cleaned" glassware, samples prepared with clean glassware show ZP values that are lower in magnitude. The additional charge from contaminants may alter the interpretation of droplet stability, especially in discussions involving extended DLVO Theory where the emphasis is on uncharged surfaces. Therefore, we ensure that the samples we have prepared are as clean as possible to minimize any trace contaminants that may influence the surface charge and thus, the stability of the droplets.

Both the increase in droplet size and reduction in ZP magnitude are strongly indicative of emulsion destabilization. We define our "uncharged" nanoemulsions as those with ZP values between −10 and +10 mV, as this range is considered "neutral" for nanoparticles.[113] Without an appreciable ZP, the nanoemulsions are more susceptible to flocculation, coalescence, and Ostwald ripening, all processes that will generally increase the droplet diameters in the sample. However, in stark contrast to what initial size measurements would suggest, despite the bulk nanoemulsion sample being comprised of larger sized, "uncharged" droplets in the presence of PNVA, we measure that these samples remain stable upward of 35 days, and the dynamics of the system are not trivial. Figure 5.3 shows the measured diameters, PDIs, and ZP of these "uncharged" nanoemulsions stabilized by SDS and 5 mM PNVA, over the course of 35 days.

Initially, nanoemulsions stabilized with SDS/PNVA are much larger than those stabilized by SDS alone. We ascribe the relative difference of ~100-300 nm in droplet diameters to the PNVA coating on the droplet surface and the formation of stratified polymer layers. The decrease in ZP magnitude due to nonionic polymer adsorption

has been observed previously for nanoparticles.[114] It is important to recall that ZP measurements are not a direct measurement of the surface charge, but rather, a measurement of the potential difference across the slipping plane of a colloid.[113, 115] The adsorption of nonionic polymers to a colloidal surface, specifically in thick layers, shifts the slipping plane further into the bulk phase, and consequently reduces the measured ZP value.[114] Ultimately, this phenomenon accounts for both the formation of larger droplets (due to polymer adsorption) and the near-zero ZP values since PNVA is nonionic.

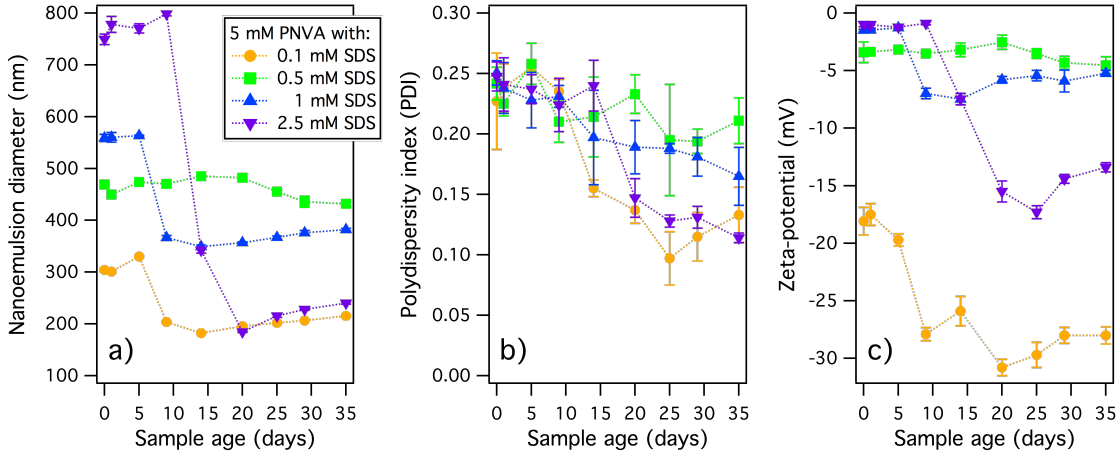

Figure 5.3. (a) Measured diameters, (b) PDIs, and (c) ZP of nanoemulsions stabilized with SDS concentrations from 0.1 (orange ●), 0.5 (green ■), 1 (blue ▲), and 2.5 (purple ▼) mM, in conjunction with 5 mM PNVA, as a function of time. Error bars represent error-propagated standard deviations from triplicate measurements of 3 different samples.

Over time, rather than growing in size, samples containing 0.1 (orange ●), 1 (blue ▲), and 2.5 (purple ▼) mM PNVA are observed to shrink in droplet diameter with time (Figure 5.3a). Accompanying the reduction in sizes is an increase in ZP magnitude (Figure 5.3c). This observation can be explained by the desorption of PNVA. As PNVA desorbs from the droplet surface, the nanoemulsion diameter shrinks and the interfacial electric field induced by SDS becomes more significant, resulting in more negative ZP values. Despite the complex dynamics of this system, we believe the nanoemulsion samples are still stable as reflected by the monodispersity of the system with PDI values < 0.3 (Figure 5.3b).[2] If the droplets were destabilizing via flocculation, coalescence, or Ostwald ripening, the sample would become more polydispersed, which would be reflected by an increase in the PDIs.

The nanoemulsions we have prepared with SDS/PNVA show interesting properties and dynamics. While deeper investigations will be necessary to fully describe

the dynamics of this system, we conclude that these "uncharged" nanoemulsions are stable, even during periods where the ZP values were ~0 mV. We believe the factors contributing to the stability of the nanoemulsions when they are "uncharged" are steric effects and the molecular structure of the adsorbed complexes, topics that will be discussed in greater detail in the sections to come.

DLVO and Extended DLVO Theory

Calculations. DLVO theory describes colloid stability through interaction pair potentials derived from attractive van der Waals and repulsive charge-charge (also described as "electric" double-layer) interactions between two spheres. The interaction potential W between two spheres (i.e., droplets) of radii R_1 and R_2 as a function of interdroplet distance D is expressed as[116, 117]

$$\begin{aligned} W(D) &= W_{vdw} + W_{elec} \\ &= -\frac{A}{6D}\frac{R_1 R_2}{(R_1 + R_2)} + \frac{R_1 R_2}{R_1 + R_2} Z e^{-\kappa D} \end{aligned} \tag{26}$$

where A is the Hamaker constant equal to 0.55×10^{-20} J for hexadecane-in-water nanoemulsions, κ^{-1} is the Debye screening length, and Z is an interaction constant.

The Hamaker constant for hexadecane-in-water nanoemulsions is[117, 118]

$$A = \frac{3}{4} k_B T \left(\frac{\varepsilon_{\text{hexadecane}} - \varepsilon_{\text{water}}}{\varepsilon_{\text{hexadecane}} + \varepsilon_{\text{water}}} \right)^2 + \frac{3h\nu_e}{16\sqrt{2}} \frac{(n^2_{\text{hexadecane}} - n^2_{\text{water}})^2}{(n^2_{\text{hexadecane}} + n^2_{\text{water}})^{\frac{3}{2}}}. \tag{27}$$

Parameters used to calculate the Hamaker constant for this work can be found in Table A.10 in the Appendix.

The Debye screening length is given by[119]

$$\kappa^{-1} = \frac{0.304}{\sqrt{I(M)}} \tag{28}$$

where I is the ionic strength in molar (M). For this work, the ionic strength and corresponding Debye length can be found in Table A.11 in the Appendix.

The interaction constant is defined as[116, 117]

$$Z = 64\pi\varepsilon_o\varepsilon \left(\frac{kT}{e} \right)^2 \tanh^2 \left(\frac{ze\psi_o}{4kT} \right) \text{J m}^{-1} \tag{29}$$

where ψ_o is the droplet surface potential in mV. In our work, we use experimentally

measured ζ-potentials to calculate the interaction potentials. This has been done as an approximation in previous work following the rationale that the ζ-potential values closely mimic the electrostatic potentials.[117, 118]

First, we note that for two droplets of roughly the same size, $R_1 \approx R_2 \equiv R$. Then Eq. 26 above becomes

$$W(D) = -\frac{AR}{12D} + \frac{1}{2}RZe^{-\kappa D} \tag{30}$$

Second, we note that at room temperature ($T = 25^{\circ}$C), the interaction constant becomes[116]

$$Z = 9.22 \times 10^{-11} \tanh^2\left(\frac{\psi_o}{103}\right) \text{J m}^{-1} \tag{31}$$

The equation describing the van der Waals attractive forces is chosen for the case where the interdroplet distance is less than the droplet radius.[116] The interdroplet distance is defined as the distance from one edge of a nanoemulsion to the next.

For our nanoemulsions stabilized by a steric polymer layer with ζ-potential measuring ~0 mV, extended DLVO theory was used to calculate the interaction potentials. Under the framework of extended DLVO theory, two additional repulsive terms are introduced[120–122]

$$W(D) = W_{vdw} + W_{elec} + W_{osmotic} + W_{entropic} \tag{32}$$

with

$$W_{osmotic} = \frac{4\pi R}{\nu}\phi_p^2\left(\frac{1}{2} - \chi\right)L^2\left(\frac{D}{2L} - \frac{1}{4} - \ln\frac{D}{L}\right) \tag{33}$$

where R is the droplet radius, ν is the volume of one solvent molecule, ϕ_p is the volume fraction of polymer, ϕ is the volume fraction of droplets, χ is the Flory-Huggins constant for polymers, L is the steric layer thickness, M_w is the polymer molecular weight, and ρ is the density of the oil core. The equations chosen for both $W_{osmotic}$ and $W_{entropic}$ are for the case where the interdroplet distance is less than the steric layer thickness.[120–122]

$$W_{entropic} = \frac{2\pi R}{M_w}\phi L^2\rho\left[\frac{D}{L}\ln\left(\frac{D}{L}\left(\frac{3-\frac{D}{L}}{2}\right)^2\right) - 6\ln\left(\frac{3-\frac{D}{L}}{2}\right) + 3\left(1+\frac{D}{L}\right)\right] \tag{34}$$

In the following sections, DLVO and extended DLVO theory will be used to calculate interaction pair potentials for SDS/PNVA-stabilized nanoemulsions.

General Application of DLVO Theory. To better understand the steric effects stabilizing our "uncharged" nanoemulsions (Figure 5.3), theoretical frameworks detailing colloid stability were applied. While DLVO theory has been predominantly employed within the context of solid particle stability, we have applied the framework to soft nanodroplets. Figure 5.4 summarizes the results from calculating interaction pair potentials using the framework described by standard DLVO theory and extended DLVO theory, as described above.[116–122]

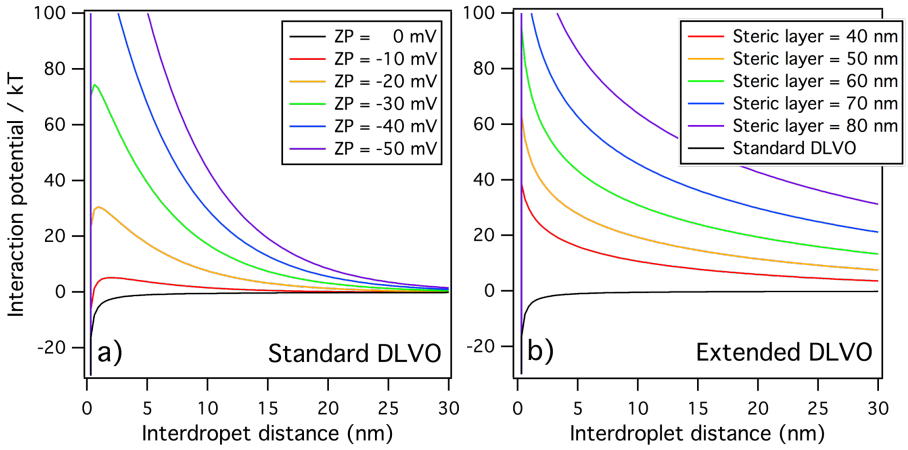

Figure 5.4. Theoretical interaction potential diagrams calculated using (a) standard and (b) extended DLVO theory. Calculations using standard DLVO theory were done for droplets with varying ZP values and no steric layers, while calculations using extended DLVO theory were done for droplets with ZP = 0 mV and varying steric layer thickness. The interaction potentials are in units of kT. Equations and parameters used to generate plots can be found in the *Calculations* section above and the Appendix.

Since the 1940s, the fundamental concepts describing colloid stability have been largely captured by DLVO theory. It explains colloid stability through the interaction potential W, at some distance D, between two droplets, which is a balance between attractive van der Waals and repulsive electrostatic forces (Equation 26). Theoretical interaction potentials were calculated using DLVO theory where all parameters were fixed, except for the ZPs, which were varied from 0 to -50 mV to progressively increase the degree of electrostatic repulsion, and can be seen in Figure 5.4a. At infinitesimally small interdroplet distances, the droplets fall into a "primary minimum" where they are not stable. A "secondary minimum" is established with a rise in an energy barrier due to charge-charge repulsion, which is a stable region for colloidal systems. In Figure 5.4a, for a colloid surface where the ZP is 0 mV (black), only a primary minimum exists. As the ZP magnitude increases, a progressive increase in the energy

barrier is observed. The larger the energy barrier, the more time the droplets spend in the secondary minimum, which demonstrates that an appreciable ZP is crucial for stability.

An important aspect of stability that is not captured by standard DLVO theory is steric hindrance, which arises from adsorbates that are larger and contain bulkier groups in their chemical structure. Especially in nanoemulsion applications where macromolecules such as polymers are adsorbed in multiple layers, the thickness of the steric layer becomes important. Extended DLVO theory accounts for these additional repulsive forces through osmotic and entropic repulsion. Osmotic repulsion occurs when the steric region of two droplets overlaps and the osmotic pressure within the overlap region increases. To offset the increased osmotic pressure, the droplets will repel one another. From an entropic perspective, entropy is decreased in the overlap region where the steric layer is compressed. To re-establish a state with higher entropy, the droplets will again repel.

Extended DLVO theory was applied to calculate the interaction potentials for droplets with ZP values fixed at 0 mV. The only parameter varied was the thickness of the steric layer, as shown in Figure 5.4b. The black trace in Figure 5.4b is the same black trace from Figure 5.4a, calculated with standard DLVO theory, to serve as a visual comparison. Immediately, we see that the energy barrier and secondary minimum is recovered, and the height of the energy barrier increases as the steric layer becomes thicker. This demonstrates that in order to accurately describe the stability of the "uncharged" nanoemulsions we have created, extended DLVO theory is certainly a more fitting model.

Applying Extended DLVO Theory to "Uncharged" Nanoemulsions. It has been demonstrated above that steric effects can provided meaningful elements to the description of colloid stability, especially in systems with marginal electrostatic repulsion such as the "uncharged" nanoemulsions prepared in this work. The top panel of Figure summarizes the interaction potentials calculated for nanoemulsions stabilized with varying concentrations of SDS (Figure a) and with SDS/PNVA complexes (Figure b). The bottom panel of Figure represents a zoomed in perspective of the interaction potentials calculated for the uncharged nanoemulsions using standard (Figure c) and extended (Figure d) DLVO theory. The concentration of PNVA was fixed at 5 mM, while the concentration of SDS varied from 0.1 (orange), 0.5 (green), 1 (blue), and 2.5 (purple) mM.

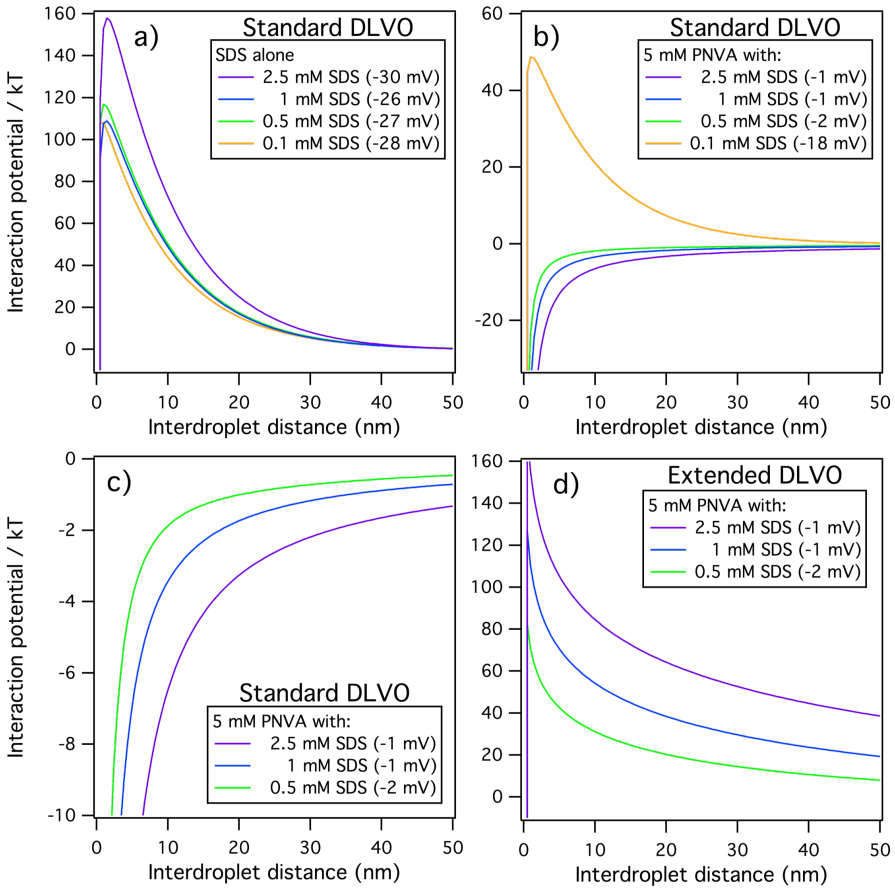

Figure 5.5. *Top panel:* Experimental interaction potentials calculated using standard DLVO theory for nanoemulsions stabilized by (a) SDS alone and (b) SDS/PNVA. *Bottom panel:* Zoomed in plot of interaction potentials calculated with (c) standard and (d) extended DLVO theory for "uncharged" nanoemulsions. The PNVA concentration was fixed at 5 mM, while the SDS concentration was varied between 0.1 (orange), 0.5 (green), 1 (blue), and 2.5 (purple) mM. The interaction potentials are in units of kT.

The stability of surfactant-stabilized nanoemulsions has been well-documented in literature.[1, 2, 4] Thus, it is expected that nanoemulsions stabilized by anionic SDS would be stable due to the high charge density at the droplet surface, as predicted by DLVO theory in Figure 5.5a, which summarizes the interaction potentials for nanoemulsions stabilized with increasing SDS concentrations. Upon the addition of 5 mM PNVA to samples with various SDS concentrations, the magnitude in ZP decreases to a constant level near zero with increased SDS concentrations (Figure 5.1c). The calculated interaction potentials using standard DLVO theory for these samples are shown in Figure 5.5b. At a low SDS concentration of 0.1 mM (orange), the DLVO interaction potential indicates that the remaining ZP is still sufficient to stabilize the

nanoemulsions, while predicting that samples with near-zero ZP are not stable at all. From the zoomed in perspective shown in Figure 5.5c using standard DLVO theory, nanoemulsions prepared with 5 mM PNVA and 0.5 (green), 1 (blue), and 2.5 mM (purple) SDS will immediately fall into the primary minimum and destabilize, according to standard DLVO theory. Without the charge-charge repulsive forces balancing the van der Waals attractive forces, there would indeed be no stabilizing mechanism for the droplets. However, the thickness of the polymer layers has not been accounted for in standard DLVO theory.

Figure 5.5d shows the interaction potentials calculated using extended DLVO theory for nanoemulsions prepared with 5 mM PNVA and 0.5 (green), 1 (blue), and 2.5 mM (purple) SDS. The parameters used to calculate the interaction potentials can be found in Table A.12 of the Appendix. The main distinguishing features between Figures 5.5c and 5.5d are the appearance of the energy barrier and secondary minimum using the extended theory. Note that the energy barrier increases with increasing polymer thickness (green to purple). This demonstrates that as more PNVA adsorbs to the nanoemulsion surface, the stability of the droplets is enhanced. We also note that in order to establish steric stabilization, the thermal energy of the system should exceed the van der Waals attraction.[118] Work done by Morozova et al. has demonstrated that the minimum thickness of the steric layer must adhere to the following criterion:

$$L > \frac{AR}{24k_BT} \tag{35}$$

where L is the steric layer thickness, A is the Hamaker constant for hexadecane-in-water nanoemulsions, R is the droplet radius, k_b is the Boltzmann constant, and T is temperature. Our estimated PNVA (i.e., steric) layer thickness satisfies this criterion, further confirming the stabilizing effects PNVA has on droplets with near-zero ZP.

Counter to standard DLVO predictions, we have demonstrated above that SDS/PNVA-stabilized nanoemulsions exhibiting nearly zero ZP can still be highly stable (Figure 5.3). We predominantly attribute the stability of these droplets to the thick steric layers formed by the adsorption of nonionic PNVA, which is supported by our interaction potential calculations. To account for the steric effects in these nanoemulsions, we applied extended DLVO theory (which has previously been exclusive to hard colloid systems such as nanoparticles)[120, 122] to calculate a different set of interaction potentials shown in Figure 5.5d. Steric hindrance introduces additional repulsive forces that prevent droplet flocculation and coalescence. However, intermolecular interactions between the oil droplet, surface adsorbates, and aqueous medium may also reveal insights that size measurements and DLVO theory cannot

predict. Thus, determining the conformational arrangement of the SDS/PNVA complexes at the droplet surface is highly informative and will be the topic of discussion for the next section.

Interfacial Bonding Effects Contributing to Droplet Stability

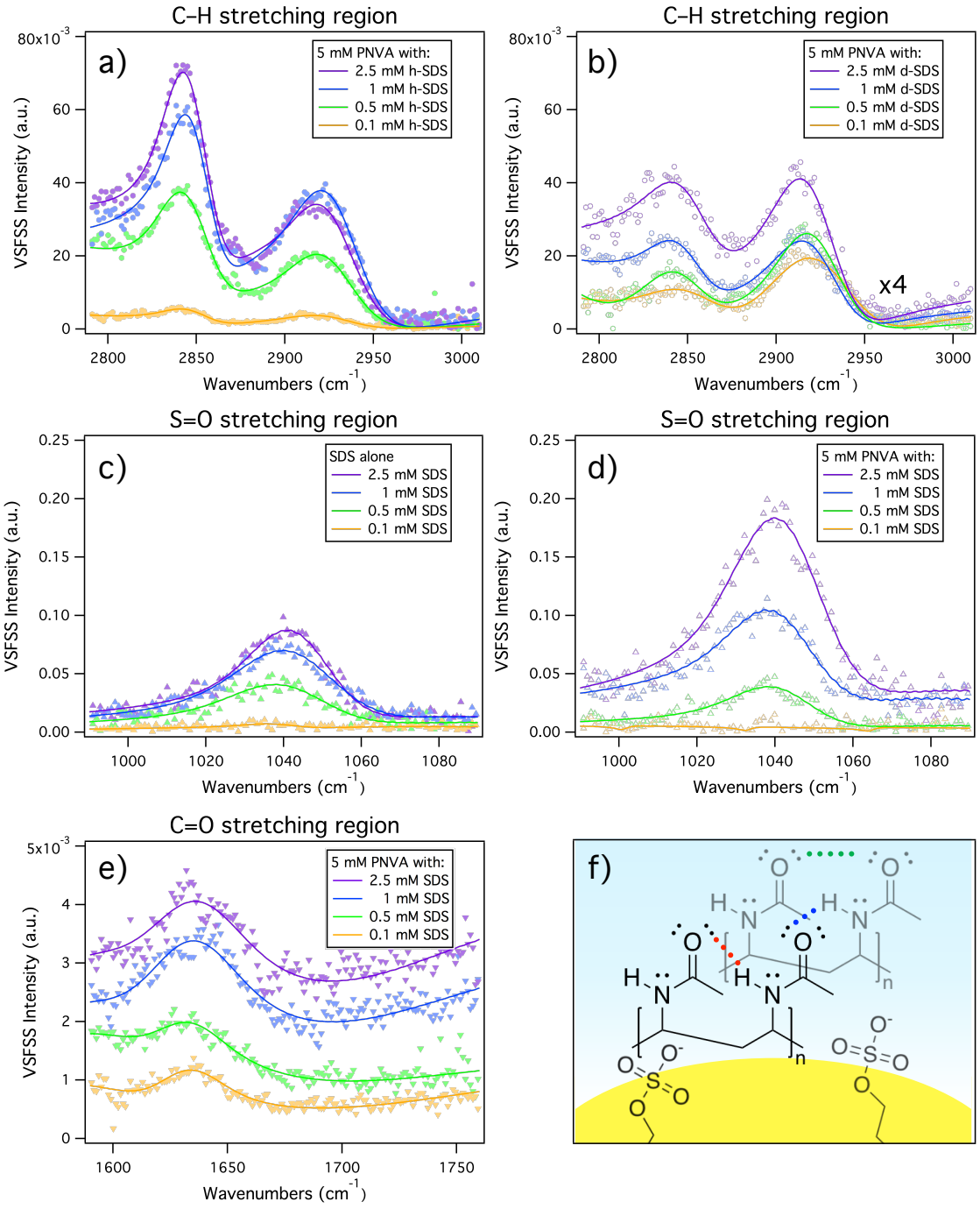

Figure 5.6. *Top panel:* VSFSS measurements of nanoemulsions stabilized by (a) h-SDS/PNVA and (b) d-SDS/PNVA in the C–H stretching region. The spectra were collected in the SSP polarization combination, probing dipole components perpendicular to the droplet surface. Note that the spectra in (b) were scaled by a factor of 4, in order to be plotted on the same intensity scale as the spectra in (a). *Middle panel:* VSFSS measurements of nanoemulsions stabilized by (c) SDS alone and (d) SDS with PNVA in the symmetric S=O stretching region. The spectra were collected in the PPP polarization combination, probing dipole components perpendicular and parallel to the droplet surface. *Bottom panel:* (e) VSFSS measurements of nanoemulsions stabilized by SDS/PNVA in the carbonyl C=O stretching region. The spectra were collected in the SSP polarization combination, probing dipole components perpendicular to the droplet surface. (f) Illustration denoting intra- (red and green dotted lines) and intermolecular (blue dotted lines) interactions between neighboring PNVA strands. For spectra with or without PNVA, the SDS concentrations were 0.1 (orange), 0.5 (green), 1 (blue), and 2.5 (purple) mM. For samples stabilized with both SDS and PNVA, the PNVA concentration was fixed at 5 mM.

Hydrophobic Interactions between PNVA Backbone and SDS Alkyl Chain. Polymer adsorption and self-assembly is often driven by electrostatic interactions between the polymer and the substrate, especially in the cases where the polymer is a polyelectrolyte.[36, 123, 124] However, because PNVA is a nonionic polymer, hydrophobic interactions become more essential in the adsorption process. To investigate the hydrophobic behavior of SDS/PNVA complexes at the oil/water droplet interface, VSFSS measurements of nanoemulsions stabilized by 5 mM PNVA and 0.1 (orange), 0.5 (green), 1 (blue), and 2.5 (purple) mM SDS in the CH stretching region were obtained and are depicted in Figure 5.6 (top panel). All spectra shown here were collected in the SSP polarization scheme, which probes dipole components perpendicular to the droplet surface. Figure 5.6a are spectra collected with standard hydrogenated SDS (h-SDS) and PNVA, which provide insight into the net conformational ordering of the SDS/PNVA complexes. In order to decouple the CH resonances of the SDS alkyl chain from the PNVA backbone, deuterated SDS (d-SDS) was used in place of h-SDS. This redshifts the CH resonances of SDS and thus, all sum frequency responses shown in Figure 5.6b are attributed solely to PNVA. We note that the spectra shown in Figure 5.6b were scaled by a factor of 4 in order to be clearly plotted on the same axis scale as the spectra in Figure 5.6a. The CH resonances observed near ~2850, 2890, and 2930 cm^{-1} correspond to the methylene CH_2 symmetric stretch, the methyl CH_3 symmetric stretch, and the methylene CH_2 asymmetric stretch, respectively, and are typical of CH containing surfactants and polymers.[59, 125]

Figure 5.6a shows the SF intensity increasing with increasing bulk h-SDS concentration. As the nanoemulsions are coated with both h-SDS and PNVA, the observed increase in intensity may be attributed to a few factors. A higher bulk h-SDS concentration can result in a greater population of h-SDS at the interface, which can consequently recruit more PNVA to adsorb. Additionally, a higher interfacial concentration of h-SDS/PNVA complexes can induce a stronger degree of net orientation within the surfactant tails and PNVA backbones via hydrophobic interactions. While these are all possible explanations for the progressively increasing SF intensity, it is not possible to decouple the contributions from h-SDS to those from PNVA, which is where utilizing deuterated SDS becomes important. The fit parameters can be found in Table A.13 of the Appendix.

Figure 5.6b shows the spectra of nanoemulsions stabilized by d-SDS and PNVA. Since d-SDS no longer contains CH resonances, all SF intensity observed here describes PNVA interfacial behavior and conformational ordering. As the bulk PNVA concentration is fixed at 5 mM, enhancement in the SF response is attributed to enhanced PNVA adsorption with increasing surfactant concentration, thus forming a thicker polymer layer. The increased SF intensity with increasing d-SDS concentration in Figure 5.6b can also be explained by PNVA adopting a stronger net orientation around the droplet surface. However, we believe a higher PNVA population adsorbing to the surface is a more likely interpretation as it is consistent with our nanoemulsion size measurements above (Figure 5.1b), depicting that droplets coated with SDS and PNVA are substantially larger in diameter than those coated with SDS alone. This is also in agreement with extended DLVO calculations above (Figure 5.5d), predicting that a thick steric layer is a considerable stabilizing factor for droplets with negligible ZP values. Figure 5.6b also illustrates that the PNVA backbone maintains a net orientation upon adsorption, likely forming strongly bonded polymer networks. Previous work in literature has reported polymer self-assembled structures to result in a stratified, interpenetrated network of polymer strands.[126–129] This network is formed through complex interactions between the polymer and neighboring species. Thus, it is likely that the net orientation of the PNVA backbone allows the polymer strands to partake in such interactions, leading to the formation of a rigid network. Table A.14 in the Appendix shows the peak assignments and fitting parameters used to fit spectra shown in Figure 5.6b.

We conclude that the hydrophobic portions of the SDS/PNVA complexes formed at the nanoemulsion surfaces have conformationally ordered surfactant alkyl tails and polymer backbones. The enhancement in adsorbed PNVA due to increasing

amounts of interfacial SDS suggests that the thick polymer layers are preventing the "uncharged" droplets from coalescence and immediate destabilization.

Bonding Environment around SDS Headgroup. Further insights into the molecular nature of the SDS/PNVA co-adsorption can be obtained from spectroscopic measurements of the polar regions of the surfactant and polymer. One would expect that the SDS head groups rest directly at the nanoemulsion surface, interacting with interfacial water and the co-adsorbed PNVA. The bonding interactions between the sulfate head group and other interfacial species can highlight additional sources of droplet stability. Figure 5.6 (middle panel) shows VSFSS spectra in the symmetric S=O stretching region of nanoemulsions stabilized by SDS alone (Figure 5.6c) and SDS/PNVA (Figure 5.6d).[58, 130–132] The PNVA concentration was fixed at 5 mM, while the SDS concentration varied between 0.1 (orange), 0.5 (green), 1 (blue), and 2.5 (purple) mM. These spectra were collected in the PPP polarization combination, probing perpendicular and parallel dipole components relative to the interface.

In both Figures 5.6c and 5.6d, the SF intensity of the symmetric S=O stretch near ~1040 cm^{-1} increases with increasing SDS concentration. For nanoemulsions stabilized with 0.1 and 0.5 mM SDS alone (Figure 5.6a) or in conjunction with PNVA (Figure 5.6b), the SF intensities were of comparable magnitude (see Table A.15 and A.16 in the Appendix for fitting parameters). However, samples containing 1 and 2.5 mM SDS *without* PNVA are appreciably lower in intensity. Our nanoemulsions are initially prepared with only SDS; PNVA is then added afterward and allowed to adsorb. Thus, we attribute the relative increase in the SF response between SDS alone (Figure 5.6c, blue and purple) versus SDS/PNVA (Figure 5.6d, blue and purple) to more highly oriented SDS head groups, induced by a thicker steric PNVA layer. Note that the largest nanoemulsions with the lowest magnitude ZP (Figure 5.1) were also prepared with 1 and 2.5 mM SDS in conjunction with PNVA. Alternatively, an increase in SDS adsorption (and thus, population) driven by PNVA adsorption would also increase the intensity of the S=O resonance. However, this interpretation is unlikely, as it is not supported by our ZP measurements above (Figure 5.1c). If PNVA encouraged more SDS to adsorb, the ZP would consequently become more negative, rather than remain nearly neutral.

As discussed above, strongly bonded networks of polymer strands would induce more rigidity to the SDS/PNVA complex at the droplet interface. This rigidity would reduce the possible orientations the SDS headgroups could adopt, resulting

in a stronger net alignment, as observed in Figure 5.6d. The enhancement in the SDS net ordering due to the presence of PNVA provides insight into the interfacial chemistry occurring at the boundary of the oil droplet and the PNVA layers. To investigate how the steric PNVA layer bonds with its environment at the droplet surface, we need to probe other functional groups on PNVA.

Bonding Environment around PNVA Monomer Units. The polar regions of PNVA are composed of secondary amide functional groups, with a carbonyl C=O resonance. This vibrational mode is sensitive to changes in bonding environment due to intermolecular forces that are attracted to the lone pairs of electrons on the oxygen. Figure 5.6e shows VSFSS spectra, collected in the SSP polarization scheme, of nanoemulsions stabilized by SDS/PNVA in the amide C=O stretching region.[125, 133–135] Again, the PNVA concentration was fixed at 5 mM, while the SDS concentration varied from 0.1 (orange), 0.5 (green), 1 (blue), to 2.5 (purple) mM. The carbonyl spectral region has been notoriously difficult to probe due to a highly intense nonresonant response that obscures any resonant responses from the species of interest.[136, 137] In order to measure the resonant C=O responses from PNVA, the visible pulse was carefully de-timed from the IR pulse by ~500-600 fs, to remain within the vibrational lifetime of C=O stretching resonance.[138] This detiming approach allows for the resonant response to be measured, while minimizing any unwanted overlapping contributions.[139–141] Its presence indicates that as the polymer adsorbs to the interface, it does so with the carbonyl mode adopting a net orientation perpendicular to the interface as opposed to solely random in orientation. Though this method has allowed us to capture a discernible peak from the C=O resonances, we note the presence of a residual elevated background in all spectra is still present. This background is likely manifested from the initial broad nonresonant response that was minimized, but not fully eliminated. Additionally, an elevated background can also be attributed to a variety of effects including: $\chi^{(3)}$ contributions, dispersive D_2O background, and a nonresonant contribution from the calcium fluoride window containing our sample.[54, 142–144]

In order to fit the C=O stretching region and obtain meaningful information on the C=O resonance, two non-physical background peaks were identified and incorporated into the fits. We emphasize that these background peaks do not present physical meaning, but rather allow us to properly fit the C=O mode of interest. Using the spectrum with the lowest C=O response (0.1 mM SDS/5 mM PNVA), two background peaks were placed at 1593 and 1777 cm^{-1}. The peak parameters were determined and fixed for all spectra in Figure 5.6e, except the peak amplitude. The background peak

amplitudes were allowed to vary because the elevated background intensity visibly varies for different samples. In doing so, we were able to fit the C=O stretching region for nanoemulsions stabilized by SDS/PNVA and extract the fit parameters shown in Table A.17 of the Appendix. This process has allowed us to fit our spectra to a peak near ~1630 cm^{-1}, corresponding to the "associated" C=O stretch for secondary amides.[125, 133–135]

Table 5.1. Fitting parameters for spectra of SDS/PNVA stabilized nanoemulsions in the C=O stretching region, corresponding to Figure 5.6e. Note that the parameters for the arbitrary background peaks have been omitted for clarity. Complete fit parameters can be found in Table A.17.

Fixed [PNVA] = 5 mM		SDS concentration:			
Peak assignment	**Parameter**	**[SDS] = 0.1 mM**	**[SDS] = 0.5 mM**	**[SDS] = 1 mM**	**[SDS] = 2.5 mM**
C=O stretch	Amplitude	0.01 ± 0.001	0.01 ± 0.001	0.03 ± 0.001	0.03 ± 0.002
	Phase	0	0	0	0
	Lorentzian	5	5	5	5
	Peak position	1629 ± 1	1628 ± 1	1629 ± 1	1629 ± 1
	Gaussian	14 ± 1	15 ± 2	20 ± 1	21 ± 2

The fit parameters for specifically the C=O peak are provided in Table 5.1 for easy reference. It can be seen that while the changes in peak amplitude are negligible, the Gaussian width broadens with increasing SDS concentration as well as with increasing thickness of the PNVA layer. This indicates that as more PNVA adsorbs to the droplet surface, there is an increase in molecular bonding between the interfacial species. A strongly bonded PNVA network would provide avenues for both *intra*– and *inter*molecular forces to exist, as illustrated in Figure 5.6f. Among the monomer units of PNVA, hydrogen bonding can occur *intra*molecularly between the N–H and the C=O moieties (illustrated by the red dotted lines). Additional hydrogen bonding can occur *inter*molecularly between the polymer N–H and C=O groups on neighboring strands (illustrated by the blue dotted lines), as well as the C=O group and interfacial water molecules. Carbonyl "head-to-head" interactions (i.e., C=O⋯C=O) are also common and will impart more stiffness to the adsorbed polymer layers (illustrated by the green dotted lines). These types of molecular interactions are consistent with what has been observed for other carbonyl-containing species.[125, 145–148] Ultimately, the broadening of the Gaussian width supports the interfacial picture that a stratified, rigid polymer network is contributing greatly to droplet stability.

Conclusions

Interfaces are ubiquitous in nature and present in various applications. Thus, the knowledge around chemical processes that occur at the junction of two immiscible liquids is highly valuable. Specifically, the interest surrounding oil and water has been predominantly motivated by efforts to develop safer dispersants for oil remediation, design stimuli-responsive nanocarriers for drug delivery, and understand complex mechanisms that contribute to oil-in-water emulsion stability. While nanoemulsions are widely prevalent in several applications, their stability is often a limiting factor in their versatility. Colloid stability has been primarily described by DLVO theory, which relates the stability to a balance of attractive van der Waals and repulsive electrostatic forces. The problem that arises with an "uncharged" nanoemulsion surface is the lack of repulsive charge-charge repulsion between neighboring droplets. As DLVO theory would predict, such a colloid system would have very minimal stability.

In the work presented in this chapter, we have created nanoemulsions stabilized by anionic surfactant SDS and nonionic PNVA, with ZP measuring ~0 mV. Contrary to what standard DLVO theory would predict, these "uncharged" nanoemulsions are stable upward to 35 days with robust size distributions and constant PDI values indicative of sample monodispersity. In order to more accurately model the stability of these nanodroplets, we applied extended DLVO theory to calculate interaction potentials that would imply a stable colloid system. We learn that the added steric effects from the PNVA layer result in additional repulsive forces that prevent immediate coalescence and destabilization.

By employing surface-specific VSFSS, we were able to confirm the presence of both the surfactant and polymer at the nanodroplet surface and develop a molecular-level understanding of how the conformational arrangement and adsorption behavior of SDS and PNVA complexes contribute to the emulsion stability. As illustrated in Figure 5.6f, the probing of interfacial C–H, S=O, and C=O vibrational modes reveals that the SDS/PNVA complexes formed at the droplet surface are in a stratified, strongly bonded network of polymer strands. The adsorbed PNVA strands interact *intra*molecularly with neighboring monomer units and *inter*molecularly with neighboring polymer strands and interfacial water molecules. This ultimately forms a rigid network that acts as a stabilizing mechanism for these "uncharged" droplets.

All in all, we have illustrated that nanoemulsions with negligible ZP can be created without them immediately coalescing. By explicitly accounting for steric effects, the extended DLVO theory underlines the importance of accounting for factors such as

steric hindrance in colloid stability. Additionally, the conformational ordering of the SDS/PNVA complexes and especially the arrangement of the PNVA layers upon adsorption are crucial stabilizing factors that DLVO theory, size, and ZP measurements alone cannot capture. Our findings provide insight into the basic science behind the interfacial phenomena aiding the stabilization of oil droplets via nonionic species, expanding the applicability of "uncharged" nanoemulsions.

CHAPTER VI

ZWITTERIONIC SURFACTANTS AND CO-STABILIZERS

This work was not yet published, but under review at the time this dissertation was submitted. Emma Tran designed the study, performed some of the experiments, analyzed the data, and wrote the manuscript. Konnor Jones and Gabrielle Cano performed some of the experiments and provided general feedback on the manuscript. Frederick Moore provided editorial assistance and general feedback on the manuscript. Lawrence Scatena was the principal investigator for this work and provided editorial assistance and general feedback.

Introduction

Amphiphilic molecules such as surfactants play a significant role in diverse processes including emulsification,[149] foaming,[150–152] interfacial property modification,[153–155] excipient formulation,[156, 157] drug delivery,[158, 159] environmental remediation[155, 160] and oil recovery.[161, 162] While surfactants have hydrophobic and hydrophilic regions, their structural details vary. Surfactant head groups generally fall into two classes: charged (i.e., anionic or cationic) and uncharged (i.e., nonionic or zwitterionic).[163] While there exists an exhaustive body of literature on the former, studies investigating the latter are an active area of research. The shift to understanding uncharged surfactants was motivated by the desire and need to incorporate more environmentally compatible chemicals into applications involving pharmaceuticals, environmental remediation, and food science. Nonionic and zwitterionic surfactants have been shown to be less ecotoxic and more biodegradable, while still exhibiting sufficient emulsifying and foaming capabilities, but details are still largely lacking.[164–166] Thus, investigating the interfacial properties and behavior of such surfactants at a molecular-level will yield additional insight and knowledge that can promote their usage in various formulations.

In this chapter, we focus on the zwitterionic surfactant dodecyl-N,N-dimethyl-3-ammonio-1-propanesulfonate (DDAPS) and investigate its interfacial behavior in the presence of different co-additives at both a planar and droplet (e.g., nanoemulsion) oil/water interface. DDAPS adsorbs spontaneously to a planar interface, but for nanoemulsions, the interface is formed through ultra-sonication and DDAPS's presence at the interface stabilizes the droplet surface. The self-assembly of ionic surfactants

at planar and colloidal surfaces has been studied to a great extent. Relatively, little work has been done to understand how zwitterionic surfactants behave at a planar versus droplet (i.e. curved) interface–and this is especially pertinent to oil spill remediation via chemical dispersant systems. In this application, a large oil slick is doused with a mixture of surfactants that are intended to disperse the oil slick into smaller oil droplets. Once the oil droplets are small enough, microbes can then naturally degrade the oil.[167, 168] In this example, the large oil slick is the thermodynamically stable, planar oil/water interface; while the dispersed oil droplets are the kinetically stable, curved oil/water interface. Thus, by comparing the two interfacial geometries, we are able to learn how DDAPS's behavior in the presence of different co-additives varies between systems governed by different energetics. The co-additives in this study include salts and charged surfactants to mimic a more application-relevant environment.[169, 170]

By utilizing interfacial tensiometry coupled with surface-specific vibrational spectroscopic techniques, we were able to elucidate the molecular-level details of DDAPS adsorption and molecular conformational ordering with and without co-additives. Traditional sum frequency (SF) spectroscopy was employed to investigate DDAPS at the planar oil/water interface, while sum frequency scattering spectroscopy was used to probe the nanoemulsion surface. The results confirm that the interfacial geometry has an effect on DDAPS's interfacial behavior, as well as the interactions between DDAPS and co-additives. DDAPS alone adsorbs to the planar oil/water interface with a net conformational ordering of its alkyl tails that is unaffected by the presence of co-additives. At the droplet oil/water interface, however, the co-additives have a more pronounced effect on DDAPS adsorption and net ordering and play an essential role in nanoemulsion stabilization. Therefore, formulations incorporating DDAPS in nanoemulsion formation necessitates co-additives such as salts or other surfactants.

The surface activity of surfactant solutions can provide insight into their emulsifying and oil dispersing capabilities. For example, highly surface-active species will readily adsorb to an interface and reduce the interfacial tension (IFT) considerably, making them effective emulsifiers.[149, 171, 172] While zwitterionic surfactant DDAPS at a concentration of 0.05 mM lowers the IFT of hexadecane and water from ~55 mN/m[173] to 20.669 ± 1.021 mN/m (dashed horizontal line in Figure 6.1), the presence of co-additives is expected to further reduce the IFT.

Figure 6.1 shows the IFT of 0.05 mM DDAPS in conjunction with varying amounts of NaCl (a, blue markers) and $MgCl_2$ (b, green markers). The salt concentrations were increased from 0.01 mM (○) to 0.1 mM (□), and finally to 1 mM (△). The horizontal dashed line present in all IFT plots represents the equilibrated IFT of 0.05 DDAPS alone, without any co-additives. This line serves as a visual guide for comparing the surface activity of DDAPS alone versus DDAPS with co-additives.

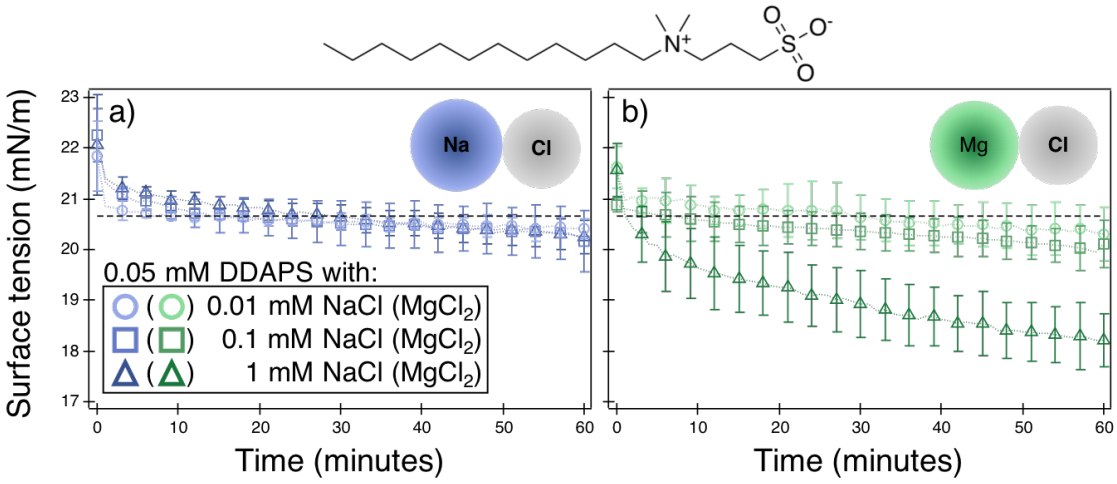

Figure 6.1. IFT as a function of time for solutions of 0.05 mM DDAPS with varying NaCl (a, blue markers) and $MgCl_2$ (b, green markers) concentrations at a hexadecane/water interface. The salt concentrations were varied from 0.01 mM (○), 0.1 mM (□), and 1 mM (△). The dashed horizontal line indicates the equilibrated IFT value of 0.05 mM DDAPS alone, absent of any salt additives. The molecular structure of DDAPS is shown above the IFT panels.

From Figure 6.1a, it can be seen that both salts lower the IFT, but to different degrees. In solutions containing DDAPS+NaCl, the IFT was not reduced significantly beyond that exhibited by DDAPS alone. This is in contrast (Figure 6.1b) to solutions

containing DDAPS+$MgCl_2$ where the IFT decreases substantially, specifically with 1 mM $MgCl_2$. IFT reduction in the presence of salts is a phenomena attributed to the screening effect, which allows more surfactants to adsorb by decreasing charge-charge repulsion between neighboring surfactant head groups.[150, 174, 175] The impact charge screening has on the surface activity is more pronounced with $MgCl_2$ than NaCl, likely due to the differences in ionic strength and valency of the cations.

In a study investigating DDAPS on foam stability, Varade et al. showed that the effects monovalent salts (including NaCl) have on DDAPS's surface activity is relatively small compared to the effects on ionic surfactants, which supports our IFT results.[150, 151, 175] For ionic surfactants, charge screening allows for more surfactant molecules to populate the interface because one ion is electrostatically attracted to the surfactant head group, whether it be positive or negatively charged. This reduces the electrostatic repulsion between neighboring surfactant head groups and allows surfactants to pack more tightly, ultimately increasing the population of surfactants at the interface. In the case of zwitterionic surfactants, while there are attractive interactions between the Na^+ and Cl^- ions with the sulfonate and quaternary ammonium regions, respectively, on the DDAPS head group, there are also repulsive interactions between ions and head group regions with like charges (e.g., Na^+ and the quaternary ammonium regions). The net result is that monovalent salts have minimal effect on DDAPS surface activity.[150, 151] $MgCl_2$ on the other hand, reduces the IFT to a greater degree than NaCl. This can be attributed to the sulfonate region of the DDAPS head group having a greater binding affinity to the divalent Mg^{2+} cation over the monovalent Na^+ cation.[176] This affinity, specific to divalent cations, can further screen neighboring sulfonate groups, increase surfactant packing, and allow for more DDAPS to adsorb–all of which explains the reduction in IFT at higher $MgCl_2$ concentrations.

In addition to salts, mixed or co-surfactant systems have also been shown to interact synergistically to achieve a greater reduction in the IFT than the individual components.[177–179] Thus, we investigate how the surface activity of DDAPS+SDS solutions compares to that of DDAPS+DTAB. Figure 6.2 contains the IFT traces of 0.05 mM DDAPS with increasing amounts of d-SDS (a, pink markers) and d-DTAB (b, purple markers). The co-surfactant concentrations were increased from 0.01 mM (○) to 0.1 mM (□), and finally to 1 mM (△). Again, the horizontal dashed line denotes the equilibrated IFT of 0.05 DDAPS alone, serving as a visual guide. We note that the use of deuterated SDS and DTAB here is simply to maintain experimental consistency between our tensiometry and spectroscopic measurements

(to be discussed later).

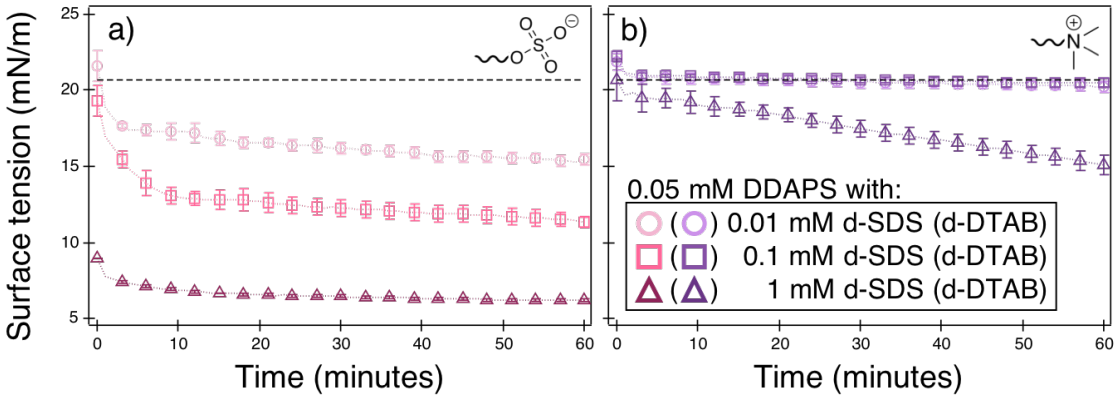

Figure 6.2. IFT as a function of time for solutions of 0.05 mM DDAPS with varying SDS (a) and DTAB (b) concentrations at a hexadecane/water interface. The surfactant concentrations were varied from 0.01 mM (○), 0.1 mM (□), and 1 mM (△). The dashed horizontal line indicates the equilibrated surface tension value of 0.05 mM DDAPS alone, absent of any co-surfactants.

Clearly, co-surfactants have a greater impact on the surface activity of the system than the salts, which is inherently due to the addition of more surfactants (i.e. d-SDS and d-DTAB) in solution. While salts can enhance the adsorption of DDAPS through charge screening, the salts themselves do not directly affect the IFT because they do not disrupt the hydrogen-bonding network at the interface, as surfactants do.[180, 181] Co-surfactants, on the other hand, may encourage more DDAPS to adsorb via synergistic interactions, and also play a direct role in reducing the IFT. By comparing the effects d-SDS and d-DTAB has on the surface activity of the mixture, it is clear that with d-SDS as the co-surfactant, there is a much greater reduction in the IFT overall. The IFT of DDAPS+d-SDS solutions decreases progressively as the concentration of d-SDS increases from 0.01 mM to 1 mM.

In the presence of d-DTAB, however, the reduction in the IFT does not become significant until d-DTAB is at a concentration of 1 mM (dark purple △). The difference in surface activity between DDAPS+d-SDS versus DDAPS+d-DTAB indicates stronger synergistic effects when an anionic surfactant is present. This can be due to d-SDS being more surface active than d-DTAB, effectively increasing the total number of surfactants at the interface.[182] The zwitterionic head group of DDAPS provides separate hydrophilic regions that can interact differently with d-SDS versus d-DTAB. The interactions between DDAPS+d-SDS results in a tighter packing of the alkyl

tails than DDAPS+d-DTAB, subsequently allowing more surfactants to adsorb and further reduce the IFT. It is possible that steric hindrance from the –($CH_2CH_2CH_2$)– between the DDAPS quaternary ammonium and sulfonate head groups prevent d-DTAB from interacting effectively with the DDAPS sulfonate group.[150, 161] This hypothesis is revisited in later sections using our surface spectroscopic technique.

Adsorption and net ordering of DDAPS at a planar oil/water interface

IFT measurements provide valuable information on the relative population of adsorbed surfactants, but do not provide molecular-level details about the net ordering of adsorbed species. To obtain such a perspective, we employ vibrational sum frequency spectroscopy (VSFS) to measure the vibrational resonances of the DDAPS alkyl tails at the planar interface. Figure 6.3 shows VSFS spectra measured in the CH stretching region of DDAPS at a planar CCl_4/water interface. The DDAPS concentrations were increased from 0.05 mM (light gray ○) to 0.5 mM (gray □) and finally to 5 mM (dark gray △). All spectra were collected in the SSP polarization scheme, which probes dipole components perpendicular to the interface. The resulting peaks are characteristic of CH vibrational resonances, which are summarized in Table 6.1 and consistent with phase-sensitive SFG results conducted at the air/water interface by Mafi et al.[163, 183] Details on the fitting routine and exact fit parameters can be found in Table A.18 of the Appendix and elsewhere.[33, 34, 65, 184] The inset in Figure 6.3 shows the d^+/r^+ ratio as a function of DDAPS concentration. The d^+/r^+ ratio allows relative net ordering of surfactants to be quantified.[54, 55, 59] A higher (lower) d^+/r^+ ratio indicates surfactant tails that are less (more) ordered.

Table 6.1. Characteristic CH resonances at an oil/water interface.[12, 185]

Peak assignment	Notation	Wavenumber (cm^{-1})
CH_2 symmetric stretch (s.s.)	d^+	2846
CH_3 symmetric stretch (s.s.)	r^+	2874
CH_2 asymmetric stretch (a.s.)	d^-	2916
CH_2 s.s. Fermi resonance (F.R.)	d^+_{FR}	2890-2930
CH_3 s.s. Fermi resonance (F.R.)	r^+_{FR}	2933
CH_3 asymmetric stretch (a.s.)	r^-	2962

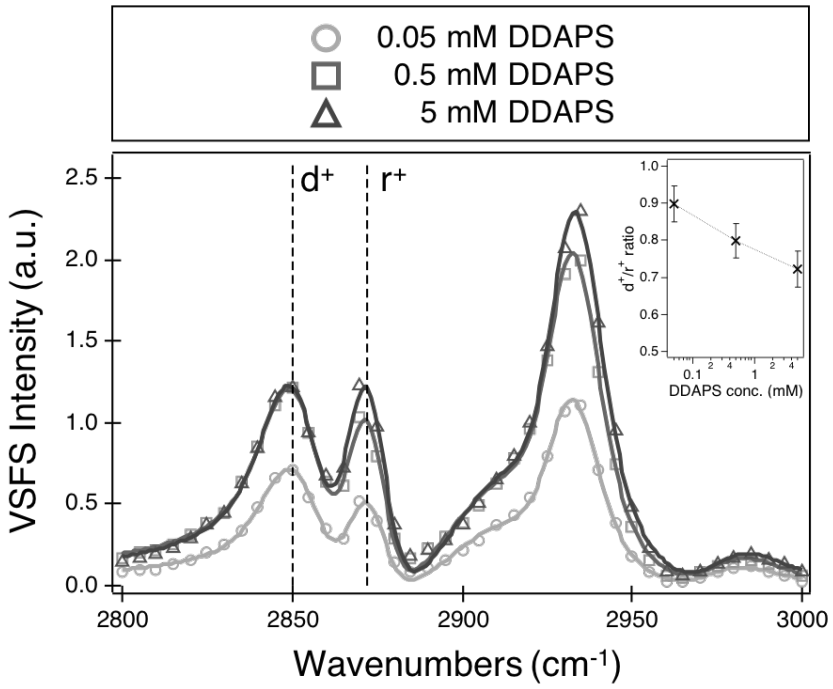

Figure 6.3. VSFS measurements of DDAPS solutions at a planar CCl_4/water interface. The DDAPS concentrations varied from 0.05 mM (light gray ○), 0.5 mM (gray □), and 5 mM (dark gray △). All spectra were collected with the SSP polarization scheme, probing molecular dipole moments perpendicular to the interface. The dashed vertical lines denote the CH_2 (d^+) and CH_3 (r^+) symmetric stretches. The inset depicts the d^+/r^+ ratio as a function of DDAPS concentration.

As the bulk DDAPS concentration increases from 0.05 mM to 0.5 mM, there is an increase in overall SF intensity, as well as a decrease in the d^+/r^+ ratio (Figure 6.3, inset), which is indicative of more tightly packed alkyl tails.[12, 54, 55, 59] Increasing the DDAPS concentration another magnitude from 0.5 to 5 mM yields minimal change in the overall SF intensity, but the d^+/r^+ ratio continues to decrease. Once an interface is saturated with surfactants, there are less gauche defects along the alkyl tails, which decreases the CH_2 s.s. (d^+) signal and increases the CH_3 s.s. (r^+). In Figure 6.3, comparing the intensities of the d^+ and r^+ peaks of 0.5 and 5 mM DDAPS, we observe no change in the d^+ amplitude, but an increase in the r^+ amplitude. This result illustrates that the interface is not yet completely saturated with DDAPS, but is becoming more populated, which induces a stronger net alignment of the r^+ resonances (and hence, an increased r^+ signal). If the interface resembled that of a fully packed DDAPS monolayer absent of any gauche defects, we would expect a decrease in the d^+ intensity, as the dipoles causing the d^+ signal would cancel. In other words, the CH_2 symmetric stretches are in a centrosymmetric environment and

thus, SF-inactive. This effect is not observed for the concentrations of DDAPS we investigated.

Now that we have developed an understanding of how DDAPS behaves at a planar oil/water interface on its own, we can investigate how co-additives such as salts and other surfactants influence its interfacial properties. As mentioned above, co-additives can cause synergistic effects that enhance the overall surface activity of the system, which can affect the packing and arrangement of interfacial species. Further, the importance of these co-additives will be underlined in later sections where we discuss the formation of nanoemulsions with DDAPS.

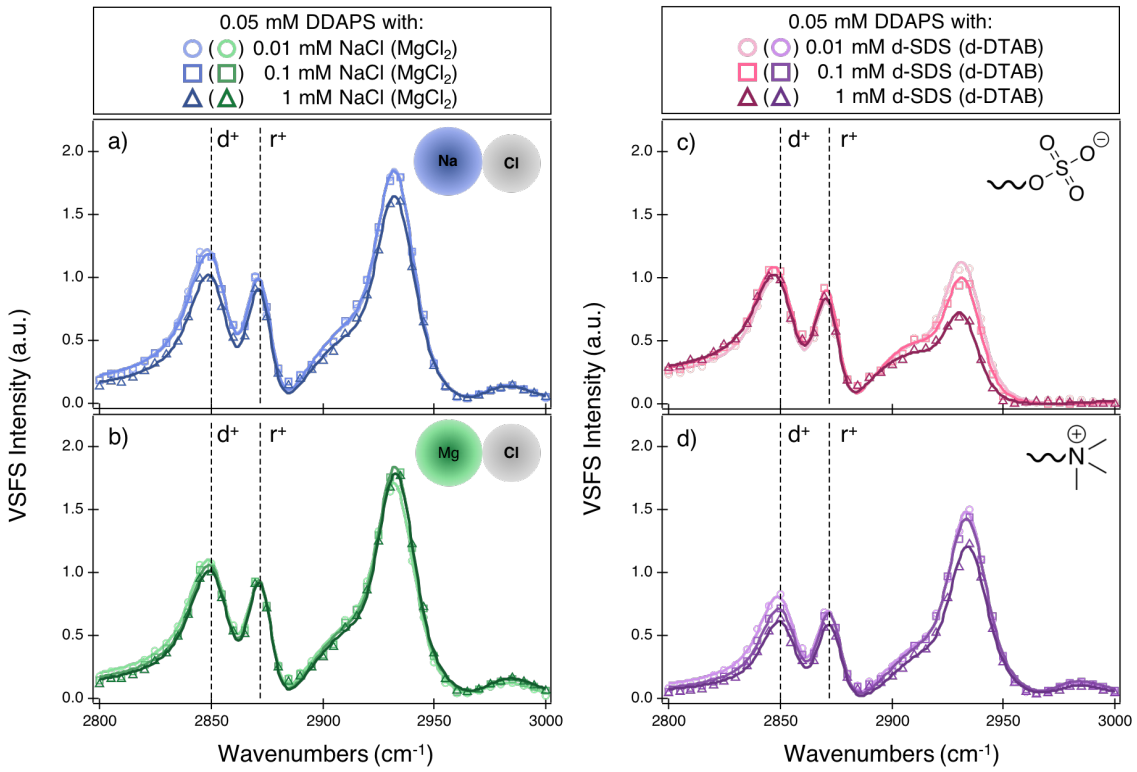

Figure 6.4. VSFS measurements of DDAPS and co-additive solutions at a planar CCl_4/water interface. The co-additives include NaCl (a, blue), $MgCl_2$ (b, green), d-SDS (c, pink), and d-DTAB (d, purple). The DDAPS concentration was fixed at 0.05 mM while the co-additive concentrations varied from 0.01 mM (○), 0.1 mM (□), and 1 mM (△). All spectra were collected with the SSP polarization scheme, probing molecular dipole moments perpendicular to the interface. The dashed vertical lines denote the CH_2 (d^+) and CH_3 (r^+) symmetric stretches.

Now that we have an understanding of how DDAPS alone orients itself at an oil/water interface, we begin to add co-additives and measure their effects. Figure 6.4 shows VSFS spectra collected in the CH stretching region of DDAPS solutions in

conjunction with different co-additives, including NaCl (a, blue), $MgCl_2$ (b, green), d-SDS (c, pink), and d-DTAB (d, purple). The DDAPS concentration was fixed at 0.05 mM, while the concentrations of co-additives varied between 0.01 mM (○), 0.1 mM (□), and 1 mM (△). All spectra shown here were collected with the SSP polarization combination. Since the primary focus of this study is to probe the DDAPS alkyl tails, deuterated co-surfactants (i.e., d-SDS and d-DTAB) were used to prevent spectral overlap of the DDAPS CH resonances with those of the co-surfactants.

While the overall surface activity of the system varies from the type and concentration of the co-additive, the net ordering of the DDAPS tails does not significantly change. From Figure 6.4, it can be seen that the CH spectral features representing the DDAPS tails are very similar across co-additives and concentrations, especially in the presence of $MgCl_2$. With d-SDS and d-DTAB, the SF intensity from the DDAPS alkyl tails decreases with increasing co-additive concentration. Fit parameters can be referenced in the Appendix, Tables A.19–A.22. Recall that IFT results above show that the lowest IFT is achieved when the co-surfactants are in excess, as the density of adsorbed surfactants is highest. Thus, the decrease in SF intensity observed here demonstrates that the co-surfactants (i.e., d-SDS or d-DTAB) are replacing DDAPS at the interface when they are in excess.

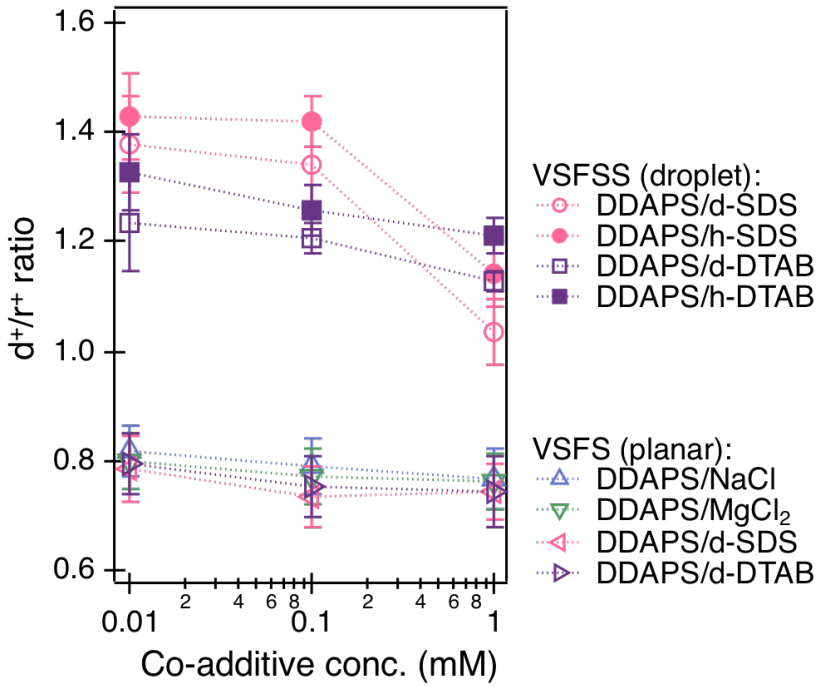

Figure 6.5. d^+/r^+ ratio of DDAPS and various co-additives at both interfaces. For VSFS measurements at the planar interface, the co-additives were NaCl (blue △), $MgCl_2$ (green ▽), d-SDS (pink ◁), and d-DTAB (purple ▷). For VSFSS measurements at the droplet interface, the co-additives were d-SDS (pink ○), h-SDS (pink ●), d-DTAB (purple □), and h-DTAB (purple ■).

The influence of each co-additive on DDAPS net conformational ordering at the planar oil/water interface is minimal, as demonstrated by the similar d^+/r^+ ratios in Figure 6.5 (open triangles). Note the d^+/r^+ ratios calculated from VSFSS data will be discussed in later sections. The differences in SF amplitude for some mixtures, are minor and do not suggest that DDAPS's interfacial net ordering is dependent on the type or concentration of co-additives. The insights gained from these planar studies will aid in our investigation of these mixed systems on nanoemulsion formation and how co-additives contribute to emulsion stability.

Zwitterionic DDAPS on nanoemulsion formation

We now investigate how DDAPS and co-additives interact to stabilize oil droplets in water. Kinetically stable oil droplets dispersed in water (i.e., nanoemulsions) can be created by ultrasonicating small amounts of oil into an aqueous solution of emulsifiers or surfactants. Nanoemulsions are generally ~100s of nanometers in diameter and the droplet distribution should have a polydispersity index < 0.3 to be considered monodispersed and appropriate for applications.[149, 171, 172] Common surfactants such as SDS and DTAB are very effective emulsifiers and oil dispersants on their own. Interestingly, zwitterionic DDAPS alone (0.1–5 mM) does not form nanoemulsions. Despite reducing the IFT of hexadencane/water by ~34 mN/m (Figure 6.1) and its net orientation at the planar CCl_4/water interface suggesting a closely packed monolayer (Figure 6.3), DDAPS is not effective at stabilizing nanoemulsions unless co-additives are also present.

Figure 6.6 summarizes droplet diameter (a) and ζ-potential (b) measurements for oil-in-water emulsions stabilized by 0.05 mM DDAPS and varying concentrations of different co-additives. The co-additives include NaCl (blue ◇), $MgCl_2$ (green △), SDS (pink ○), and DTAB (purple □) ranging from 0.01 to 1 mM. The emulsion diameters increased with increasing concentrations of salt, especially in the presence of $MgCl_2$, but were not as affected by increasing concentrations of co-surfactants. Under all concentrations of SDS and DTAB, the nanoemulsion diameters remained below 500 nm, but at high concentrations of NaCl and $MgCl_2$, the diameters

enter the size regime of 'macroemulsions' (i.e., diameter ~1-100 μm). This is important to note for two reasons: 1) emulsions classified under this category are only weakly kinetically stable and thus, governed by different energetics compared to nanoemulsions; 2) the theory behind sum frequency scattering from spherical droplets begins to break down for larger particle diameters.[14, 17] With these two notions in mind, we do not probe oil droplets larger than 800 nm in diameter with our VSFSS technique.

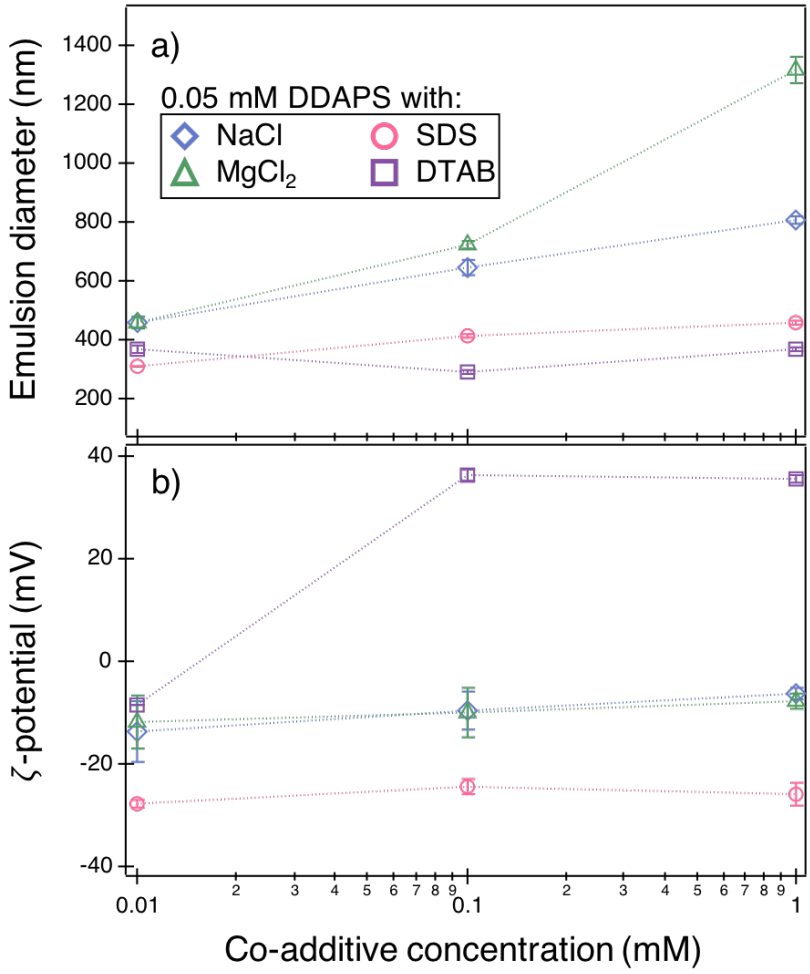

Figure 6.6. Diameter (a) and ζ-potential (b) measurements of oil-in-water emulsions stabilized by 0.05 mM DDAPS and varying concentrations of NaCl (blue $\diamond$), $MgCl_2$ (green $\triangle$), SDS (pink $\circ$), and DTAB (purple $\square$).

The ζ-potentials of the different emulsions are shown in Figure 6.6b. In the presence of NaCl and $MgCl_2$, the ζ-potentials are negative overall and similar across all salt concentrations. Recall that DDAPS is a zwitterionic surfactant and its head

group has a net neutral charge. Thus, the negative ζ-potentials are likely due to the adsorption of hydroxyl ions to an interface,[151, 186, 187] which is consistent with ζ-potentials of DDAPS alone measured at the hexane/water interface.[151] Additionally, it is also possible that the sulfonate portion on DDAPS extends farther away from the droplet surface, placing it closer to the slip plane, and making the negative charge more sensitive to ζ-potential measurements. With the addition of SDS as a co-surfactant, the ζ-potentials become more negative and conversely, with the addition of DTAB, the ζ-potentials become more positive. This indicates that the co-surfactants are adsorbed to the droplet surface and assisting DDAPS with stabilizing the nanoemulsions. We hypothesize that the added salts contribute to stabilizing the nanoemulsions by allowing more DDAPS to adsorb to the droplet surface. This idea cannot be discussed fully with ζ-potential measurements alone, and is investigated more deeply with our VSFSS technique in the following section.

DDAPS in the presence of salts at the droplet interface

At the planar oil/water interface, we found through IFT and VSFS measurements that DDAPS adsorption and net ordering change only marginally in the presence of various salt concentrations. This result suggests that these co-additives have little influence over DDAPS's interfacial behavior. However, regarding the formation and stabilization of nanoemulsions, NaCl and $MgCl_2$ play an essential role, as DDAPS alone cannot form nanoemulsions. 6.7 depicts the VSFSS spectra of nanoemulsions coated by DDAPS in the presence of NaCl (a, blue) and $MgCl_2$ (b, green), measured in the CH stretching region using the SSP polarization scheme. This provides information on the net alignment of the DDAPS alkyl tails, specifically dipole components perpendicular to the droplet surface. The DDAPS concentration was 0.05 mM, and the salt concentrations were either 0.01 mM (○) or 0.1 mM (□). The dashed vertical lines denote the CH_2 (d^+) and CH_3 (r^+) symmetric stretches. Fit parameters are provided in Tables A.23 and A.24 in the Appendix.

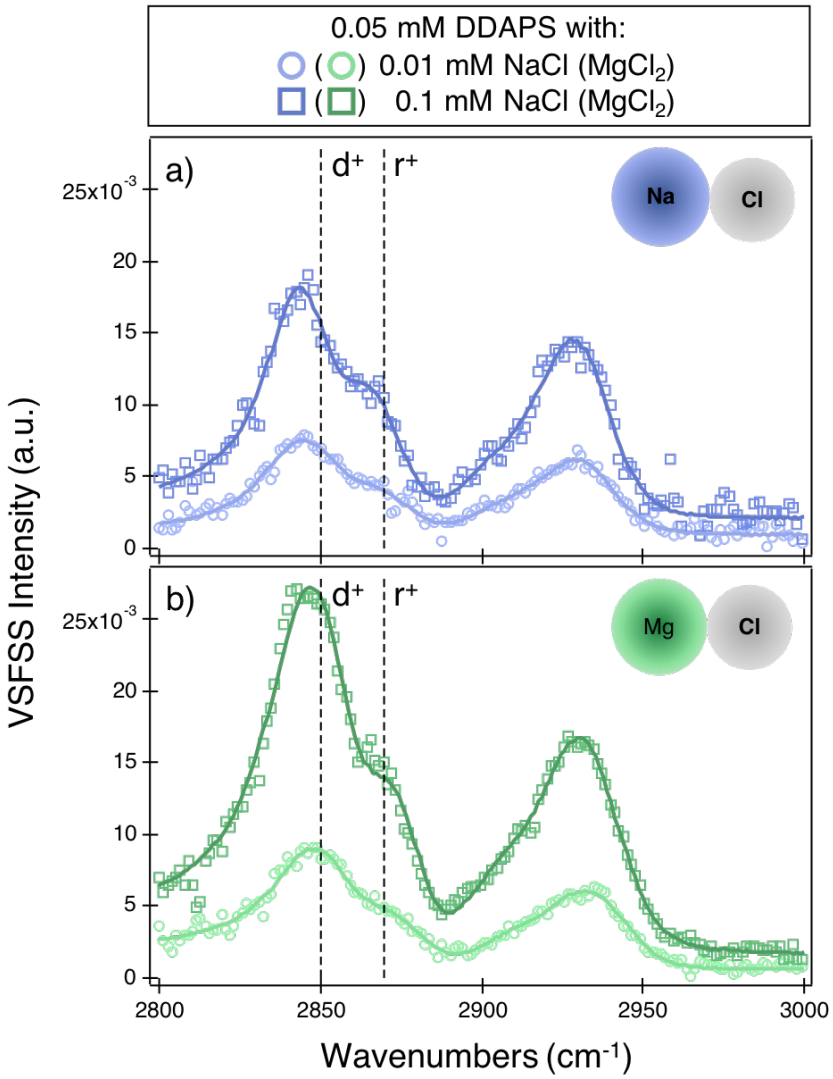

Figure 6.7. VSFSS spectra of nanoemulsions stabilized by DDAPS in the presence of NaCl (a, blue) and $MgCl_2$ (b, green) in the CH stretching region, using the SSP polarization scheme. The DDAPS concentration was fixed at 0.05 mM and the salt concentrations were increased from 0.01 mM (○) to 0.1 mM (□). The dashed vertical lines denote the CH_2 (d^+) and CH_3 (r^+) symmetric stretches.

Unlike the VSFS spectra collected at the planar oil/water interface (Figure 6.4), the presence of NaCl and $MgCl_2$ at the droplet interface significantly influences the adsorption of DDAPS, which contributes to the nanoemulsion stability. With both NaCl (6.7a) and $MgCl_2$ (6.7b) as co-additives, a higher concentration of either salt results in an enhancement in the SF intensity of the DDAPS tails. This enhancement can be ascribed to a greater population of DDAPS at the droplet surface. Because the d^+/r^+ ratio decreases from low to high concentrations of salt, the DDAPS tails

are adopting a more ordered conformation with less gauche defects.

The differences in adsorption behavior of various DDAPS solutions at the planar versus droplet oil/water interface is likely due to the differences in surface areas. For example, a surfactant concentration that would constitute maximum surface coverage at the planar interface may not have the same result at the nanoemulsion interface, since spherical droplets have a higher surface area-to-volume ratio. Therefore, the same concentration of surfactants and co-additives at the two interfaces can result in very different interfacial phenomena. At the planar interface, the introduction of a salt will have a less pronounced effect on DDAPS adsorption if the interface is already well populated. However, for a given amount of oil that is dispersed as droplets, the droplet surface area is much larger and results in surfactants that are less densely packed. Thus, the screening effect from added salts will have a more significant impact on the interfacial surfactant population, which is reflected in the VSFSS spectra. The increase in DDAPS number density at the droplet interface explains the need for salts to stabilize the nanoemulsions. Additionally, this result highlights that the system's energetics play an important role in understanding surfactant interfacial properties.

Synergy between DDAPS and co-surfactants at the droplet interface

The addition of salts as co-additives was shown above to enhance the adsorption of DDAPS to the nanoemulsion surface. We now investigate how co-surfactants such as SDS and DTAB influence DDAPS adsorption and net ordering at the droplet interface. Figure 6.8 depicts VSFSS spectra of the CH stretching region measuring the surfactant alkyl tails. The nanoemulsions were stabilized by 0.05 mM DDAPS and either 0.01 mM (○/●), 0.1 mM (□/■), or 1 mM (△/▲) SDS (Figure 6.8a and 8b, pink) or DTAB (Figure 6.8c and 8d, purple) as co-surfactants. The open markers denote the use of deuterated co-surfactants, such that all CH resonances detected are attributed to DDAPS; while the filled markers denote the use of hydrogenated co-surfactants. In the presence of hydrogenated co-surfactants (i.e., h-SDS or h-DTAB), we note that the measured SF response is from the alkyl tails of both DDAPS and the co-surfactant. All spectra were collected with the SSP polarization scheme, which probes dipoles containing a component perpendicular to the droplet surface. For exact fit parameters, see Tables A.25–A.28 in the Appendix.

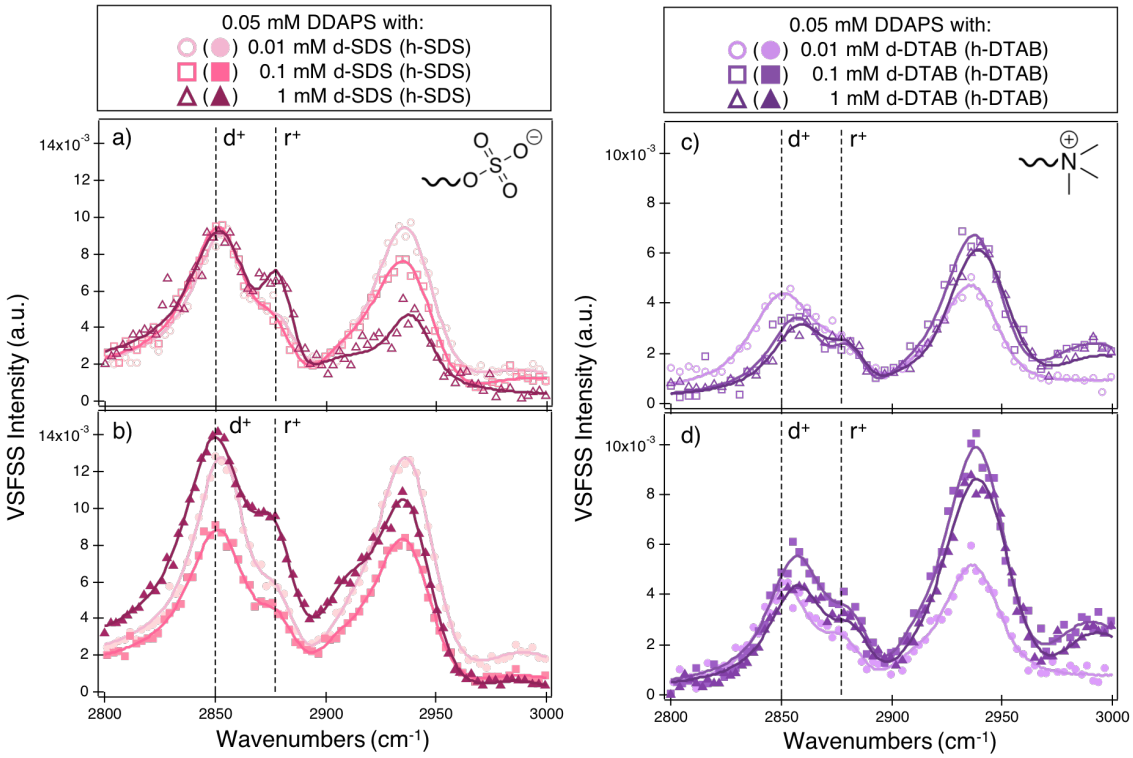

Figure 6.8. VSFSS spectra of nanoemulsions coated by DDAPS in conjunction with d-SDS (a), h-SDS (b), d-DTAB (c), and h-DTAB (d). The concentration of DDAPS was fixed at 0.05 mM, while the co-additive concentrations were varied from 0.01 mM (○/●), 0.1 mM (□/■), and 1 mM (△/▲). The open markers denote deuterated co-surfactants and the filled markers denote hydrogenated co-surfactants. All spectra were collected with the SSP polarization scheme, probing molecular dipole moments perpendicular to the interface. The dashed vertical lines denote the CH_2 (d^+) and CH_3 (r^+) symmetric stretches.

The VSFSS spectra of DDAPS in conjunction with d-SDS (Figure 6.8a) and d-DTAB (Figure 6.8c) do not show large changes in the SF amplitude with increasing co-surfactant concentration, as was seen with increasing salt concentrations (Figure 6.7). The behavior of DDAPS+d-DTAB at the droplet surface is similar to the planar surface, with DDAPS having similar adsorption across different d-DTAB concentrations. From the slight decrease in d^+/r^+ ratios (Figure 6.5, purple □), the DDAPS alkyl tails are becoming more ordered with increasing concentration of d-DTAB, albeit the effect is subtle. However, with d-SDS as the co-surfactant, there is a more pronounced decrease in the d^+/r^+ ratio with increasing concentration of d-SDS (Figure 6.5, pink ○). Thus, for the DDAPS+d-SDS system, we conclude that there is a higher population of surfactants at the droplet surface allowing for tighter packing of the alkyl tails, which is consistent with the high surface activity of this system

(Figure 6.2).

Figures 6.7b and 6.7d are VSFSS measurements containing the contributions from the co-surfactant alkyl tails, as they are no longer deuterated. This allows us to determine the adsorption behavior of h-SDS and h-DTAB in conjunction with DDAPS. Because the bulk DDAPS concentration was fixed throughout this study, changes to the SF intensity in Figures 6.7b and 6.7d can be attributed to the increasing concentrations of h-SDS and h-DTAB, respectively. In the presence of h-SDS, the SF intensity progressively increases from 0.01 mM h-SDS (●) to 1 mM h-SDS (▲), which indicates an increase in adsorption of h-SDS, DDAPS, or both due to cooperative adsorption. The increased adsorption of total surfactants allows for a more tightly packed surfactant layer at the droplet surface, which is reflected in a lower d^+/r^+ ratio (Figure 6.5, pink ●). With h-DTAB as the co-surfactant however, the change in SF intensity is less pronounced which indicates that increasing the bulk concentration of h-DTAB does not greatly affect the overall surfactant packing. This result further supports our hypothesis that for the mixed DDAPS+SDS system, there is a greater interfacial population of surfactants than mixed DDAPS+DTAB system. Additionally, because the surface activity of DDAPS+DTAB is not as strong as DDAPS+SDS, we do not observe a large decrease in the d^+/r^+ ratio for the former mixed system as we do for the latter.

Conclusions

In this chapter, we have demonstrated that is it possible for some surfactants, specifically zwitterionic DDAPS in this case, to exhibit different interfacial properties depending on the surface geometry. Although DDAPS alone is surface active and readily adsorbs to the planar oil/water interface, it cannot stabilize nanoemulsions without the aid of co-additives such as salts or other surfactants. Moreover, the molecular structure of DDAPS at the planar interface is largely invariant with co-additives, but DDAPS adopts tighter packing with co-additives at the droplet surface.

The results from this work highlight the importance of accounting for the interfacial geometry and system energetics when analyzing surfactant properties. For example, DDAPS on its own would not be effective at dispersing oil for remediation purposes, as it cannot stabilize tiny oil droplets (kinetically stable). Thus, the oil droplets will eventually coalesce back into the large oil slick (thermodynamically stable) before any oil can be degraded. However, in a mixed system containing salts and other surfactants (which is likely the case in a natural environment), DDAPS's oil dispersing

performance is enhanced. This insight is valuable for scientists developing surfactant mixtures for various applications via rational design. By developing an understanding of the synergy between DDAPS and other species, formulations for cleaning products, cosmetics, and oil dispersants can reduce the amount of harsh chemicals used by incorporating more DDAPS as a less toxic alternative, all while preserving the efficacy of the product.

CHAPTER VII

SUMMARY AND OUTLOOK

This dissertation is a compilation of work investigating the interfacial phenomena of nanoemulsions, surfactant/polymer self-assembly, and colloidal stability. Experimental techniques spanning dynamic light scattering, ζ-potential measurements, interfacial tensiometry, and surface-specific spectroscopy were employed to reveal valuable insights into surface chemistry. Chapter III demonstrated that the interfacial behavior of PEI can be tuned by adjusting the solution pH. Under acidic conditions PEI is not surface-active, but under basic conditions the hydrophobicity of PEI facilitates its adsorption to the nanoemulsion surface. Building up from a single polymer layer, the work discussed in Chapter IV focuses on multi-polymer layering around nanoemulsion surfaces. Additional pH-dependent properties were observed, further underlining the utility of polymer layers as surface modifiers. Polymer adsorption plays a crucial role in colloidal stability via steric effects. The system studied in Chapter V provided a unique avenue to investigate colloidal stability via steric stabilization, absent of electrostatic repulsive forces. The nonionic polymer PNVA forms layers of strongly bonded, rigid polymer networks that stabilizes the droplet surface. This level of molecular detail was made possible with our VSFSS technique. Continuing the work that probes droplet surfaces coated by neutral (or net neutral) species, Chapter VI investigates the interfacial behavior of zwitterionic DDAPS in the presence of various co-additives. The work in this chapter sheds light on how the geometry and energetics of the interface can influence surfactant behavior.

Interfacial phenomena is an area of research that is continually expanding with the development of instrumentation, technology, and surface-active molecules. The diversity and sheer number of applications that involve any type of interface (e.g., solid/air, liquid/air, liquid/liquid) or colloid (e.g., emulsions, foams, aerosols) necessitates the advancement of surface-specific characterization techniques accompanied by appropriate analysis methods. As researchers push the boundaries of spectral regions and chemical systems that can be studied with sum frequency scattering spectroscopy, the complexity of the interface grows leaving creative and challenging fundamental questions to be investigated. Moreover, with developments such as two-dimensional electronic SFG spectroscopy,[188, 189] SFG imaging,[190, 191] and dual resonant SFG spectroscopy,[192] there is no doubt the outlook of colloid and interface science is a bright one, *pun very much intended.*

APPENDIX

Fitting parameters for all spectra shown in Chapter III

Table A.2. Fitting parameters and d^+/r^+ ratios for h-SDS and PEI/h-SDS spectra shown in Figure 3.5b. Nanoemulsions were either stabilized with 1 mM h-SDS or 5.2 mM PEI and 1 mM h-SDS at constant pH 3.

Peak assignment	**Parameter**	**h-SDS alone**	**PEI/h-SDS**
CH_2 symmetric stretch (d^+)	Amplitude	0.05 ± 0.005	0.07 ± 0.005
	Phase	0	0
	Lorentizian linewidth	2	2
	Peak position	2850 ± 1	2851 ± 1
	Gaussian linewidth	5 ± 1	8 ± 1
CH_3 symmetric stretch (r^+)	Amplitude	0.03 ± 0.004	0.06 ± 0.006
	Phase	0	0
	Lorentizian linewidth	2	2
	Peak position	2875 ± 6	2873 ± 1
	Gaussian linewidth	19 ± 7	13 ± 2
CH_3 asymmetric stretch & Fermi resonance	Amplitude	0.05 ± 0.005	0.08 ± 0.004
	Phase	0	0
	Lorentizian linewidth	2	2
	Peak position	2935 ± 2	2935 ± 1
	Gaussian linewidth	20 ± 2	24 ± 1
Non-resonant contribution	Amplitude	0.05 ± 0.006	0.03 ± 0.003
	Phase	0	0
d^+/r^+ ratio		1.7 ± 0.2	1.2 ± 0.1

Table A.3. Fitting parameters for PEI/d-SDS spectra shown in Figure 3.6a for pH 7.5, 8, 10, and 11. PEI and d-SDS concentrations were fixed at 5.2 mM and 0.1 mM, respectively.

Peak assignment	**Parameter**	**pH 7.5**	**pH 8**	**pH 10**	**pH 11**
CH_2 symmetric stretch	Amplitude	0.04 ± 0.04	0.09 ± 0.01	0.1 ± 0.001	0.1 ± 0.001
	Phase	0	0	0	0
	Lorentzian	2	2	2	2
	Peak position	2850 ± 5	2851 ± 2	2851 ± 2	2850 ± 2
	Gaussian	19 ± 5	26 ± 0.6	27 ± 0.4	28 ± 0.3
CH_3 symmetric stretch	Amplitude	0.02 ± 0.005	0.008 ± 0.04	0.009 ± 0.003	0.01 ± 0.002
	Phase	0	0	0	0
	Lorentzian	2	2	2	2
	Peak position	2880 ± 26	2890 ± 5	2894 ± 4	2900 ± 4
	Gaussian	29 ± 12	14 ± 6	11 ± 5	17 ± 6
CH_3 asymmetric stretch	Amplitude	0.02 ± 0.005	0.04 ± 0.007	0.03 ± 0.002	0.02 ± 0.002
	Phase	0	0	0	0
	Lorentzian	2	2	2	2
	Peak position	2935 ± 9	2964 ± 3	2956 ± 2	2953 ± 2
	Gaussian	28 ± 9	63 ± 1	48 ± 3	30 ± 5
N.R. contribution	Amplitude	0	0.02 ± 0.001	0.04 ± 0.001	0.05 ± 0.001
	Phase	0	0	0	0

Table A.4. Fitting parameters for PEI/d-SDS and PEI/h-SDS spectra shown in Figure 3.6b for pH 11. PEI and d-SDS/h-SDS concentrations were fixed at 5.2 mM and 1 mM, respectively.

Peak assignment	**Parameter**	**PEI/d-SDS**	**PEI/h-SDS**
CH_2 symmetric stretch	Amplitude	0.05 ± 0.008	0.09 ± 0.002
	Phase	0	0
	Lorentzian	2	2
	Peak position	2851 ± 2	2852 ± 3
	Gaussian	27 ± 2	26 ± 4
CH_3 symmetric stretch	Amplitude	0.009 ± 0.008	0.05 ± 0.003
	Phase	0	0
	Lorentzian	2	2
	Peak position	2885 ± 7	2875 ± 2
	Gaussian	32 ± 3	28 ± 6
CH_3 asymmetric stretch & Fermi resonance	Amplitude	0.007 ± 0.003	0.04 ± 0.002
	Phase	0	0
	Lorentzian	2	2
	Peak position	2935 ± 9	2935 ± 3
	Gaussian	27 ± 5	32 ± 3
Non-resonant contribution	Amplitude	0.02 ± 0.007	0.03 ± 0.003
	Phase	0	0

Table A.5. Fitting parameters for PEI/d-DTAB spectra shown in Figure 3.8a for pH 8, 10, and 11. PEI and d-DTAB concentrations were fixed at 5.2 mM and 0.1 mM, respectively.

Peak assignment	**Parameter**	**pH 8**	**pH 10**	**pH 11**
CH_2 symmetric stretch	Amplitude	0.03 ± 0.04	0.08 ± 0.007	0.1 ± 0.007
	Phase	0	0	0
	Lorentzian	2	2	2
	Peak position	2854 ± 10	2852 ± 2	2853 ± 2
	Gaussian	19 ± 7	25 ± 2	22 ± 2
CH_3 symmetric stretch	Amplitude	0.02 ± 0.02	0.03 ± 0.006	0.03 ± 0.007
	Phase	0	0	0
	Lorentzian	2	2	2
	Peak position	2891 ± 14	2881 ± 2	2889 ± 2
	Gaussian	25 ± 16	56 ± 4	67 ± 2
CH_3 asymmetric stretch	Amplitude	0.04 ± 0.002	0.04 ± 0.004	0.03 ± 0.004
	Phase	0	0	0
	Lorentzian	2	2	2
	Peak position	2938 ± 6	2943 ± 3	2945 ± 5
	Gaussian	56 ± 3	28 ± 3	32 ± 8
Non-resonant contribution	Amplitude	0	0	0
	Phase	0	0	0

Table A.6. Fitting parameters for PEI/d-DTAB and PEI/h-DTAB spectra shown in Figure 3.8b for pH 11. PEI and d-DTAB/h-DTAB concentrations were fixed at 5.2 mM and 1 mM, respectively.

Peak assignment	**Parameter**	**PEI/d-DTAB**	**PEI/h-DTAB**
CH_2 symmetric stretch	Amplitude	0.01 ± 0.001	0.05 ± 0.001
	Phase	0	0
	Lorentzian	2	2
	Peak position	2849 ± 3	2852 ± 1
	Gaussian	25 ± 3	26 ± 2
CH_3 symmetric stretch	Amplitude	0.009 ± 0.008	0.02 ± 0.001
	Phase	0	0
	Lorentzian	2	2
	Peak position	2881 ± 4	2870 ± 2
	Gaussian	29 ± 2	28 ± 4
CH_3 asymmetric stretch & Fermi resonance	Amplitude	0.02 ± 0.001	0.04 ± 0.002
	Phase	0	0
	Lorentzian	2	2
	Peak position	2940 ± 2	2938 ± 2
	Gaussian	30 ± 3	31 ± 4
Non-resonant contribution	Amplitude	0.005 ± 0.009	0.002 ± 0.001
	Phase	0	0

Fitting parameters for all spectra shown in Chapter IV

Table A.7. Fit parameters for VSFSS spectra of nanoemulsions stabilized by either 0, 0.1, or 1 mM d-DTAB, in conjunction with 5 mM PSS, shown in Figure 4.4.

Alkane CH Stretches d-DTAB + 5 mM PSS (pH 7)				
Peak Assignment	**Parameter**	**0 mM d-DTAB**	**0.1 mM d-DTAB**	**1 mM d-DTAB**
CH_2 symmetric stretch (s.s.)	Amplitude Phase Lorentzian Peak position Gaussian	N/A	0.03 ± 0.002 0 2 2852 ± 1 13 ± 2	0.04 ± 0.003 0 2 2848 ± 2 11 ± 2
CH_3 symmetric stretch (s.s.)	Amplitude Phase Lorentzian Peak position Gaussian	N/A	0.02 ± 0.002 0 2 2877 ± 2 50 ± 3	0.02 ± 0.002 0 2 2879 ± 3 36 ± 4
CH_2 asymmetric stretch (a.s.)	Amplitude Phase Lorentzian Peak position Gaussian	N/A	0.03 ± 0.002 0 2 2909 ± 1 13 ± 1	0.03 ± 0.003 0 2 2908 ± 3 16 ± 2
CH_3 asymmetric stretch (a.s.)	Amplitude Phase Lorentzian Peak position Gaussian	N/A	0.01 ± 0.001 0 2 2975 ± 2 88 ± 5	0.02 ± 0.004 0 2 2980 ± 3 73 ± 6
Non-resonant contribution	Amplitude Phase	N/A	0 0	0 0
Aromatic CH Stretches d-DTAB + 5 mM PSS (pH 7)				
Peak Assignment	**Parameter**	**0 mM d-DTAB**	**0.1 mM d-DTAB**	**1 mM d-DTAB**
Aromatic CH stretch 1	Amplitude Phase Lorentzian Peak position Gaussian	N/A	N/A	0.03 ± 0.003 0 2 3020 ± 10 40 ± 5
Aromatic CH stretch 2	Amplitude Phase Lorentzian Peak position Gaussian	N/A	N/A	0.05 ± 0.007 0 2 3059 ± 2 7 ± 2
Non-resonant contribution	Amplitude Phase	N/A	N/A	0 0

Table A.8. Fit parameters for VSFSS spectra of nanoemulsions stabilized by 0.1 mM d-DTAB, 5 mM PSS, and either 0, 1, or 10 mM cationic PEI at pH 3, shown in Figure 4.6).

Alkane CH Stretches 0.1 mM d-DTAB + 5 mM PSS + **cationic** PEI (pH 3)				
Peak Assignment	**Parameter**	**0 mM PEI**	**1 mM PEI**	**10 mM PEI**
D_2O stretch + libration	Amplitude	0.1 ± 0.0009	0.07 ± 0.001	N/A
	Phase	0	0	
	Lorentzian	5	5	
	Peak position	2782 ± 2	2784 ± 2	
	Gaussian	65 ± 8	60 ± 10	
CH_2 symmetric stretch (s.s.)	Amplitude	0.06 ± 0.008	0.07 ± 0.009	0.09 ± 0.002
	Phase	0	0	0
	Lorentzian	2	2	2
	Peak position	2840 ± 1	2841 ± 1	2850 ± 2
	Gaussian	20 ± 2	20 ± 2	12 ± 1
CH_3 symmetric stretch (s.s.)	Amplitude	0.03 ± 0.005	0.03 ± 0.005	0.04 ± 0.003
	Phase	0	0	0
	Lorentzian	2	2	2
	Peak position	2882 ± 3	2882 ± 4	2880 ± 1
	Gaussian	11 ± 4	17 ± 4	20 ± 2
CH_2 asymmetric stretch (a.s.)	Amplitude	0.03 ± 0.005	0.03 ± 0.001	0.04 ± 0.003
	Phase	0	0	0
	Lorentzian	2	2	2
	Peak position	2910 ± 2	2909 ± 2	2914 ± 1
	Gaussian	9 ± 2	10 ± 2	13 ± 1
CH_3 asymmetric stretch (a.s.)	Amplitude	0.01 ± 0.003	0.02 ± 0.002	0.01 ± 0.004
	Phase	0	0	0
	Lorentzian	2	2	2
	Peak position	2975 ± 1	2976 ± 1	2980 ± 2
	Gaussian	86 ± 4	86 ± 5	85 ± 3
Non-resonant contribution	Amplitude	0	0	0
	Phase	0	0	0
Aromatic CH Stretches 0.1 mM d-DTAB + 5 mM PSS + **cationic** PEI (pH 3)				
Peak Assignment	**Parameter**	**0 mM PEI**	**1 mM PEI**	**10 mM PEI**
Aromatic CH stretch 1	Amplitude	0.01 ± 0.002	0.04 ± 0.004	0.06 ± 0.003
	Phase	0	0	0
	Lorentzian	2	2	2
	Peak position	3020 ± 1	3020 ± 2	3023 ± 2
	Gaussian	71 ± 3	21 ± 4	29 ± 7
Aromatic CH stretch 2	Amplitude	0.02 ± 0.006	0.08 ± 0.006	0.1 ± 0.009
	Phase	0	0	0
	Lorentzian	2	2	2
	Peak position	3059 ± 1	3060 ± 2	3062 ± 1
	Gaussian	60 ± 3	15 ± 1	14 ± 1
Non-resonant contribution	Amplitude	0.006 ± 0.003	0.02 ± 0.003	0.03 ± 0.001
	Phase	0	0	0

Table A.9. Fit parameters for VSFSS spectra of nanoemulsions stabilized by 0.1 mM d-DTAB, 5 mM PSS, and either 0, 1, or 10 mM nonionic PEI at pH 10, shown in Figure 4.8.

Alkane CH Stretches 0.1 mM d-DTAB + 5 mM PSS + **nonionic** PEI (pH 10)				
Peak Assignment	**Parameter**	**0 mM PEI**	**1 mM PEI**	**10 mM PEI**
D_2O stretch + libration	Amplitude	0.03 ± 0.002	0.05 ± 0.003	0.02 ± 0.001
	Phase	0	0	0
	Lorentzian	5	5	5
	Peak position	2785 ± 4	2790 ± 5	2790 ± 5
	Gaussian	40 ± 4	43 ± 3	± 30 ± 2
CH_2 symmetric stretch (s.s.)	Amplitude	0.02 ± 0.0007	0.03 ± 0.002	0.05 ± 0.004
	Phase	0	0	0
	Lorentzian	2	2	2
	Peak position	2853 ± 1	2850 ± 1	2852 ± 1
	Gaussian	14 ± 1	16 ± 2	21 ± 1
CH_3 symmetric stretch (s.s.)	Amplitude	0.02 ± 0.001	0.02 ± 0.006	0.01 ± 0.006
	Phase	0	0	0
	Lorentzian	2	2	2
	Peak position	2880 ± 1	2879 ± 3	2880 ± 2
	Gaussian	70 ± 4	64 ± 4	60 ± 4
CH_2 asymmetric stretch (a.s.)	Amplitude	0.01 ± 0.001	0.009 ± 0.005	0.02 ± 0.005
	Phase	0	0	0
	Lorentzian	2	2	2
	Peak position	2916 ± 2	2914 ± 5	2930 ± 7
	Gaussian	12 ± 3	20 ± 3	26 ± 5
Non-resonant contribution	Amplitude	0.02 ± 0.0005	0.02 ± 0.002	0.01 ± 0.002
	Phase	0	0	0
Aromatic CH Stretches 0.1 mM d-DTAB + 5 mM PSS + **nonionic** PEI (pH 10)				
Peak Assignment	**Parameter**	**0 mM PEI**	**1 mM PEI**	**10 mM PEI**
Aromatic CH stretch 1	Amplitude	N/A	N/A	0.02 ± 0.003
	Phase			0
	Lorentzian			2
	Peak position			3026 ± 6
	Gaussian			42 ± 3
Aromatic CH stretch 2	Amplitude	N/A	N/A	0.05 ± 0.003
	Phase			0
	Lorentzian			2
	Peak position			3058 ± 2
	Gaussian			10 ± 2
Non-resonant contribution	Amplitude	N/A	N/A	0.02 ± 0.005
	Phase			0

Inputs for DLVO calculations and fitting parameters for all spectra shown in Chapter V

Table A.10. Parameters used to calculate the Hamaker constant for hexadecane-in-water nanoemulsions from Equation 27.

Variable	Description	Value
k_b	Boltzmann constant	1.380649×10^{-23} m^2 kg s^{-2} K^{-1}
T	Temperature (K)	297.15
$\varepsilon_{\text{hexadecane}}$	Dielectric constant of hexadecane	2.09
$n_{\text{hexadecane}}$	Refractive index of hexadecane	1.43
$\varepsilon_{\text{water}}$	Dielectric constant of water	78
n_{water}	Refractive index of water	1.33

Table A.11. Concentrations of SDS used and the corresponding Debye length calculated from Equation 28.

SDS concentration (mM)	Ionic strength (mM)	Debye length
0.01	0.01	96.1
0.1	0.1	30.4
0.5	0.5	13.6
1	1	9.6
2.5	2.5	6.1

Table A.12. Parameters used to calculate the interaction pair potentials in Figure 5.5d using extended DLVO theory for nanoemulsions stabilized by SDS/PNVA.

Variable	Description	Value
ν	Volume of ones solvent (water) molecule	2.99×10^{-20} m^3
ϕ_p	Volume fraction of polymer	0.05
ϕ	Volume fraction of droplets	0.01
χ	Flory-Huggins constant	0.495$*$
M_w	Polymer molecular weight	4060000 g/mol
ρ	Density of oil core	0.887×10^{6} g/m^3
L	Steric layer thickness†	varies (m)

$*$ Flory-Huggins constant for PNVA was approximated using the constant for polyacrylamide in water, due to the similar chemical moieties between the two polymers

† Steric layer thickness ≈ Radius of SDS/PNVA nanoemulsions − Radius of SDS nanoemulsions

Table A.13. Fitting parameters for spectra of h-SDS/PNVA stabilized nanoemulsions in the C–H stretching region, corresponding to Figure 5.6a.

Fixed [PNVA] = 5 mM		Hydrogenated SDS concentration:			
Peak assignment	**Parameter**	**[h-SDS] = 0.1 mM**	**[h-SDS] = 0.5 mM**	**[h-SDS] = 1 mM**	**[h-SDS] = 2.5 mM**
Water combination band	Amplitude	0.03 ± 0.005	0.06 ± 0.006	0.03 ± 0.008	0.06 ± 0.006
	Phase	0	0	0	0
	Lorentzian	2	2	2	2
	Peak position	2770 ± 2	2777 ± 1	2774 ± 2	2774 ± 1
	Gaussian	78 ± 3	67 ± 3	70 ± 4	71 ± 2
CH_2 symmetric stretch	Amplitude	0.04 ± 0.003	0.1 ± 0.003	0.4 ± 0.003	0.5 ± 0.003
	Phase	0	0	0	0
	Lorentzian	2	2	2	2
	Peak position	2850 ± 1	2849 ± 1	2852 ± 1	2850 ± 1
	Gaussian	15 ± 2	17 ± 1	14 ± 1	15 ± 1
CH_3 symmetric stretch	Amplitude	0.02 ± 0.004	0.06 ± 0.005	0.07 ± 0.005	0.09 ± 0.004
	Phase	0	0	0	0
	Lorentzian	2	2	2	2
	Peak position	2891 ± 2	2891 ± 1	2891 ± 1	2891 ± 1
	Gaussian	67 ± 5	67 ± 2	62 ± 1	62 ± 1
CH_2 asymmetric stretch	Amplitude	0.04 ± 0.003	0.06 ± 0.003	0.3 ± 0.002	0.3 ± 0.003
	Phase	0	0	0	0
	Lorentzian	2	2	2	2
	Peak position	2929 ± 2	2928 ± 1	2931 ± 1	2929 ± 1
	Gaussian	24 ± 4	22 ± 1	23 ± 1	22 ± 1
Non-resonant contribution	Amplitude	0.05 ± 0.002	0.09 ± 0.003	0.1 ± 0.002	0.1 ± 0.002
	Phase	0	0	0	0

Table A.14. Fitting parameters for spectra of d-SDS/PNVA stabilized nanoemulsions in the C–H stretching region, corresponding to Figure 5.6b.

Fixed [PNVA] = 5 mM		Deuterated SDS concentration:			
Peak assignment	**Parameter**	**[d-SDS] = 0.1 mM**	**[d-SDS] = 0.5 mM**	**[d-SDS] = 1 mM**	**[d-SDS] = 2.5 mM**
Water combination band	Amplitude	0.02 ± 0.005	0.02 ± 0.001	0.05 ± 0.002	0.07 ± 0.00
	Phase	0	0	0	0
	Lorentzian	2	2	2	2
	Peak position	2775 ± 2	2770 ± 3	2769 ± 1	2770 ± 3
	Gaussian	71 ± 3	61 ± 2	80 ± 2	80 ± 5
CH_2 symmetric stretch	Amplitude	0.01 ± 0.008	0.03 ± 0.004	0.04 ± 0.001	0.06 ± 0.002
	Phase	0	0	0	0
	Lorentzian	2	2	2	2
	Peak position	2848 ± 2	2849 ± 2	2852 ± 1	2850 ± 1
	Gaussian	27 ± 4	20 ± 2	18 ± 1	20 ± 3
CH_3 symmetric stretch	Amplitude	0.02 ± 0.009	0.02 ± 0.01	0.03 ± 0.002	0.04 ± 0.003
	Phase	0	0	0	0
	Lorentzian	2	2	2	2
	Peak position	2880 ± 1	2884 ± 2	2883 ± 2	2884 ± 1
	Gaussian	76 ± 1	72 ± 1	75 ± 1	74 ± 2
CH_2 asymmetric stretch	Amplitude	0.04 ± 0.006	0.06 ± 0.003	0.06 ± 0.001	0.08 ± 0.003
	Phase	0	0	0	0
	Lorentzian	2	2	2	2
	Peak position	2931 ± 1	2928 ± 2	2927 ± 1	2926 ± 1
	Gaussian	29 ± 2	21 ± 2	21 ± 1	21 ± 2
Non-resonant contribution	Amplitude	0.04 ± 0.001	0.05 ± 0.002	0.05 ± 0.001	0.06 ± 0.002
	Phase	0	0	0	0

Table A.15. Fitting parameters for spectra of SDS (alone) stabilized nanoemulsions in the S=O stretching region, corresponding to Figure 5.6c.

NO PNVA		SDS concentration:			
Peak assignment	**Parameter**	**[SDS] = 0.1 mM**	**[SDS] = 0.5 mM**	**[SDS] = 1 mM**	**[SDS] = 2.5 mM**
S=O symmetric stretch 1	Amplitude	0.03 ± 0.01	0.1 ± 0.008	0.2 ± 0.007	0.2 ± 0.006
	Phase	0	0	0	0
	Lorentzian	2	2	2	2
	Peak position	1045 ± 3	1043 ± 2	1045 ± 1	1046 ± 1
	Gaussian	12 ± 4	15 ± 1	15 ± 1	12 ± 1
S=O symmetric stretch 2	Amplitude	0.07 ± 0.004	0.09 ± 0.005	0.1 ± 0.004	0.1 ± 0.004
	Phase	0	0	0	0
	Lorentzian	2	2	2	2
	Peak position	1095 ± 1	1091 ± 2	1090 ± 1	1089 ± 1
	Gaussian	67 ± 3	62 ± 4	62 ± 2	61 ± 2
Non-resonant contribution	Amplitude	0.02 ± 0.006	0.03 ± 0.008	0.03 ± 0.006	0.05 ± 0.006
	Phase	0	0	0	0

Table A.16. Fitting parameters for spectra of SDS/PNVA stabilized nanoemulsions in the S=O stretching region, corresponding to Figure 5.6d.

Fixed [PNVA] = 5 mM		SDS concentration:			
Peak assignment	**Parameter**	**[SDS] = 0.1 mM**	**[SDS] = 0.5 mM**	**[SDS] = 1 mM**	**[SDS] = 2.5 mM**
S=O symmetric stretch 1	Amplitude	0.02 ± 0.01	0.2 ± 0.007	0.2 ± 0.008	0.3 ± 0.008
	Phase	0	0	0	0
	Lorentzian	2	2	2	2
	Peak position	1045 ± 3	1043 ± 1	1044 ± 1	1045 ± 1
	Gaussian	12 ± 4	12 ± 1	13 ± 1	13 ± 1
S=O symmetric stretch 2	Amplitude	0.07 ± 0.004	0.07 ± 0.006	0.2 ± 0.006	0.2 ± 0.005
	Phase	0	0	0	0
	Lorentzian	2	2	2	2
	Peak position	1095 ± 1	1096 ± 2	1092 ± 1	1091 ± 1
	Gaussian	67 ± 3	69 ± 3	65 ± 2	64 ± 2
Non-resonant contribution	Amplitude	0.02 ± 0.006	0.04 ± 0.007	0.08 ± 0.008	0.06 ± 0.007
	Phase	0	0	0	0

Table A.17. Fitting parameters for spectra of SDS/PNVA stabilized nanoemulsions in the C=O stretching region, corresponding to Figure 5.6e.

Fixed [PNVA] = 5 mM		SDS concentration:			
Peak assignment	**Parameter**	**[SDS] = 0.1 mM**	**[SDS] = 0.5 mM**	**[SDS] = 1 mM**	**[SDS] = 2.5 mM**
Background peak 1	Amplitude	0.04 ± 0.0006	0.06 ± 0.0006	0.06 ± 0.0008	0.07 ± 0.0009
	Phase	0	0	0	0
	Lorentzian	10	10	10	10
	Peak position	1593	1593	1593	1593
	Gaussian	45	45	45	45
C=O stretch	Amplitude	0.01 ± 0.001	0.01 ± 0.001	0.03 ± 0.001	0.03 ± 0.002
	Phase	0	0	0	0
	Lorentzian	5	5	5	5
	Peak position	1629 ± 1	1628 ± 1	1629 ± 1	1629 ± 1
	Gaussian	14 ± 1	15 ± 2	20 ± 1	21 ± 2
Background peak 2	Amplitude	0.03 ± 0.0003	0.04 ± 0.0004	0.06 ± 0.0003	0.06 ± 0.0004
	Phase	3.14	3.14	3.14	3.14
	Lorentzian	5	5	5	5
	Peak position	1777	1777	1777	1777
	Gaussian	106	106	106	106
Non-resonant contribution	Amplitude	0.01 ± 0.0006	0.01 ± 0.0008	0.02 ± 0.0008	0.02 ± 0.0009
	Phase	0	0	0	0

Fitting parameters for all spectra shown in Chapter VI

Table A.18. Fit parameters for VSFS experiments at the planar CCl_4/water interface with DDAPS alone, corresponding to Figure 6.3.

Peak assignment	**Parameter**	**[DDAPS] = 0.05 mM**	**[DDAPS] = 0.5 mM**	**[DDAPS] = 5 mM**
CH_2 symmetric stretch (d^+)	Amplitude	0.8 ± 0.02	0.9 ± 0.03	0.9 ± 0.03
	Phase	0	0	0
	Lorentzian	2	2	2
	Peak position	2854 ± 1	2854 ± 1	2854 ± 1
	Gaussian	10 ± 1	10 ± 1	10 ± 1
CH_2 symmetric stretch (r^+)	Amplitude	0.9 ± 0.03	1.2 ± 0.04	1.3 ± 0.04
	Phase	0	0	0
	Lorentzian	2	2	2
	Peak position	2873 ± 1	2873 ± 1	2873 ± 1
	Gaussian	6 ± 1	7 ± 1	7 ± 1
CH_2 asymmetric stretch (d^-)	Amplitude	0.6 ± 0.02	0.7 ± 0.03	0.8 ± 0.03
	Phase	0	0	0
	Lorentzian	2	2	2
	Peak position	2915 ± 2	2917 ± 2	2916 ± 3
	Gaussian	21 ± 2	24 ± 2	23 ± 3
CH_3 symmetric stretch Fermi resonance (r^+_{FR})	Amplitude	0.9 ± 0.08	1 ± 0.07	1.3 ± 0.1
	Phase	0	0	0
	Lorentzian	2	2	2
	Peak position	2932 ± 1	2932 ± 1	2933 ± 1
	Gaussian	8 ± 1	8 ± 1	8 ± 1
CH_3 asymmetric stretch (r^-)	Amplitude	0.3 ± 0.04	0.3 ± 0.05	0.3 ± 0.05
	Phase	0	0	0
	Lorentzian	2	2	2
	Peak position	2977 ± 2	2978 ± 2	2979 ± 2
	Gaussian	12 ± 2	13 ± 3	12 ± 3
Non-resonant background	Amplitude	0.08 ± 0.01	0.1 ± 0.02	0.1 ± 0.02
	Phase	0	0	0

Table A.19. Fit parameters for VSFS experiments at the planar CCl_4/water interface with DDAPS and NaCl, corresponding to Figure 6.4a.

Fixed DDAPS concentration = 0.05 mM		Varying NaCl concentrations		
Peak assignment	**Parameter**	**[NaCl] = 0.01 mM**	**[NaCl] = 0.1 mM**	**[NaCl] = 1 mM**
CH_2 symmetric stretch (d^+)	Amplitude	0.9 ± 0.03	0.9 ± 0.03	0.8 ± 0.03
	Phase	0	0	0
	Lorentzian	2	2	2
	Peak position	2854 ± 1	2854 ± 1	2854 ± 1
	Gaussian	10 ± 1	10 ± 1	9 ± 1
CH_2 symmetric stretch (r^+)	Amplitude	1 ± 0.04	1 ± 0.04	1 ± 0.04
	Phase	0	0	0
	Lorentzian	2	2	2
	Peak position	2873 ± 1	2873 ± 1	2873 ± 1
	Gaussian	7 ± 1	7 ± 1	6 ± 1
CH_2 asymmetric stretch (d^-)	Amplitude	0.7 ± 0.03	0.7 ± 0.04	0.6 ± 0.04
	Phase	0	0	0
	Lorentzian	2	2	2
	Peak position	2916 ± 3	2916 ± 3	2915 ± 3
	Gaussian	25 ± 2	25 ± 2	24 ± 3
CH_3 symmetric stretch Fermi resonance (r^+_{FR})	Amplitude	1 ± 0.09	1 ± 0.09	1 ± 0.1
	Phase	0	0	0
	Lorentzian	2	2	2
	Peak position	2932 ± 1	2932 ± 1	2932 ± 1
	Gaussian	9 ± 1	9 ± 1	9 ± 1
CH_3 asymmetric stretch (r^-)	Amplitude	0.3 ± 0.05	0.3 ± 0.05	0.3 ± 0.05
	Phase	0	0	0
	Lorentzian	2	2	2
	Peak position	2978 ± 2	2979 ± 2	2978 ± 2
	Gaussian	13 ± 3	14 ± 3	13 ± 3
Non-resonant background	Amplitude	0.2 ± 0.02	0.2 ± 0.02	0.1 ± 0.02
	Phase	0	0	0

Table A.20. Fit parameters for VSFS experiments at the planar CCl_4/water interface with DDAPS and $MgCl_2$, corresponding to Figure 6.4b.

	Fixed DDAPS concentration = 0.05 mM	Varying $MgCl_2$ concentrations		
Peak assignment	**Parameter**	**[$MgCl_2$] = 0.01 mM**	**[$MgCl_2$] = 0.1 mM**	**[$MgCl_2$] = 1 mM**
CH_2 symmetric stretch (d^+)	Amplitude	0.8 ± 0.03	0.9 ± 0.03	0.9 ± 0.03
	Phase	0	0	0
	Lorentzian	2	2	2
	Peak position	2854 ± 1	2854 ± 1	2854 ± 1
	Gaussian	10 ± 1	9 ± 1	10 ± 1
CH_2 symmetric stretch (r^+)	Amplitude	1 ± 0.04	1 ± 0.04	1 ± 0.04
	Phase	0	0	0
	Lorentzian	2	2	2
	Peak position	2873 ± 1	2873 ± 1	2873 ± 1
	Gaussian	7 ± 1	6 ± 1	6 ± 1
CH_2 asymmetric stretch (d^-)	Amplitude	0.7 ± 0.04	0.7 ± 0.03	0.6 ± 0.04
	Phase	0	0	0
	Lorentzian	2	2	2
	Peak position	2916 ± 3	2917 ± 3	2915 ± 3
	Gaussian	25 ± 3	24 ± 2	23 ± 3
CH_3 symmetric stretch Fermi resonance (r^+_{FR})	Amplitude	1 ± 0.09	1 ± 0.08	1 ± 0.1
	Phase	0	0	0
	Lorentzian	2	2	2
	Peak position	2932 ± 1	2932 ± 1	2932 ± 1
	Gaussian	9 ± 1	9 ± 1	9 ± 1
CH_3 asymmetric stretch (r^-)	Amplitude	0.3 ± 0.05	0.3 ± 0.05	0.3 ± 0.04
	Phase	0	0	0
	Lorentzian	2	2	2
	Peak position	2978 ± 2	2978 ± 2	2979 ± 2
	Gaussian	13 ± 4	13 ± 3	13 ± 3
Non-resonant background	Amplitude	0.2 ± 0.02	0.1 ± 0.02	0.1 ± 0.02
	Phase	0	0	0

Table A.21. Fit parameters for VSFS experiments at the planar CCl_4/water interface with DDAPS and SDS, corresponding to Figure 6.4c.

Fixed DDAPS concentration = 0.05 mM		Varying d-SDS concentrations		
Peak assignment	**Parameter**	**[d-SDS] = 0.01 mM**	**[d-SDS] = 0.1 mM**	**[d-SDS] = 1 mM**
CH_2 symmetric stretch (d^+)	Amplitude	0.8 ± 0.03	0.8 ± 0.03	0.7 ± 0.02
	Phase	0	0	0
	Lorentzian	2	2	2
	Peak position	2853 ± 1	2853 ± 1	2853 ± 1
	Gaussian	9 ± 1	9 ± 1	10 ± 1
CH_2 symmetric stretch (r^+)	Amplitude	1 ± 0.05	1 ± 0.04	1 ± 0.04
	Phase	0	0	0
	Lorentzian	2	2	2
	Peak position	2873 ± 1	2873 ± 1	2873 ± 1
	Gaussian	7 ± 1	7 ± 1	6 ± 1
CH_2 asymmetric stretch (d^-)	Amplitude	0.6 ± 0.04	0.6 ± 0.04	0.5 ± 0.03
	Phase	0	0	0
	Lorentzian	2	2	2
	Peak position	2916 ± 4	2916 ± 4	2917 ± 3
	Gaussian	23 ± 4	23 ± 4	26 ± 3
CH_3 symmetric stretch Fermi resonance (r^+_{FR})	Amplitude	0.9 ± 0.1	0.8 ± 0.1	0.6 ± 0.09
	Phase	0	0	0
	Lorentzian	2	2	2
	Peak position	2933 ± 1	2933 ± 1	2933 ± 1
	Gaussian	9 ± 1	8 ± 1	8 ± 1
Non-resonant background	Amplitude	0.3 ± 0.02	0.3 ± 0.02	0.3 ± 0.02
	Phase	0	0	0

Table A.22. Fit parameters for VSFS experiments at the planar CCl_4/water interface with DDAPS and DTAB, corresponding to Figure 6.4d.

Fixed DDAPS concentration = 0.05 mM		Varying d-DTAB concentrations		
Peak assignment	**Parameter**	**[d-DTAB] = 0.01 mM**	**[d-DTAB] = 0.1 mM**	**[d-DTAB] = 1 mM**
CH_2 symmetric stretch (d^+)	Amplitude	0.8 ± 0.03	0.8 ± 0.03	0.7 ± 0.03
	Phase	0	0	0
	Lorentzian	2	2	2
	Peak position	2854 ± 1	2854 ± 1	2854 ± 1
	Gaussian	9 ± 1	9 ± 1	8 ± 1
CH_2 symmetric stretch (r^+)	Amplitude	1 ± 0.04	1 ± 0.04	1 ± 0.05
	Phase	0	0	0
	Lorentzian	2	2	2
	Peak position	2873 ± 1	2873 ± 1	2873 ± 1
	Gaussian	7 ± 1	7 ± 1	7 ± 1
CH_2 asymmetric stretch (d^-)	Amplitude	0.6 ± 0.03	0.6 ± 0.04	0.5 ± 0.05
	Phase	0	0	0
	Lorentzian	2	2	2
	Peak position	2916 ± 3	2915 ± 4	2916 ± 5
	Gaussian	23 ± 3	21 ± 4	19 ± 5
CH_3 symmetric stretch Fermi resonance (r^+_{FR})	Amplitude	1 ± 0.1	1 ± 0.2	1 ± 0.2
	Phase	0	0	0
	Lorentzian	2	2	2
	Peak position	2933 ± 1	2933 ± 1	2933 ± 1
	Gaussian	9 ± 1	9 ± 1	9 ± 1
CH_3 asymmetric stretch (r^-)	Amplitude	0.3 ± 0.04	0.3 ± 0.04	0.2 ± 0.05
	Phase	0	0	0
	Lorentzian	2	2	2
	Peak position	2978 ± 2	2978 ± 2	2978 ± 3
	Gaussian	13 ± 3	13 ± 3	12 ± 4
Non-resonant background	Amplitude	0.1 ± 0.02	0.06 ± 0.02	0.06 ± 0.02
	Phase	0	0	0

Table A.23. Fit parameters for VSFSS experiments on nanoemulsions stabilized by DDAPS and NaCl, corresponding to Figure 6.7a.

Fixed DDAPS concentration = 0.05 mM		Varying NaCl concentrations	
Peak assignment	**Parameter**	**[NaCl] = 0.01 mM**	**[NaCl] = 0.1 mM**
CH_2 symmetric stretch (d^+)	Amplitude	0.06 ± 0.01	0.08 ± 0.008
	Phase	0	0
	Lorentzian	2	2
	Peak position	2849 ± 2	2847 ± 2
	Gaussian	13 ± 2	10 ± 1
CH_2 symmetric stretch (r^+)	Amplitude	0.05 ± 0.006	0.08 ± 0.003
	Phase	0	0
	Lorentzian	2	2
	Peak position	2871 ± 3	2869 ± 2
	Gaussian	14 ± 4	14 ± 2
CH_2 asymmetric stretch (d^-)	Amplitude	0.04 ± 0.004	0.04 ± 0.004
	Phase	0	0
	Lorentzian	2	2
	Peak position	2914 ± 1	2914 ± 1
	Gaussian	23 ± 5	25 ± 4
CH_3 symmetric stretch Fermi resonance (r^+_{FR})	Amplitude	0.04 ± 0.005	0.07 ± 0.003
	Phase	0	0
	Lorentzian	2	2
	Peak position	2931 ± 1	2930 ± 1
	Gaussian	12 ± 1	12 ± 1
CH_3 asymmetric stretch (r^-)	Amplitude	0.03 ± 0.002	0.05 ± 0.002
	Phase	0	0
	Lorentzian	2	2
	Peak position	2985 ± 5	2985 ± 3
	Gaussian	128 ± 2	125 ± 3
Non-resonant background	Amplitude	0.007 ± 0.002	0.01 ± 0.002
	Phase	0	0

Table A.24. Fit parameters for VSFSS experiments on nanoemulsions stabilized by DDAPS and $MgCl_2$, corresponding to Figure 6.7b.

Fixed DDAPS concentration = 0.05 mM		Varying $MgCl_2$ concentrations	
Peak assignment	**Parameter**	**[$MgCl_2$] = 0.01 mM**	**[$MgCl_2$] = 0.1 mM**
CH_2 symmetric stretch (d^+)	Amplitude	0.06 ± 0.03	0.1 ± 0.002
	Phase	0	0
	Lorentzian	2	2
	Peak position	2854 ± 1	2853 ± 1
	Gaussian	13 ± 1	14 ± 1
CH_2 symmetric stretch (r^+)	Amplitude	0.05 ± 0.002	0.08 ± 0.004
	Phase	0	0
	Lorentzian	2	2
	Peak position	2875 ± 1	2875 ± 1
	Gaussian	14 ± 2	14 ± 1
CH_2 asymmetric stretch (d^-)	Amplitude	0.02 ± 0.003	0.05 ± 0.003
	Phase	0	0
	Lorentzian	2	2
	Peak position	2914 ± 1	2914 ± 1
	Gaussian	18 ± 4	26 ± 3
CH_3 symmetric stretch Fermi resonance (r^+_{FR})	Amplitude	0.06 ± 0.004	0.07 ± 0.003
	Phase	0	0
	Lorentzian	2	2
	Peak position	2936 ± 1	2933 ± 1
	Gaussian	14 ± 1	13 ± 1
CH_3 asymmetric stretch (r^-)	Amplitude	0.03 ± 0.001	0.04 ± 0.002
	Phase	0	0
	Lorentzian	2	2
	Peak position	2985 ± 2	2985 ± 2
	Gaussian	126 ± 2	125 ± 2
Non-resonant background	Amplitude	0.02 ± 0.001	0.02 ± 0.001
	Phase	0	0

Table A.25. Fit parameters for VSFSS experiments on nanoemulsions stabilized by DDAPS and d-SDS, corresponding to Figure 6.8a.

Fixed DDAPS concentration = 0.05 mM		Varying d-SDS concentrations		
Peak assignment	**Parameter**	**[d-SDS] = 0.01 mM**	**[d-SDS] = 0.1 mM**	**[d-SDS] = 1 mM**
CH_2 symmetric stretch (d^+)	Amplitude	0.04 ± 0.002	0.05 ± 0.003	0.04 ± 0.002
	Phase	0	0	0
	Lorentzian	2	2	2
	Peak position	2859 ± 1	2858 ± 1	2859 ± 1
	Gaussian	13 ± 1	13 ± 1	14 ± 1
CH_2 symmetric stretch (r^+)	Amplitude	0.03 ± 0.004	0.04 ± 0.004	0.04 ± 0.003
	Phase	0	0	0
	Lorentzian	2	2	2
	Peak position	2881 ± 1	2879 ± 1	2880 ± 1
	Gaussian	12 ± 1	12 ± 2	8 ± 1
CH_2 asymmetric stretch (d^-)	Amplitude	0.02 ± 0.002	0.03 ± 0.002	0.02 ± 0.002
	Phase	0	0	0
	Lorentzian	2	2	2
	Peak position	2915 ± 1	2915 ± 1	2915 ± 1
	Gaussian	31 ± 6	27 ± 5	46 ± 9
CH_3 symmetric stretch Fermi resonance (r^+_{FR})	Amplitude	0.05 ± 0.003	0.05 ± 0.003	0.03 ± 0.002
	Phase	0	0	0
	Lorentzian	2	2	2
	Peak position	2939 ± 1	2939 ± 1	2939 ± 1
	Gaussian	15 ± 1	15 ± 1	11 ± 1
CH_3 asymmetric stretch (r^-)	Amplitude	0.03 ± 0.001	0.03 ± 0.0008	0.01 ± 0.002
	Phase	0	0	0
	Lorentzian	2	2	2
	Peak position	2985 ± 3	2984 ± 3	2985 ± 2
	Gaussian	40 ± 7	46 ± 9	45 ± 4
Non-resonant background	Amplitude	0.01 ± 0.0007	0.01 ± 0.0007	0.02 ± 0.001
	Phase	0	0	0

Table A.26. Fit parameters for VSFSS experiments on nanoemulsions stabilized by DDAPS and h-SDS, corresponding to Figure 6.8b.

Fixed DDAPS concentration = 0.05 mM		Varying h-SDS concentrations		
Peak assignment	**Parameter**	**[h-SDS] = 0.01 mM**	**[h-SDS] = 0.1 mM**	**[h-SDS] = 1 mM**
CH_2 symmetric stretch (d^+)	Amplitude	0.08 ± 0.002	0.07 ± 0.002	0.08 ± 0.004
	Phase	0	0	0
	Lorentzian	2	2	2
	Peak position	2859 ± 1	2858 ± 1	2857 ± 1
	Gaussian	13 ± 1	14 ± 1	14 ± 1
CH_2 symmetric stretch (r^+)	Amplitude	0.06 ± 0.003	0.05 ± 0.009	0.08 ± 0.01
	Phase	0	0	0
	Lorentzian	2	2	2
	Peak position	2879 ± 1	2880 ± 1	2879 ± 1
	Gaussian	12 ± 1	12 ± 2	13 ± 2
CH_2 asymmetric stretch (d^-)	Amplitude	0.06 ± 0.008	0.05 ± 0.01	0.08 ± 0.009
	Phase	0	0	0
	Lorentzian	2	2	2
	Peak position	2922 ± 6	2915 ± 11	2916 ± 8
	Gaussian	30 ± 5	26 ± 5	26 ± 6
CH_3 symmetric stretch Fermi resonance (r^+_{FR})	Amplitude	0.08 ± 0.02	0.07 ± 0.04	0.07 ± 0.05
	Phase	0	0	0
	Lorentzian	2	2	2
	Peak position	2939 ± 1	2937 ± 1	2938 ± 1
	Gaussian	14 ± 1	14 ± 2	13 ± 3
CH_3 asymmetric stretch (r^-)	Amplitude	0.04 ± 0.002	0.03 ± 0.001	0.02 ± 0.004
	Phase	0	0	0
	Lorentzian	2	2	2
	Peak position	2985 ± 3	2985 ± 3	2984 ± 6
	Gaussian	27 ± 5	30 ± 9	20 ± 12
Non-resonant background	Amplitude	0.02 ± 0.0008	0.02 ± 0.0009	0.03 ± 0.002
	Phase	0	0	0

Table A.27. Fit parameters for VSFSS experiments on nanoemulsions stabilized by DDAPS and d-DTAB, corresponding to Figure 6.8c.

Fixed DDAPS concentration = 0.05 mM		Varying d-DTAB concentrations		
Peak assignment	**Parameter**	**[d-DTAB] = 0.01 mM**	**[d-DTAB] = 0.1 mM**	**[d-DTAB] = 1 mM**
CH_2 symmetric stretch (d^+)	Amplitude	0.03 ± 0.003	0.03 ± 0.002	0.03 ± 0.003
	Phase	0	0	0
	Lorentzian	2	2	2
	Peak position	2855 ± 1	2862 ± 1	2864 ± 1
	Gaussian	15 ± 1	13 ± 1	13 ± 1
CH_2 symmetric stretch (r^+)	Amplitude	0.03 ± 0.002	0.03 ± 0.005	0.02 ± 0.01
	Phase	0	0	0
	Lorentzian	2	2	2
	Peak position	2878 ± 2	2882 ± 1	2882 ± 1
	Gaussian	16 ± 3	10 ± 2	10 ± 3
CH_2 asymmetric stretch (d^-)	Amplitude	0.02 ± 0.01	0.02 ± 0.002	0.02 ± 0.002
	Phase	0	0	0
	Lorentzian	2	2	2
	Peak position	2919 ± 5	2915 ± 2	2914 ± 6
	Gaussian	21 ± 5	26 ± 3	23 ± 6
CH_3 symmetric stretch Fermi resonance (r^+_{FR})	Amplitude	0.03 ± 0.04	0.05 ± 0.002	0.05 ± 0.02
	Phase	0	0	0
	Lorentzian	2	2	2
	Peak position	2937 ± 2	2938 ± 1	2939 ± 2
	Gaussian	13 ± 4	15 ± 1	17 ± 2
CH_3 asymmetric stretch (r^-)	Amplitude	0.02 ± 0.0008	0.03 ± 0.0008	0.02 ± 0.0007
	Phase	0	0	0
	Lorentzian	2	2	2
	Peak position	2986 ± 1	2982 ± 2	2985 ± 2
	Gaussian	122 ± 2	29 ± 3	30 ± 4
Non-resonant background	Amplitude	0	0	0
	Phase	0	0	0

Table A.28. Fit parameters for VSFSS experiments on nanoemulsions stabilized by DDAPS and h-DTAB, corresponding to Figure 6.8d.

Fixed DDAPS concentration = 0.05 mM		Varying h-DTAB concentrations		
Peak assignment	**Parameter**	**[h-DTAB] = 0.01 mM**	**[h-DTAB] = 0.1 mM**	**[h-DTAB] = 1 mM**
CH_2 symmetric stretch (d^+)	Amplitude	0.06 ± 0.001	0.06 ± 0.002	0.05 ± 0.004
	Phase	0	0	0
	Lorentzian	2	2	2
	Peak position	2857 ± 1	2862 ± 1	2862 ± 1
	Gaussian	13 ± 1	13 ± 1	13 ± 1
CH_2 symmetric stretch (r^+)	Amplitude	0.04 ± 0.003	0.05 ± 0.008	0.04 ± 0.01
	Phase	0	0	0
	Lorentzian	2	2	2
	Peak position	2879 ± 1	2882 ± 1	2883 ± 1
	Gaussian	12 ± 1	12 ± 1	12 ± 1
CH_2 asymmetric stretch (d^-)	Amplitude	0.03 ± 0.005	0.05 ± 0.02	0.03 ± 0.03
	Phase	0	0	0
	Lorentzian	2	2	2
	Peak position	2916 ± 6	2916 ± 7	2915 ± 4
	Gaussian	26 ± 5	23 ± 6	25 ± 6
CH_3 symmetric stretch Fermi resonance (r^+_{FR})	Amplitude	0.05 ± 0.01	0.09 ± 0.05	0.09 ± 0.07
	Phase	0	0	0
	Lorentzian	2	2	2
	Peak position	2936 ± 1	2938 ± 2	2939 ± 3
	Gaussian	13 ± 2	15 ± 2	17 ± 3
CH_3 asymmetric stretch (r^-)	Amplitude	0.02 ± 0.002	0.04 ± 0.001	0.04 ± 0.001
	Phase	0	0	0
	Lorentzian	2	2	2
	Peak position	2980 ± 1	2982 ± 1	2985 ± 1
	Gaussian	69 ± 2	23 ± 2	20 ± 2
Non-resonant background	Amplitude	0	0	0
	Phase	0	0	0

REFERENCES

References

(1) Gupta, A.; Eral, H. B.; Hatton, T. A.; Doyle, P. S. Nanoemulsions: formation, properties and applications. *Soft Matter* **2016**, *12*, 2824–41.

(2) Mason, T.; Wilking, J.; Meleson, K.; Chang, C.; Graves, S. Nanoemulsions: formation, structure, and physical properties. *J. Phys.: Condens. Matter* **2006**, *18*, R635–R666.

(3) McClements, D. J. Nanoemulsions versus microemulsions: terminology, differences, and similarities. *Soft Matter* **2012**, *8*, 1719–1729.

(4) Tadro, T.; Izquierdo, P.; Esquena, J.; Solans, C. Formation and stability of nano-emulsions. *Advances in Colloid and Interface Science* **2004**, *108-109*, 303–318.

(5) Guerra-Rosas, M. I.; Morales-Castro, J.; Ochoa-Martinez, L. A.; Salvia-Trujillo, L.; Martin-Belloso, O. Long-term stability of food-grade nanoemulsions from high methoxyl pectin containing essential oils. *Food Hydrocolloids* **2016**, *52*, 438–446.

(6) Klang, V.; Matsko, N.; Zimmermann, A.-M.; Vojnikovic, E.; Valenta, C. Enhancement of stability and skin permeation by sucrose stearate and cyclodextrins in progesterone nanoemulsions. *International Journal of Pharmaceutics* **2010**, *393*, 153–161.

(7) Donsì, F.; Sessa, M.; Mediouni, H.; Mgaidi, A.; Ferrari, G. Encapsulation of bioactive compounds in nanoemulsion- based delivery systems. *Procedia Food Science* **2011**, *1*, 1666–1671.

(8) Aziz, Z. A. A.; Mohd-Nasir, H.; Ahmad, A.; Setapar, S. H. M.; Peng, W. L.; Chuo, S. C.; Khatoon, A.; Umar, K.; Yaqoob, A. A.; Ibrahim, M. N. M. Role of Nanotechnology for Design and Development of Cosmeceutical: Application in Makeup and Skin Care. *Frontiers in Chemistry* **2019**, *7*.

(9) Kurapatia, R.; Groth, T. W.; Raichur, A. M. Recent Developments in Layer-by-Layer Technique for Drug Delivery Applications. *ACS Appl. Bio Mater.* **2019**, *2*, 5512–5527.

(10) Zakeri, A.; Kouhbanani, M. A. J.; Beheshtkhoo, N.; Beigi, V.; Mousavi, S. M.; Hashemi, S. A. R.; Zade, A. K.; Amani, A. M.; Savardashtaki, A.; Mirzaei, E.; Jahandideh, S.; Movahedpour, A. Polyethylenimine-based nanocarriers in co-delivery of drug and gene: a developing horizon. *Nano Reviews & Experiments* **2018**, *9*, 1488497.

(11) Ariga, K.; Lvov, Y. M.; Kawakami, K.; Ji, Q.; Hill, J. P. Layer-by-layer self-assembled shells for drug delivery. *Advanced Drug Delivery Reviews* **2011**, *63*, 762–771.

(12) Lambert, A. G.; Davies, P. B.; Neivandt, D. J. Implementing the Theory of Sum Frequency Generation Vibrational Spectroscopy: A Tutorial Review. *Applied Spectroscopy Reviews* **2005**, *40*, 103–145.

(13) Superfine, R.; Huang, J. Y.; Shen, Y. R. Phase measurement for surface infrared–visible sum-frequency generation. *Optics Letters* **1990**, *15*, 1276–1278.

(14) Roke, S.; Roeterdink, W. G.; Wijnhoven, J. E. G. J.; Petukhov, A. V.; Kleyn, A. W.; Bonn, M. Vibrational Sum Frequency Scattering from a Submicron Suspension. *Phys. Rev. Lett.* **2003**, *91*, 258302.

(15) De Beer, A. G. F.; Roke, S. Sum frequency generation scattering from the interface of an isotropic particle: Geometrical and chiral effects. *Phys. Rev. B* **2007**, *75*, 245438.

(16) Roke, S.; Bonn, M.; Petukhov, A. V. Nonlinear optical scattering: The concept of effective susceptibility. *Physical Review B* **2004**, *70*, 115106.

(17) De Beer, A. G. F.; Roke, S. Nonlinear Mie theory for second-harmonic and sum-frequency scattering. *Physical Review B* **2000**, *79*, 155420.

(18) De Beer, A. G. F.; Campen, R. K.; Roke, S. Separating surface structure and surface charge with second-harmonic and sum-frequency scattering. *Physical Review B* **2010**, *82*, 235431.

(19) Carpenter, A. P.; Tran, E.; Altman, R. M.; Richmond, G. L. Formation and surface-stabilizing contributions to bare nanoemulsions created with negligible surface charge. *Proceedings of the National Academy of Sciences* **2019**, *116*, 9214–9219.

(20) Krezel, A.; Bal, W. A formula for correlating pK_a values determined in D_2O and H_2O. *Journal of Inorganic Biochemistry* **2004**, *98*, 161–166.

(21) Goldburg, W. Dynamic light scattering. *American Journal of Physics* **1999**, *67*, 1152–1160.

(22) Stetefeld, J.; McKenna, S.; Patel, T. Dynamic light scattering: a practical guide and applications in biomedical sciences. *Biophysical reviews* **2016**, *8*, 409–427.

(23) Malvern Zetasizer Nano Series User Manual. **2009**, *Mano317 Issue 5.0*.

(24) Kaszuba, M.; Corbett, J.; Watson, F.; Jones, A. High-concentration zeta potential measurements using light-scattering techniques. *Philos. Trans. R. Soc. A: Math., Phys. Eng. Sci.* **2010**, *368*, 4439–4451.

(25) De Aguiar, H. B.; Strader, M. L.; de Beer, A. G. F.; Roke, S. Surface Structure of Sodium Dodecyl Sulfate Surfactant and Oil at the Oil-in-Water Droplet Liquid/Liquid Interface: A Manifestation of a Nonequilibrium Surface State. *J. Phys. Chem. B* **2011**, *115*, 2970–2978.

(26) Smolentsev, N.; Smit, W. J.; Bakker, H. J.; Roke, S. The interfacial structure of water droplets in a hydrophobic liquid. *Nature Communications* **2017**, *8*, 15548.

(27) Beaman, D. K.; Robertson, E. J.; Richmond, G. L. From Head to Tail: Structure, Solvation, and Hydrogen Bonding of Carboxylate Surfactants at the Organic–Water Interface. *The Journal of Physical Chemistry C* **2011**, *115*, 12508–12516.

(28) Beaman, D. K.; Robertson, E. J.; Richmond, G. L. Unique Assembly of Charged Polymers at the OilWater Interface. *Langmuir* **2011**, *27*, 2104–2106.

(29) Altman, R. M.; Richmond, G. L. Coming to Order: Adsorption and Structure of Nonionic Polymer at the Oil/Water Interface as Influenced by Cationic and Anionic Surfactants. *Langmuir* **2020**, *36*, 1975–1984.

(30) Robertson, E. J. Vibrational Sum Frequency Spectroscopic Investigations of Carboxylic Acid-Containing Polyelectrolytes at the Oil-Water Interface. *University of Oregon* **2014**, *Eugene, OR*.

(31) Beaman, D. K. Vibrational sum-frequency spectroscopy investigations of carboxylic acid based surfactants and polymers at the oil-water interface. *University of Oregon* **2010**, *Eugene, OR*.

(32) Schabes, B. K. Mixtures of Polyelectrolytes and Surfactants at the Oil/Water Interface. *University of Oregon* **2019**, *Eugene, OR*.

(33) Bain, C. D.; Davies, P. B.; Ong, T. H.; Ward, R. N.; Brown, M. A. The Structure of Interfaces Probed by Sum-frequency Spectroscopy. *Surface and Interface Analysis* **1991**, *17*, 529–541.

(34) Bain, C. D.; Davies, P. B.; Ong, T. H.; Ward, R. N.; Brown, M. A. Quantitative analysis of monolayer composition by sum-frequency vibrational spectroscopy. *Langmuir* **1991**, *7*, 1563–1566.

(35) Fred G. Moore, K. A. B.; Richmond, G. L. Challenges in Interpreting Vibrational Sum Frequency Spectra: Deconvoluting Spectral Features as Demonstrated in the Calcium Fluoride—Water—Sodium Dodecylsulfate System. *Applied Spectroscopy* **2002**, *56*, DOI: https://doi.org/10.1366/000370202321116048.

(36) Szczepanowicz, K.; Bazylińska, U.; Pietkiewicz, J.; Szyk-Warszyńska, L.; Wilk, K. A.; Warszyński, P. Biocompatible long-sustained release oil-core polyelectrolyte nanocarriers: From controlling physical state and stability to biological impact. *Advances in Colloid and Interface Science* **2015**, *222*, 678–691.

(37) Miyake, M. Recent progress of the characterization of oppositely charged polymer/surfactant complex in dilution deposition system. *Advances in Colloid and Interface Science* **2017**, *239*, 146–157.

(38) Petkova, R.; Tcholakova, S.; Denkov, N. D. Foaming and Foam Stability for Mixed Polymer–Surfactant Solutions: Effects of Surfactant Type and Polymer Charge. *Langmuir* **2012**, *28*, 4996–5009.

(39) Li, Y.; Ghoreishi, S. M.; Warr, J.; Bloor, D. M.; Holzwarth, J. F.; Wyn-Jones, E. Binding of Sodium Dodecyl Sulfate to Some Polyethyleneimines and Their Ethoxylated Derivatives at Different pH Values. Electromotive Force and Microcalorimetry Studies. *Langmuir* **2000**, *16*, 3093–3100.

(40) Halacheva, S. S.; Penfold, J.; Thomas, R. K.; Webster, J. R. P. Effect of Polymer Molecular Weight and Solution pH on the Surface Properties of Sodium Dodecylsulfate-Poly(Ethyleneimine) Mixtures. *Langmuir* **2012**, *28*, 14909–14916.

(41) Halacheva, S. S.; Penfold, J.; Thomas†, R. K.; Webster, J. R. P. Solution pH and Oligoamine Molecular Weight Dependence of the Transition from Monolayer to Multilayer Adsorption at the Air–Water Interface from Sodium Dodecyl Sulfate/Oligoamine Mixtures. *Langmuir* **2013**, *29*, 5832–5840.

(42) Penfold, J.; Tucker, I.; Thomas, R. K.; Taylor, D. J. F.; Zhang, J.; Bell, C. Influence of the Polyelectrolyte Poly(ethyleneimine) on the Adsorption of Surfactant Mixtures of Sodium Dodecyl Sulfate and Monododecyl Hexaethylene Glycol at the AirSolution Interface. *Langmuir* **2006**, *22*, 8840–8849.

(43) Penfold, J.; Tucker, I.; Thomas, R. K.; Zhang, J. Adsorption of Polyelectrolyte/Surfactant Mixtures at the AirSolution Interface: Poly(ethyleneimine)/Sodium Dodecyl Sulfate. *Langmuir* **2005**, *21*, 10061–10073.

(44) Tucker, I. M.; Petkov, J. T.; Jones, C.; Penfold, J.; Thomas, R. K.; Rogers, S. E.; Terry, A. E.; Heenan, R. K.; Grillo, I. Adsorption of Polymer–Surfactant Mixtures at the Oil–Water Interface. *Langmuir* **2012**, *28*, 14974–14982.

(45) Penfold, J.; Thomas, R. K.; Zhang, X. L.; Taylor, D. J. F. Nature of AmineSurfactant Interactions at the AirSolution Interface. *Langmuir* **2009**, *25*, 3972–3980.

(46) Penfold, J.; Tucker, I.; Thomas, R. K.; Taylor, D. J. F.; Zhang, J.; Zhang, X. L. The Impact of Electrolyte on the Adsorption of Sodium Dodecyl Sulfate/Polyethyleneimine Complexes at the AirSolution Interface. *Langmuir* **2007**, *23*, 3690–3698.

(47) Zhao, X.; Pan, F.; Lu, J. R. Adsorption of polyethyleneimine characterized by spectroscopic ellipsometry. *Progress in Natural Science* **2005**, *15*, 56–59.

(48) Angus-Smyth, A.; Bain, C. D.; Vargac, I.; Campbell, R. A. Effects of bulk aggregation on PEI–SDS monolayers at the dynamic air–liquid interface: depletion due to precipitation versus enrichment by a convection/spreading mechanism. *Soft Matter* **2013**, *26*, 6103–6117.

(49) Robertson, E. J.; Richmond, G. L. Chunks of Charge: Effects at Play in the Assembly of Macromolecules at Fluid Surfaces. *Langmuir* **2013**, *29*, 10980–10989.

(50) Beaman, D. K.; Robertson, E. J.; Richmond, G. L. Ordered polyelectrolyte assembly at the oil–water interface. *Proceedings of the National Academy of Sciences* **2012**, *9*, 3226–3231.

(51) Windsor, R.; Neivandt, D. J.; Davies, P. B. Adsorption of Sodium Dodecyl Sulfate in the Presence of Poly(ethylenimine) and Sodium Chloride Studied Using Sum Frequency Vibrational Spectroscopy. *Langmuir* **2001**, *17*, 7306–7312.

(52) Wang, H.; Wang, Y.; Yan, H.; Zhang, J.; Thomas, R. K. Binding of Sodium Dodecyl Sulfate with Linear and Branched Polyethyleneimines in Aqueous Solution at Different pH Values. *Langmuir* **2006**, *22*, 1526–1533.

(53) Curtis, K. A.; Miller, D.; Millard, P.; Basu, S.; Horkay, F.; Chandran, P. L. Unusual Salt and pH Induced Changes in Polyethylenimine Solutions. *PLoS ONE* **2016**, *11*, DOI: https://doi.org/10.1371/journal.pone.0158147.

(54) De Aguiar, H. B.; Strader, M. L.; de Beer, A. G. F.; Roke, S. Surface Structure of Sodium Dodecyl Sulfate Surfactant and Oil at the Oil-in-Water Droplet Liquid/Liquid Interface: A Manifestation of a Nonequilibrium Surface State. *J. Phys. Chem. B* **2011**, *115*, 2970–2978.

(55) Becraft, K. A.; Moore, F. G.; Richmond, G. L. Charge Reversal Behavior at the CaF_2/H_2O/SDS Interface as Studied by Vibrational Sum Frequency Spectroscopy. *J. Phys. Chem. B* **2003**, *107*, 3675–3678.

(56) Conboy, J. C.; Messmer, M. C.; Richmond, G. L. Investigation of Surfactant Conformation and Order at the LiquidLiquid Interface by Total Internal Reflection Sum-Frequency Vibrational Spectroscopy. *J. Phys. Chem.* **1996**, *100*, 7617–7622.

(57) Khan, N.; Brettmann, B. Intermolecular Interactions in Polyelectrolyte and Surfactant Complexes in Solution. *Polymers* **2019**, *11*, 7617–7622.

(58) Hensel, J. K.; Carpenter, A. P.; Ciszewski, R. K.; Schabes, B. K.; Kittredge, C. T.; Moore, F. G.; Richmond, G. L. Molecular characterization of water and surfactant AOT at nanoemulsion surfaces. *Proceedings of the National Academy of Sciences* **2017**, *114*, 13351–13356.

(59) Scheu, R.; Chen, Y.; de Aguiar, H. B.; Rankin, B. M.; Ben-Amotz, D.; Roke, S. Specific Ion Effects in Amphiphile Hydration and Interface Stabilization. *J. Am. Chem. Soc.* **2014**, *136*, 2040–2047.

(60) Schabes, B. K.; Hopkins, E. J.; Richmond, G. L. Molecular Interactions Leading to the Coadsorption of Surfactant Dodecyltrimethylammonium Bromide and Poly(styrenesulfonate) at the Oil/Water Interface. *Langmuir* **2019**, *35*, 7268–7276.

(61) Altman, R. M.; Richmond, G. L. Coming to Order: Adsorption and Structure of Nonionic Polymer at the Oil/Water Interface as Influenced by Cationic and Anionic Surfactants. *Langmuir* **2020**, *36*, 1975–1984.

(62) Sheth, N.; Ngo, D.; Banerjee, J.; Zhou, Y.; Pantano, C. G.; Kim, S. H. Probing Hydrogen-Bonding Interactions of Water Molecules Adsorbed on Silica, Sodium Calcium Silicate, and Calcium Aluminosilicate Glasses. *J. Phys. Chem. C* **2018**, *122*, 17792–17801.

(63) Makarem, M.; Lee, C. M.; Sawada, D.; O'Neill, H. M.; Kim, S. H. Distinguishing Surface versus Bulk Hydroxyl Groups of Cellulose Nanocrystals Using Vibrational Sum Frequency Generation Spectroscopy. *J. Phys. Chem. Lett.* **2018**, *9*, 70–75.

(64) Olsson, A.-M.; Salmén, L. The association of water to cellulose and hemicellulose in paper examined by FTIR spectroscopy. *Carbohydrate Research* **2004**, *339*, 813–818.

(65) Brown, M. G.; Raymond, E. A.; Allen, H. C.; Scatena, L. F.; Richmond, G. L. The Analysis of Interference Effects in the Sum Frequency Spectra of Water Interfaces. *J. Phys. Chem. A* **2000**, *104*, 10220–10226.

(66) Batchelor, S. N.; Tucker, I.; Petkov, J. T.; Penfold, J.; Thomas, R. K. Sodium Dodecyl Sulfate–Ethoxylated Polyethylenimine Adsorption at the Air–Water Interface: How the Nature of Ethoxylation Affects the Pattern of Adsorption. *Langmuir* **2014**, *30*, 9761–9769.

(67) Zhang, X. L.; Taylor, D. J. F.; Thomas, R. K.; Penfold, J. Adsorption of Polyelectrolyte/Surfactant Mixtures at the AirWater Interface: Modified Poly(ethyleneimine) and Sodium Dodecyl Sulfate. *Langmuir* **2011**, *27*, 2601–2612.

(68) Windsor, R.; Neivandt, D. J.; Davies, P. B. Temperature and pH Effects on the Coadsorption of Sodium Dodecyl Sulfate and Poly(ethylenimine). *Langmuir* **2002**, *18*, 2199–2204.

(69) Decher, G.; Hong, J. D.; Schmitt, J. Buildup of ultrathin multilayer films by a self- assembly process: III. Consecutively alternating adsorption of anionic and cationic polyelectrolytes on charged surfaces. *Thin Solid Films* **1992**, *210-211*, 831–835.

(70) Sun, B.; Flessner, R.; Saurer, E.; Jewell, C.; Fredin, N.; Lynn, D. Characterization of pH-induced changes in the morphology of polyelectrolyte multilayers assembled from poly(allylamine) and low molecular weight poly(acrylic acid). *J. Colloid Interface Sci.* **2011**, *335*, 431–441.

(71) DeRocher, J. P.; Mao, P.; Han, J.; Rubner, M. F.; Cohen, R. E. Layer-by-Layer Assembly of Polyelectrolytes in Nanofluidic Devices. *Macromolecules* **2010**, *43*, 2430–2437.

(72) Andreeva, D. V.; Skorb, E. V.; Shchukin, D. G. Layer-by-Layer Polyelectrolyte/Inhibitor Nanostructures for Metal Corrosion Protection. *ACS Appl. Mater. Interfaces* **2010**, *7*, 1954–1962.

(73) L.Macdonald, M.; E.Samuel, R.; J.Shah, N.; F.Padera, R.; M.Beben, Y.; T.Hammond, P. Tissue integration of growth factor-eluting layer-by-layer polyelectrolyte multilayer coated implants. *Biomaterials* **2011**, *32*, 1446–1453.

(74) Stekolshchikova, A. A.; Radaev, A. V.; Orlova, O. Y.; Nikolaev, K. G.; Skorb, E. V. Thin and Flexible Ion Sensors Based on Polyelectrolyte Multilayers Assembled onto the Carbon Adhesive Tape. *ACS Omega* **2019**, *4*, 15421–15427.

(75) M.Budy, S.; J.Hamilton, D.; Cai, Y.; Knowles, M. K.; M.Reed, S. Polymer mediated layer-by-layer assembly of different shaped gold nanoparticles. *Journal of Colloid and Interface Science* **2017**, *487*, 336–347.

(76) Jin, H.; Choi, S.; Lee, H. J.; Kim, S. Layer-by-Layer Assemblies of Semiconductor Quantum Dots for Nanostructured Photovoltaic Devices. *J. Phys. Chem. Lett.* **2013**, *4*, 2461–2470.

(77) Rochin-Wong, S.; Rosas-Durazo, A.; Zavala-Rivera, P.; Maldonado, A.; Martinez-Barbosa, M.; Velaz, I.; Tanori, J. Drug Release Properties of Diflunisal from Layer-By-Layer Self-Assembled κ-Carrageenan/Chitosan Nanocapsules: Effect of Deposited Layers. *Polymers* **2018**, *10*.

(78) Singh, Y.; Meher, J. G.; Raval, K.; AliKhan, F.; Chaurasia, M.; K.Jain, N.; Chourasia, M. K. Nanoemulsion: Concepts, development and applications in drug delivery. *Journal of Controlled Release* **2017**, *252*, 28–49.

(79) Schmitt, J.; Gruenewald, T.; Decher, G.; Pershan, P. S.; Kjaer, K.; Loesche, M. Internal structure of layer-by-layer adsorbed polyelectrolyte films: a neutron and x-ray reflectivity study. *Macromolecules* **1993**, *26*, 7058–7063.

(80) Forzani, E. S.; Otero, M.; Perez, M. A.; Teijelo, M. L.; Calvo, E. J. The Structure of Layer-by-Layer Self-Assembled Glucose Oxidase and $Os(Bpy)_2ClPyCH_2NHPoly(allylamine)$ Multilayers: Ellipsometric and Quartz Crystal Microbalance Studies. *Langmuir* **2002**, *18*, 4020–4029.

(81) Cassier, T.; Lowack, K.; Decher, G. Layer-by-layer assembled protein/polymer hybrid films: nanoconstruction via specific recognition. *Supramolecular Science* **1998**, *5*, 309–315.

(82) Kolasinska, M.; Krastev, R.; Warszynski, P. Characteristics of polyelectrolyte multilayers: Effect of PEI anchoring layer and posttreatment after deposition. *Journal of Colloid and Interface Science* **2007**, *305*, 46–56.

(83) Czerwieniec, B.; Strawski, M.; Granicka, L.; Szklarczyk, M. AFM study of adhesion and interactions between polyelectrolyte bilayers assembly. *Colloids and Surfaces A: Physicochemical and Engineering Aspects* **2018**, *555*, 465–472.

(84) Kett, P.; Casford, M.; Yang, A.; Lane, T.; Johal, M.; Davies, P. Structural Changes in a Polyelectrolyte Multilayer Assembly Investigated by Reflection Absorption Infrared Spectroscopy and Sum Frequency Generation Spectroscopy. *J. Phys. Chem. B* **2009**, *113*, 1559–1568.

(85) Silva, H. S.; Miranda, P. B. Molecular Ordering of Layer-by-Layer Polyelectrolyte Films Studied by Sum-Frequency Vibrational Spectroscopy. *J. Phys. Chem. B* **2009**, *113*, 10068–10071.

(86) Zhang, R.; Zhang, Z.; McClements, D. J. Nanoemulsions: An emerging platform for increasing the efficacy of nutraceuticals in foods. *Colloids and Surfaces B: Biointerfaces* **2020**, *194*, 111202.

(87) Kharat, M.; Aberg, J.; Dai, T.; McClements, D. J. Comparison of Emulsion and Nanoemulsion Delivery Systems: The Chemical Stability of Curcumin Decreases as Oil Droplet Size Decreases. *J. Agric. Food Chem.* **2020**, *68*, 9205–9212.

(88) Sonneville-Aubrun, O.; L'Alloret, J.-T. S. F. Nanoemulsions: a new vehicle for skincare products. *Advances in Colloid and Interface Science* **2004**, *108-109*, 145–149.

(89) Stanimirova, R. D.; Kralchevsky, P. A.; Danov, K. D.; Xu, H.; Ung, Y. W.; Petkov, J. T. Oil drop deposition on solid surfaces in mixed polymer-surfactant solutions in relation to hair- and skin-care applications. *Colloids and Surfaces A: Physicochemical and Engineering Aspects* **2019**, *577*, 53–61.

(90) Nazarzadeh, E.; Anthonypillai, T.; Sajjadi, S. On the growth mechanisms of nanoemulsions. *Journal of Colloid and Interface Science* **2013**, *397*, 154–162.

(91) Kabong, M. A.; Focke, W. W.; Toit, E. L. D.; Rolfes, H.; Ramjee, S. Breakdown mechanisms of oil-in-water emulsions stabilised with Pluronic F127 and co-surfactants. *Colloids and Surfaces A: Physicochemical and Engineering Aspects* **2020**, *585*, 124101.

(92) Wang, L.; Tabor, R.; Eastoe, J.; Li, X.; Heenanc, R. K.; Dong, J. Formation and stability of nanoemulsions with mixed ionic–nonionic surfactants. *Physical Chemistry Chemical Physics* **2009**, *11*, 9772–9778.

(93) Ning, J.; Wei, B.; Mao, R.; Wang, Y.; Shang, J.; Sun, L. Pore-Level Observations of an Alkali-Induced Mild O/W Emulsion Flooding for Economic Enhanced Oil Recovery. *Energy Fuels* **2018**, *32*, 10595–10604.

(94) Lua, Y.; Sun, D.; Ralston, J.; Liu, Q.; Xua, Z. CO_2-responsive surfactants with tunable switching pH. *Journal of Colloid and Interface Science* **2019**, *557*, 185–195.

(95) Adamczak, M.; Para, G.; Simon, C.; Warszyński, P. Natural oil nanoemulsions as cores for layer-by-layer encapsulation. *Journal of Microencapsulation* **2013**, *30*, 479–489.

(96) Ábrahám, Á.; Kardos, A.; Mezei, A.; Campbell, R. A.; Varga, I. Effects of Ionic Strength on the Surface Tension and Nonequilibrium Interfacial Characteristics of Poly(sodium styrenesulfonate)/Dodecyltrimethylammonium Bromide Mixtures. *Langmuir* **2014**, *30*, 4970–4979.

(97) Ritaccoa, H.; Albouy, P.-A.; Bhattacharyya, A.; Langevin, D. Influence of the polymer backbone rigidity on polyelectrolyte–surfactant complexes at the air/water interface. *Physical Chemistry Chemical Physics* **2000**, *2*, 5243–5251.

(98) Kristen-Hochrein, N.; Laschewsky, A.; Miller, R.; von Klitzing, R. Stability of Foam Films of Oppositely Charged Polyelectrolyte/Surfactant Mixtures: Effect of Isoelectric Point. *J. Phys. Chem. B* **2011**, *115*, 14475–14483.

(99) Tummino, A.; J.T.; Sebastiani, F.; Noskov, B.; Varga, I.; Campbell, R. Effects of Aggregate Charge and Subphase Ionic Strength on the Properties of Spread Polyelectrolyte/Surfactant Films at the Air/Water Interface under Static and Dynamic Conditions. *Langmuir* **2018**, *34*, 2312–2323.

(100) Zhang, Y.; He, S.; Li, Y.; Tang, H. The physical stability and digestibility of b-carotene in oil-in-water sodium caseinate nanoemulsion. *Journal of Food Measurement and Characterization* **2016**, *22*, 864–871.

(101) Ozturk, B.; Sanem; Argin; Ozilgen, M.; McClements, D. J. Formation and stabilization of nanoemulsion-based vitamin E delivery systems using natural biopolymers: Whey protein isolate and gum arabic. *Food Chemistry* **2015**, *188*, 256–263.

(102) Bazylińska, U.; Skrzela, R.; Szczepanowicz, K.; Warszyński, P.; Wilk, K. A. Novel approach to long sustained multilayer nanocapsules: influence of surfactant head groups and polyelectrolyte layer number on the release of hydrophobic compounds. *Soft Matter* **2011**, *7*, 6113–6124.

(103) Tran, E.; Carpenter, A. P.; Richmond, G. L. Probing the Molecular Structure of Coadsorbed Polyethylenimine and Charged Surfactants at the Nanoemulsion Droplet Surface. *Langmuir* **2020**, *36*, 9081–9089.

(104) Knock, M. M.; Bell, G. R.; Hill, E. K.; Turner, H. J.; Bain, C. D. Sum-Frequency Spectroscopy of Surfactant Monolayers at the Oil–Water Interface. *J. Phys. Chem. B* **2003**, *107*, 10801–10814.

(105) Goloub, T.; Pugh, R. J. The role of the surfactant head group in the emulsification process: Single surfactant systems. *J. Colloid Interface Sci.* **2003**, *257*, 337–343.

(106) Altman, R. M.; Richmond, G. L. Twist and Stretch: Assignment and Surface Charge Sensitivity of a Water Combination Band and Its Implications for Vibrational Sum Frequency Spectra Interpretations. *J. Phys. Chem. B* **2021**, *125*, 6717–6726.

(107) Cejka, J.; van Bekkum, H.; Corma, A.; Schueth, F., *Introduction to Zeolite Science and Practice*, 2007; Vol. 168.

(108) Jadhav, C.; Kate, V.; Payghan, S. A. Investigation of effect of non-ionic surfactant on preparation of griseofulvin non-aqueous nanoemulsion. *Journal of Nanostructure in Chemistry* **2015**, *5*, 107113.

(109) Koroleva, M.; Nagovitsina, T.; Yurtov, E. Nanoemulsions stabilized by non-ionic surfactants: stability and degradation mechanisms. *Physical Chemistry Chemical Physics* **2018**, *20*, 1036910377.

(110) Zhao, Y.; Peng, F.; Ke, Y. Design and characterization of oil-in-water nanoemulsion for enhanced oil recovery stabilized by amphiphilic copolymer, nonionic surfactant, and LAPONITE RD. *RSC Advances* **2021**, *11*, 1952–1959.

(111) Hoeller, S.; Sperger, A.; Valenta, C. Lecithin based nanoemulsions: A comparative study of the influence of non-ionic surfactants and the cationic phytosphingosine on physicochemical behaviour and skin permeation. *International Journal of Pharmaceutics* **2009**, *370*, 181–186.

(112) Sonneville-Aubrun, O.; Babayan, D.; Bordeaux, D.; Lindner, P.; Rata, G.; Cabane, B. Phase transition pathways for the production of 100 nm oil-in-water emulsions. *Physical Chemistry Chemical Physics* **2009**, *11*, 101–110.

(113) Clogston, J. D.; Patri, A. K., *Zeta Potential Measurement. In: McNeil, S. (eds) Characterization of Nanoparticles Intended for Drug Delivery. Methods in Molecular Biology (Methods and Protocols)*, 2011; Vol. 697, pp 63–63.

(114) Barany, S. Polymer adsorption and electrokinetic potential of dispersed particles in weak and strong electric fields. *Advances in Colloid and Interface Science* **2015**, *222*, 58–69.

(115) Kaszuba, M.; Corbett, J.; Watson, F. M.; Jones, A. High-concentration zeta potential measurements using light-scattering techniques. *Philos. Trans. R. Soc., A* **2010**, *368*, 44394451.

(116) Israelachvili, J. N., *Intermolecular and Surface Forces*, 1991; Vol. 2 Ed. P 480.

(117) Zdrali, E.; Okur, H. I.; Roke, S. Specific Ion Effects at the Interface of Nanometer-Sized Droplets in Water: Structure and Stability. *J. Phys. Chem. C* **2019**, *123*, 1662116630.

(118) Morozova, T. I.; Lee, V. E.; Panagiotopoulos, A. Z.; Prud'homme, R. K.; Priestley, R. D.; Nikoubashman, A. On the Stability of Polymeric Nanoparticles Fabricated through Rapid Solvent Mixing. *Langmuir* **2019**, *35*, 709–717.

(119) Smith, A. M.; Lee, A. A.; Perkin, S. The Electrostatic Screening Length in Concentrated Electrolytes Increases with Concentration. *J. Phys. Chem. Lett.* **2016**, *7*, 2157–2163.

(120) Worthen, A. J.; Tran, V.; Cornell, K. A.; Truskett, T. M.; Johnston, K. P. Steric stabilization of nanoparticles with grafted low molecular weight ligands in highly concentrated brines including divalent ions. *Soft Matter* **2016**, *12*, 2025–2039.

(121) J.Babchin, A.; L.Schramm, L. Osmotic repulsion force due to adsorbed surfactants. *Colloids and Surfaces B: Biointerfaces* **2012**, *91*, 137–143.

(122) Fritz, G.; Schädler, V.; Willenbacher, N.; Wagner, N. J. Electrosteric Stabilization of Colloidal Dispersions. *Langmuir* **2002**, *18*, 6381–6390.

(123) Zhang, C. Sum Frequency Generation Vibrational Spectroscopy for Characterization of Buried Polymer Interfaces. *Applied Spectroscopy* **2017**, *71*, 1717–1749.

(124) Conboy, J. C.; Messmer, M. C.; Richmond, G. L. Investigation of Surfactant Conformation and Order at the LiquidLiquid Interface by Total Internal Reflection Sum-Frequency Vibrational Spectroscopy. *J. Phys. Chem.* **1996**, *100*, 7617–7622.

(125) Maeda, Y.; Nakamura, T.; Ikeda, I. Changes in the Hydration States of Poly(N-alkylacrylamide)s during Their Phase Transitions in Water Observed by FTIR Spectroscopy. *Macromolecules* **2001**, *34*, 1391–1399.

(126) Bucatariu, F.; Ghiorghita, C.-A.; Schwarz, D.; Boita, T.; Mihai, M. Layer-by-layer polyelectrolyte architectures with ultra-fast and high loading/release properties for copper ions. *Colloids and Surfaces A: Physicochemical and Engineering Aspects* **2019**, *579*, 123704.

(127) Zaldivar, G.; Tagliazucchi, M. Layer-by-Layer Self-Assembly of Polymers with Pairing Interactions. *ACS Macro Lett.* **2016**, *5*, 862–866.

(128) Bai, S.; Wang, Z.; Gao, J.; Zhang, X. Hydrogen-bonding-directed layer-by-layer polymer films: Substrate effect on the microporous morphology variation. *European Polymer Journal* **2006**, *42*, 900–907.

(129) Kharlampieva, E.; Kozlovskaya, V.; Ankner, J. F.; Sukhishvili, S. A. Hydrogen-Bonded Polymer Multilayers Probed by Neutron Reflectivity. *Langmuir* **2008**, *24*, 11346–11349.

(130) Hafizah, M. A. E.; Riyadi, A. F.; Manaf, A.; Andreas Particle Size Reduction of Polyaniline Assisted by Anionic Emulsifier of Sodium Dodecyl Sulphate (SDS) Through Emulsion Polymerization. *IOP Conf. Ser.: Mater. Sci. Eng.* **2019**, *515*, 012080.

(131) Gao, X.; Chorover, J. Adsorption of sodium dodecyl sulfate (SDS) at ZnSe and α-Fe_2O_3 surfaces: Combining infrared spectroscopy and batch uptake studies. *Journal of Colloid and Interface Science* **2010**, *348*, 167–176.

(132) Hore, D. K.; Beaman, D. K.; Parks, D. H.; Richmond, G. L. Whole-Molecule Approach for Determining Orientation at Isotropic Surfaces by Nonlinear Vibrational Spectroscopy. *J. Phys. Chem. B* **2005**, *109*, 16846–16851.

(133) Wang, Z.; Morales-Acosta, M. D.; Li, S.; Liu, W.; Kanai, T.; Liu, Y.; Chen, Y.-N.; Walker, F. J.; Ahn, C. H.; Leblanc, R. M.; Yan, E. C. Y. A narrow amide I vibrational band observed by sum frequency generation spectroscopy reveals highly ordered structures of a biofilm protein at the air/water interface. *Chemical Communications* **2016**, *52*, 2956–2959.

(134) Takemoto, Y.; Ajiro, H.; Akashi, M. Hydrogen-Bonded Multilayer Films Based on Poly(N-vinylamide) Derivatives and Tannic Acid. *Langmuir* **2015**, *31*, 6863–6869.

(135) Takemoto, Y.; Ajiro, H.; Akashi, M. Amphiphilic Poly(N-vinyl acetamide) Gels Strengthened with Swelling Solvent. *Macromolecular Chemistry and Physics* **2014**, *215*, 384–390.

(136) Schmüser, L.; Golbek, T. W.; Weidner, T. Windowless detection geometry for sum frequency scattering spectroscopy in the C–D and amide I regions. *Biointerfaces* **2021**, *16*, 011201.

(137) Foster, M. J.; Carpenter, A. P.; Richmond, G. L. Dynamic Duo: Vibrational Sum Frequency Scattering Investigation of pH-Switchable Carboxylic Acid/Carboxylate Surfactants on Nanodroplet Surfaces. *J. Phys. Chem. B* **2021**, *125*, 9629–9640.

(138) Laß, K.; Han, X.; Hasselbrink, E. The surprisingly short vibrational lifetime of the internal stretch of CO adsorbed on Si(100). *J. Chem. Phys.* **2005**, *123*, 051102.

(139) Schulze-Zachau, F.; Bachmann, S.; Braunschweig, B. Effects of Ca^{2+} Ion Condensation on the Molecular Structure of Polystyrene Sulfonate at Air–Water Interfaces. *Langmuir* **2018**, *34*, 11714–11722.

(140) Curtis, A. D.; Reynolds, S. B.; Calchera, A. R.; Patterson, J. E. Understanding the Role of Nonresonant Sum-Frequency Generation from Polystyrene Thin Films. *J. Phys. Chem. Lett.* **2010**, *1*, 2435–2439.

(141) Lagutchev, A.; Hambir, S. A.; Dlott, D. D. Nonresonant Background Suppression in Broadband Vibrational Sum-Frequency Generation Spectroscopy. *J. Phys. Chem. C* **2007**, *111*, 13645–13647.

(142) Ohno, P. E.; Wang, H.-f.; Geiger, F. M. Second-order spectral lineshapes from charged interfaces. *Nature Communications* **2017**, *8*, DOI: `https://doi.org/10.1038/s41467-017-01088-0`.

(143) Gonella, G.; Lütgebaucks, C.; de Beer, A. G. F.; Roke, S. Second Harmonic and Sum-Frequency Generation from Aqueous Interfaces Is Modulated by Interference. *J. Phys. Chem. C* **2016**, *120*, 9165–9173.

(144) Wang, H.-f. Sum frequency generation vibrational spectroscopy (SFG-VS) for complex molecular surfaces and interfaces: Spectral lineshape measurement and analysis plus some controversial issues. *Progress in Surface Science* **2016**, *91*, 155–182.

(145) Matsusaki, M.; Ajiro, H.; Kida, T.; Serizawa, T.; Akash, M. Layer-by-Layer Assembly Through Weak Interactions and Their Biomedical Applications. *Advanced Materials* **2011**, *24*, 454–474.

(146) Oda, Y.; Horinouchi, A.; Kawaguchi, D.; Matsuno, H.; Kanaoka, S.; Aoshima, S.; Tanaka, K. Effect of Side-Chain Carbonyl Groups on the Interface of Vinyl Polymers with Water. *Langmuir* **2014**, *30*, 1215–1219.

(147) Panarin, E. F.; Kalnin'sh, K. K.; Azanova, V. V. IR spectra and structure of poly(vinylamide) complexes with hydrogen peroxide. *Polym. Sci. Ser. A* **2007**, *49*, 275–283.

(148) Fayzullin, R. R.; Shteingolts, S. A.; Lodochnikova, O. A.; Mamedova, V. L.; Korshin, D. E.; Mamedov, V. A. Intermolecular head-to-head interaction of carbonyl groups in bicyclic hydrogen-bonded synthon based on -hydroxy ketones. *CrystEngComm* **2019**, *21*, 1587–1599.

(149) Pu, W.; Yuan, C.; Hu, W.; Tan, T.; Hui, J.; Zhao, S.; Wang, S.; Tang, Y. Effects of interfacial tension and emulsification on displacement efficiency in dilute surfactant flooding. *RSC Advances* **2016**, *6*, 50640.

(150) Varade, S. R.; Ghosh, P. Foaming in Aqueous Solutions of Zwitterionic Surfactant: Effects of Oil and Salts. *Journal of Dispersion Science and Technology* **2017**, *38*, 1532–2351.

(151) Varade, S. R.; Ghosh, P. Foaming in aqueous solutions of zwitterionic surfactant in presence of monovalent salts: The specific ion effect. *Chemical Engineering Communications* **2019**, *207*, 1563–5201.

(152) Petkova, R.; Tcholakova, S.; Denkov, N. D. Foaming and Foam Stability for Mixed PolymerSurfactant Solutions: Effects of Surfactant Type and Polymer Charge. *Langmuir* **2012**, *28*, 49965009.

(153) Xu, Z. P.; Braterman, P. S. High affinity of dodecylbenzene sulfonate for layered double hydroxide and resulting morphological changes. *Journal of Materials Chemistry* **2003**, *13*, 268–273.

(154) Yoon, I.-H.; Yoon, S. B.; Sihn, Y.; Choi, M.-S.; Jung, C.-H.; Choi, W.-K. Stabilizing decontamination foam using surface-modified silica nanoparticles containing chemical reagent: foam stability, structures, and dispersion properties. *RSC Advances* **2021**, *11*, 1841–1849.

(155) Tamjidi, S.; Moghadas, B. K.; Esmaeili, H.; Khoo, F. S.; Gholami, G.; Ghasemi, M. Improving the surface properties of adsorbents by surfactants and their role in the removal of toxic metals from wastewater: A review study. *Process Safety and Environmental Protection* **2021**, *148*, 775–795.

(156) Sharifi, F.; Jahangiri, M.; Nazir, I.; Asim, M. H.; Ebrahimnejad, P.; Hupfauf, A.; Gust, R.; Bernkop-Schnürch, A. Zeta potential changing nanoemulsions based on a simple zwitterion. *Journal of Colloid and Interface Science* **2021**, *585*, 126–137.

(157) Van der Merwe, J.; Steenekamp, J.; Steyn, D.; Hamman, J. The Role of Functional Excipients in Solid Oral Dosage Forms to Overcome Poor Drug Dissolution and Bioavailability. *Pharmaceutics* **2020**, *12*, 393.

(158) Harwansh, R. K.; Deshmukh, R.; Rahman, M. A. Nanoemulsion: Promising nanocarrier system for delivery of herbal bioactives. *Journal of Drug Delivery Science and Technology* **2019**, *51*, 224–233.

(159) Dien, S. M.; Anton, N.; Bouriat, P.; Thioune, O.; Sy, P. M.; Massaddeq, N.; Enharrar, S.; Diarra, M.; Vandamme, T. Pickering nano-emulsions stabilized by solid lipid nanoparticles as a temperature sensitive drug delivery system. *Soft Matter* **2019**, *15*, 8164–8174.

(160) Karlapudi, A. P.; Venkateswarulu, T.; Tammineedi, J.; Kanumuri, L.; Ravuru, B. K.; ramu Dirisala, V.; Kodali, V. P. Role of biosurfactants in bioremediation of oil pollution-a review. *Petroleum* **2018**, *4*, 241–249.

(161) Zhao, J.; Dai, C.; Ding, Q.; Du, M.; Feng, H.; Wei, Z.; Chen, A.; Zhao, M. The structure effect on the surface and interfacial properties of zwitterionic sulfobetaine surfactants for enhanced oil recovery. *RSC Advances* **2015**, *5*, 13993–14001.

(162) Mariyate, J.; Bera, A. A critical review on selection of microemulsions or nanoemulsions for enhanced oil recovery. *Journal of Molecular Liquids* **2022**, *353*, 118791.

(163) Hu, D.; Mafi, A.; Chou, K. C. Revisiting the Thermodynamics of Water Surfaces and the Effects of Surfactant Head Group. *J. Phys. Chem. B* **2016**, *120*, 22572261.

(164) Andrews, M. Y.; Santelli, C. M.; Duckworth, O. W. Digital image quantification of siderophores on agar plates. *Data in Brief* **2016**, *6*, 890–898.

(165) Mohamad-Aziz, S. N.; Zularisam, A.; Sakinah, A. M. Reverse micellar modified mixed anionic and zwitterionic surfactant system for antibiotic extraction. *Separation and Purification Technology* **2019**, *229*, 115816.

(166) McLachlan, A. A.; Marangoni, D. G. Interactions between zwitterionic and conventional anionic and cationic surfactants. *Journal of Colloid and Interface Science* **2006**, *295*, 243–248.

(167) Ramdass, A. C.; Rampersad, S. N. Diversity and Oil Degradation Potential of Culturable Microbes Isolated from Chronically Contaminated Soils in Trinidad. *Microorganisms* **2021**, *9*, 1167.

(168) Zhang, X.; Kong, D.; Liu, X.; Xie, H.; Lou, X.; Zeng, C. Combined microbial degradation of crude oil under alkaline conditions by *Acinetobacter baumannii* and *Talaromyces sp. Chemosphere* **2021**, *273*, 129666.

(169) Place, B. J.; Perkins, M. J.; Sinclair, E.; Barsamian, A. L.; Blakemore, P. R.; Field, J. A. Trace analysis of surfactants in Corexit oil dispersant formulations and seawater. *Deep Sea Res Part 2 Top Stud Oceanogr.* **2016**, *129*, 273–281.

(170) Place, B.; Anderson, B.; Mekebri, A.; Furlong, E. T.; Gray, J. L.; Tjeerdema, R.; Field, J. A Role for Analytical Chemistry in Advancing our Understanding of the Occurrence, Fate, and Effects of Corexit Oil Dispersants. *Environ. Sci. Technol.* **2010**, *44*, 6016–6018.

(171) Schroën, K.; de Ruiter, J.; Berton-Carabin, C. The Importance of Interfacial Tension in Emulsification: Connecting Scaling Relations Used in Large Scale Preparation with Microfluidic Measurement Methods. *ChemEngineering* **2020**, *4*, 63.

(172) Dziza, K.; Santini, E.; Liggieri, L.; Jarek, E.; Krzan, M.; Fischer, T.; Ravera, F. Interfacial Properties and Emulsification of Biocompatible Liquid-Liquid Systems. *Coatings* **2020**, *10*.

(173) Goebel, A.; Lunkenheimer, K. Interfacial Tension of the Water/n-Alkane Interface. *Langmuir* **1997**, *13*, 369–372.

(174) Qazi, M. J.; Schlegel, S. J.; Backus, E. H.; Bonn, M.; Bonn, D.; Shahidzadeh, N. Dynamic Surface Tension of Surfactants in the Presence of High Salt Concentrations. *Langmuir* **2020**, *36*, 79567964.

(175) Dickhout, J. M.; Virga, E.; Lammertink, R. G.; de Vos, W. M. Surfactant specific ionic strength effects on membrane fouling during produced water treatment. *Journal of Colloid and Interface Science* **2019**, *556*, 12–23.

(176) Anachkov, S. E.; Tcholakova, S.; Dimitrova, D. T.; Denkov, N. D.; Subrahmaniam, N.; Bhunia, P. Adsorption of linear alkyl benzene sulfonates on oil–water interface: Effects of Na^{+}, Mg^{2+} and Ca^{2+} ions. *Colloids and Surfaces A: Physicochemical and Engineering Aspects* **2015**, *466*, 18–27.

(177) Bera, A.; Ojha, K.; Mandal, A. Synergistic Effect of Mixed Surfactant Systems on Foam Behavior and Surface Tension. *J Surfact Deterg* **2013**, *12*, 621–630.

(178) Kanoje, B.; Padshala, S.; Parikh, J.; Sahoo, S. K.; Kuperkar, K.; Bahadur, P. Synergism and aggregation behaviour in an aqueous binary mixture of cationic–zwitterionic surfactants: physico-chemical characterization with molecular simulation approach. *Phys. Chem. Chem. Phys.* **2018**, *20*, 670–681.

(179) Li, F.; Li, G.-Z.; Chen, J.-B. Synergism in mixed zwitterionic–anionic surfactant solutions and the aggregation numbers of the mixed micelles. *Colloids and Surfaces A: Physicochemical and Engineering Aspects* **1998**, *145*, 167–174.

(180) Bruce, E. E.; Okur, H. I.; Stegmaier, S.; Drexler, C. I.; Rogers, B. A.; van der Vegt, N. F. A.; Roke, S.; Cremer, P. S. Molecular Mechanism for the Interactions of Hofmeister Cations with Macromolecules in Aqueous Solution. *J. Am. Chem. Soc.* **2020**, *142*, 1909419100.

(181) Pegram, L. M.; Jr., M. T. R. Hofmeister Salt Effects on Surface Tension Arise from Partitioning of Anions and Cations between Bulk Water and the Air-Water Interface. *J. Phys. Chem. B* **2007**, *111*, 5411–5417.

(182) Conboy, J. C.; Messmer, M. C.; Richmond, G. L. Dependence of Alkyl Chain Conformation of Simple Ionic Surfactants on Head Group Functionality As Studied by Vibrational Sum-Frequency Spectroscopy. *J. Phys. Chem. B* **1997**, *101*, 6724–6733.

(183) Mafi, A.; Hu, D.; Chou, K. C. Interactions of Sulfobetaine Zwitterionic Surfactants with Water on Water Surface. *Langmuir* **2016**, *32*, 1090510911.

(184) Monson, P.; Patumtevapibal, S.; Kaufmann, K. J.; Robinson, C. W. Dominance of methyl groups in picosecond vibrational relaxation in hydrocarbons. *Chemical Physics Letters* **1974**, *28*, 312–315.

(185) Viana, R. B.; da Silva, A. B. F.; Pimentel, A. S. Infrared Spectroscopy of Anionic, Cationic, and Zwitterionic Surfactants. *Advances in Physical Chemistry* **2012**, 1–12.

(186) Drzymala, J.; Sadowski, Z.; Holysz, L.; Chibowski, E. Ice/Water Interface: Zeta Potential, Point of Zero Charge, and Hydrophobicity. *Journal of Colloid and Interface Science* **1999**, *220*, 229–234.

(187) Takahashi, M. ζ-Potential of Microbubbles in Aqueous Solutions: Electrical Properties of the GasWater Interface. *J. Phys. Chem. B* **2005**, *109*, 21858–21864.

(188) Deng, G.-H.; Qian, Y.; Wei, Q.; Zhang, T.; Rao, Y. Interface-Specific Two-Dimensional Electronic Sum Frequency Generation Spectroscopy. *J. Phys. Chem. Lett.* **2020**, *11*, 1738–1745.

(189) Deng, G.-H.; Qian, Y.; Zhang, T.; Han, J.; Chen, H.; Rao, Y. Two-dimensional electronic–vibrational sum frequency spectroscopy for interactions of electronic and nuclear motions at interfaces. *Proceedings of the National Academy of Sciences* **2021**, *118*, 4257–4321.

(190) Abe, T.; Shimada, H.; Hoshino, T.; Kawaguchi, D.; Tanaka, K. Sum frequency generation imaging for semi-crystalline polymers. *Polymer Journal* **2022**, DOI: `https://doi.org/10.1038/s41428-021-00613-9`.

(191) Shah, S. A.; S.Baldelli Vibrational Ground-State depletion for enhanced resolution sum frequency generation microscopy. *Chemical Physics Letters* **2022**, *787*, 139252.

(192) Kim, Y.; Kim, H.; Jang, H.; Ahn, J.-H.; Lee, J. Dual Resonant Sum Frequency Generations from Two-Dimensional Materials. *Nano Lett.* **2020**, *20*, 4530–4536.